Copyright

Samuel D. Hanlon

2012

Neutrophil Interstitial Migration

By

SAMUEL D. HANLON, O.D., M.S.

DISSERTATION

In Partial Fulfillment of the requirements for the degree of

DOCTOR OF PHILOSOPHY

In

PHYSIOLOGICAL OPTICS

Presented to the Graduate Faculty of the

College of Optometry

University of Houston

May, 2012

Approved:

_____

Alan R. Burns, PhD (Chair)

_____

Alison M. McDermott, PhD

_____

William L. Miller, OD, PhD

_____

C. Wayne Smith, MD

Committee in Charge

This dissertation and all the work associated with it are dedicated to my father, William

Francis (Fritz) Hanlon. Through his role-modeling I developed a deep-seated scientific

curiosity from a very young age. Regretfully, I was not able to complete this work during

his life time so that he could see the fruits of his inspiration.

individual graduate student, I received much needed encouragement and advice from Dr. Frishman. In the graduate office, Michele Stafford was extremely helpful assuring my adherence to university protocol and pro-active in notification of required deadlines and procedures.

During these past 5 years my two sons and their wives provided me with two lovely grandchildren. My sons have been supportive in my educational endeavor and have remained patient with me postponing my visits. Hopefully, my grand children and I will make up for lost time in the near future.

A recent graduate and former lab mate, Dr. Jenny Gagen "hit the nail on the head" when she described our excellent lab technician as her "lab mom". Mrs. Evelyn Brown is a kind, dedicated, amazing person. She makes coming to the lab every day a pleasure.

I would also like to acknowledge the time and support provided by the additional members of my dissertation committee: Dr. Alison McDermott, Dr. William Miller, and Dr. C. Wayne Smith. Each member has provided support and guidance in making this dissertation meet their high standards.

Neutrophil Interstitial Migration

By

SAMUEL D. HANLON, O.D., M.S.

May, 2012

Abstract:

Purpose: Molecular events regulating neutrophil extravasation have been extensively researched and described. However, relatively little is known about extravascular interstitial migration of neutrophils and then, much of what we do know has come from *in vitro* 2-D or 3-D matrix models. These models are limited by their ability to duplicate the nuances of the physiological or physical native environment. Neutrophils often migrate a considerable distance from the site of extravasation through the avascular corneal stroma to reach the site of injury. This migration involves contact with extracellular matrix and resident keratocytes. Ultrastructural morphometric data suggest neutrophil contacts with keratocytes are mediated by the leukocyte β2 (CD18) integrins and ICAM-1(a β2 ligand). While β1 (CD29) and β3 (CD61) integrin families are also expressed on extravascular migrating neutrophils, *in vitro* studies have shown that locomotion of activated neutrophils is dependent on integrin binding on 2-D surfaces, but not in 3-D matrixes. The role of integrin binding during *in vivo* corneal stroma migration has yet to be clearly defined. A greater understanding of this migration holds the promise of a more effective means for modulating neutrophil activity to control inflammation and improve the outcome of wound healing. Additionally, it may elicit details of motility applicable to other types of cells. The purpose of this dissertation is to provide insights into the mechanisms of neutrophil migration through the corneal stroma. Specifically, it addresses the influence of the keratocyte network on migrating neutrophils and the relative contribution of β1 (CD29), β2 (CD18) and β3 (CD61) integrins to neutrophil locomotion in the inflamed mouse cornea. *In vivo* data obtained using Heidelberg Retinal Tomographer III with Rostock Corneal Module (HRT-RCM) time lapse sequences provided the means, for the first time, to quantify speed and directionality of cellular movement while observing neutrophil interaction with stromal keratocytes in the living eye.

Methods: Corneal inflammation was induced in female wild type C57BL/6 mice by mechanical removal of the epithelium using an Algerbrush. Eight hours after injury the corneas were imaged with the HRT-RCM. Scanning sequences provided the means to track individual cells for extended time periods to determine motility characteristics. The contribution of integrin binding to neutrophil migration was assessed by blocking antibody (anti-β1-, β2-, or β3-integrin) or IgG control antibody applied to the cornea at the time of epithelial injury. Image stabilization, cell tracking and movement analysis were accomplished with a custom MatLab program.

Results: Time-lapse imaging showed an unequivocal preference for neutrophils to follow the network of keratocytes. Neutrophils in control eyes moved with an average speed of 7.56$\pm$0.20 (SE) μm/minute. The average confinement ratio (CR) of the neutrophil population was 0.55$\pm$0.02, where a value of 1.0 indicates confinement to a perfectly straight path. Compared to the results from control eyes, anti- β1-integrin antibody resulted in a 31 % reduction in speed ($p<0.05$) and a 33% reduction in CR ($p<0.05$), while anti-β2- or β3- integrin antibodies had no significant effect on cell speed or CR.

Conclusions: Results clearly show that the keratocyte network is the preferred route for neutrophil migration within the corneal stroma. Contrary to expectations based on previously published histological and *in vitro* evidence, blockade of β2-integrin does not affect *in vivo* motility and the same is true for β3-integrin blockade. However, β1 blockade produced a significant, but not total, reduction in cell speed and resulted in migrating cells being less confined to a straight path. Therefore, neutrophil locomotion within the physically confined environment of the corneal stroma does not require integrin binding, though β1 binding facilitates the process.

3

Table of Contents:

CHAPTER 1 - INTRODUCTION

CHAPTER 2 - MATERIALS AND METHODS

List of figures:

List of Tables:

Abbreviations:

CCT	-	Central Corneal Thickness
CD	-	Cluster of Differentiation
CR	-	Confinement Ratio
CS	-	Cell Speed
CV	-	Cell Velocity
GAG	-	Glycosaminoglycan
HRT	-	Heidelberg Retinal Tomographer
ICAM	-	Inter-Cell Adhesion Molecule
IL-1b	-	Interleukin - 1 beta
IOP	-	IntraOcular Pressure
KSPG	-	Keratocan Sulphate Proteglycan
MA	-	Migration Angle
MDP	-	Mean Displacement Plot
MMP	-	Matrix Metalloproteinase
MV	-	Migration Velocity
N.A.	-	Numerical Aperature
NIH	-	National Institutes of Health
NSAID	-	Non-Steroidal Anti-Inflammatory Drug
OCT	-	Optical Coherence Tomography
PECAM	-	Platelet Endothelial Cell Adhesion Molecule
PMMA	-	PolyMethyl Methacrylate
RCM	-	Rostock Corneal Module
SD-OCT	-	Spectral Domain OCT
SE	-	Standard Error
TI	-	Tactic Index
TNF-α	-	Tumor Necrosis Factor - alpha
VCAM	-	Vascular Cell Adnesion Molecule
VLA	-	Very Late Antigen

CHAPTER 1 – INTRODUCTION

1.1 – Inflammation

Inflammation is a potentially dangerous process. Even though the body has an elaborate system of initiating and modulating inflammation, in patient care, it is frequently considered an undesirable event that should be diminished or suppressed. While that is true in many instances, it must be remembered that inflammation is the initiation of the highly effective and conserved innate immune system present in all animals. Inflammation involves a complex series of events and interactions between a variety of cells and chemical mediators [1]. It is a vital aspect of clearing pathogens and wound healing. Neutrophils are the most abundant cellular component and first line of defense of the innate immune system and are key components of all phases of the inflammatory response.

1.1.1 Neutrophils and Hematopoiesis

Metchnikoff, who first discovered neutrophils, was also the first to describe phagocytosis and identify developing phagocytes (including neutrophils) in the bone marrow [3]. Neutrophils and macrophages originate from the same bone marrow stem cells that differentiate through common progenitors. The bone marrow contains a delicate meshwork of collagen fibers and other extracellular matrix components along with stem cells and leukocyte precursor cells. Mature leukocytes are discharged into the many thin-walled sinuses in the bone marrow. From there they join the systemic circulation.

The surface of neutrophils consists of ridges and folds with sites for interaction between the neutrophil and its surroundings including Fc receptors, Toll-like receptors, chemotactic receptors and adhesions molecules such as selectins and integrins [4]. "Resting" PMNs are medium-sized leukocytes, measuring roughly 6-10 μm in diameter, although this changes dramatically upon activation and transmigration [5, 6].

Neutrophils contain many granules which store large amounts of potent antimicrobial molecules, proteolytic enzymes and chemical mediators, many of which are highly cytotoxic and potentially destructive to host tissue. These neutrophil granules were first recognized by Ehrlich and Metchnikoff. The granules were later shown to be reservoirs of antimicrobial molecules and proteases that play a role in tissue destruction during inflammation [7]. Even though neutrophils were first described by Metchnikoff in 1905, it was not until late in the 20th century when neutrophils were classified, along with monocytes/macrophages, as "professional phagocytes" [1]. Because of this potentially destructive nature of the neutrophils, they are tightly controlled and kept in reserve as quiescent cells in the systemic circulation and bone marrow. There is often collateral damage from neutrophils during response to inflammation [3].

Prolonged neutrophil recruitment and activation may lead to tissue damage and protein alterations thus promoting antigen-antibody reactions leading to chronic inflammation [8]. Chronic inflammation has been linked to numerous diseases such as atherosclerosis, myocardial infarction, diabetes, hypertension, and even some cancers [9]. In the eye it has been linked to ocular surface disease and age-related macular degeneration [10, 11]. Understanding the cause of unresolved inflammation has been the focus of extensive research efforts.

Circulating ("resting") neutrophils have been (historically) reported to have a lifespan of 6-12 hours which is prolonged to 24-48 hours (perhaps longer) by delaying senescent apoptosis after their activation. If this prolongation is not properly controlled it may contribute to collateral tissue damage [1, 12]. When quiescent neutrophils are recruited from the blood by inflammation they are phenotypically transformed and armed with potent toxic molecules (Figure 1). When, where and for how long they remain in the tissue is determined, in part, by the tissue environment. Most neutrophils spend their entire life span in systemic circulation, ready to be called into service but never recruited to participate in an inflammatory response.
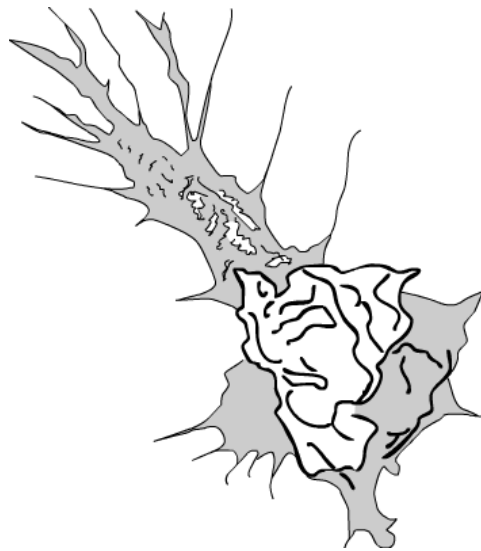
Figure 1 – Extravascular neutrophil

Example of an extravascular neutrophil that has become activated after transendothelial migration and transformed into a highly motile phenotype armed with numerous granules containing potent toxic molecules.

1.1.2 Overview of inflammation

Acute inflammation is the body's reaction to injury (or infection), providing a defense against microbial pathogens that might gain access through wounds or otherwise. It is by design self-limiting and self-resolving while setting in motion the chain of events that result in wound healing. Ultimately and ideally, healing restores tissue form and function.

Celsus was credited with first describing the four cardinal signs of inflammation (*De Medicina* volume I written in first century A.D., first printed in 1478) : rubor (redness), tumor (swelling), calor (heat), and dolor (pain). A fifth sign, functio laesa (loss of function) was added by Galen in 100 A.D. The response to injury is fairly consistent, showing that severity rather than etiology determines the response. Initially there is very brief vasoconstriction followed by a more prolonged period of vasodilation. In addition, previously inactive capillaries are filled with blood thus producing hyperemia (rubor) and heat (calor) due to the increased blood flow. The main vascular effect is in the post capillary venules which dilate. Subsequently the vascular endothelial cells contract which increases vascular permeability to where fluid and plasma proteins leak into the surrounding tissue (swelling). In more severe injury the increase in permeability may extend to include even the capillaries and arterioles.

There are many inflammatory mediators including histamine, serotonin, bradykinin, platelet activating factor, and prostaglandins from a variety of sources. In addition neuropeptides such as calcitonin gene-related protein and substance P produced by sensory nerves stimulated directly by injury also serve as inflammatory mediators. All of these produce increased swelling (tumor) which puts pressure on sensory nerves made

hypersensitive by the same mediators, thereby causing pain (dolor). Table 1 summarizes the processes and mediators of inflammation.

Table 1 – Inflammation

Acute	Plasma derived	Bradykinin, C3, C5a, MAC, Factor XII, plasmin, thrombin	
	Cell derived	Preformed	Lysosome granules, histamine, serotonin
		De novo	IFN, IL-8, TNF, IL-1, eicosanoids, NO, kinins
Chronic	Macrophage, epithelioid cell, giant cell, granuloma		
Processes	Traditional	Rubor, calor, tumor, dolor, (functio laesa)	
	Modern	Vasodilation, vascular permeability, exudates, leukocyte extravasation, chemotaxis	

[adapted from http://en.wikipedia.org/wiki/Functio_laesa]

Glucocorticoids are the most commonly prescribed anti-inflammatory drugs but they have the potential for producing significant and sometimes irreversible adverse reactions [13, 14]. They reduce inflammation and control pain by suppressing or inhibiting pro-inflammatory pathways, but do not treat the underlying cause. They provide temporary palliative treatment but can also potentially encourage bacterial infection due to the suppressed inflammation [15].

Most non-steroidal anti-inflammatory drugs (NSAIDs) work in a similar fashion but have less potential for encouraging bacterial infection. Both non-steroidal anti-inflammatory drugs and corticosteroids target the formation of eicosanoids (Figure 2) and it is now known that several members of the eiconsanoid family are anti-inflammatory regulators and promote resolution of inflammation [16-19]. This opens the door for potential continual re-initiation of inflammation and inflammatory disease [8]. Aspirin (acetylsalicylic acid) is an exception since it not only blocks the formation of eicosanoids,

but also is responsible for triggering formation of lipoxin LXA4 which actively helps to

resolve inflammation [20].
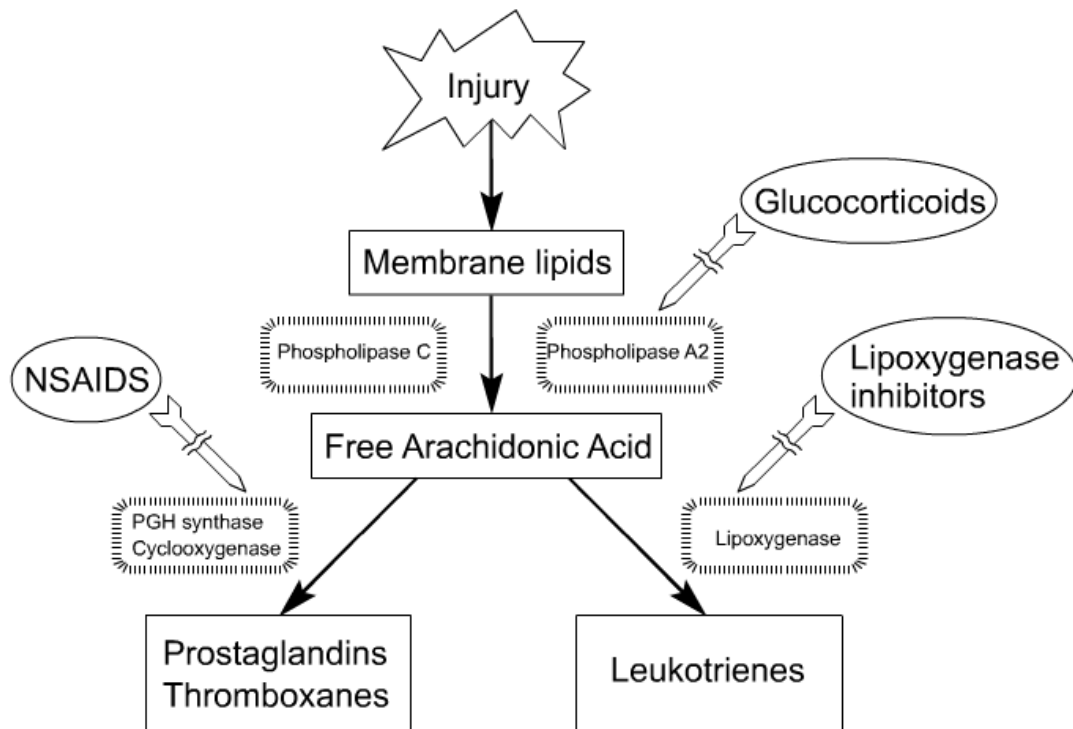
Figure 2 – Glucocorticoids and NSAIDS

Both glucocorticoids and NSAIDS inhibit the production of eicosanoids

(prostaglandins and leukotrienes) and generally dampen the inflammatory response.

However, anti-inflammatory eicosanoids may be inhibited in the process.

1.1.3 Neutrophil role in inflammation

Damaged or inflamed tissue produces chemokines which attract the infiltrating inflammatory cells and results in large numbers of these cells arriving at the site of inflammation. Other signal molecules are released into the circulating blood and stimulate the bone marrow to produce and release more leukocytes.

If successful in breaching the formidable epithelial barrier, invading pathogens encounter the innate immune system. Neutrophils, the most abundant leukocyte, mount a rapid and robust response to a breech in the physical barrier which protects the underlying tissues. The inflammatory response is the result of many different signal molecules produced by mast cells, nerve endings, platelets, leukocytes, and complement. Some of these molecules result in increased vascular permeability and activation of the vascular endothelium [1].

At the sites of inflammation, neutrophils are recruited from the systemic circulation and stimulated to transmigrate through the vascular endothelium into the extravascular interstitium. During this process they become activated, express different proteins, and transform from a round, non-motile cell into a polarized highly motile cell (Figure 1) with a greatly extended life span [2, 21, 22]. In order to reach the site of inflammation they must then migrate through the extravascular interstitium. Figure 3 summarizes the role of neutrophils in acute inflammation and illustrates the activation of the adaptive immune system.
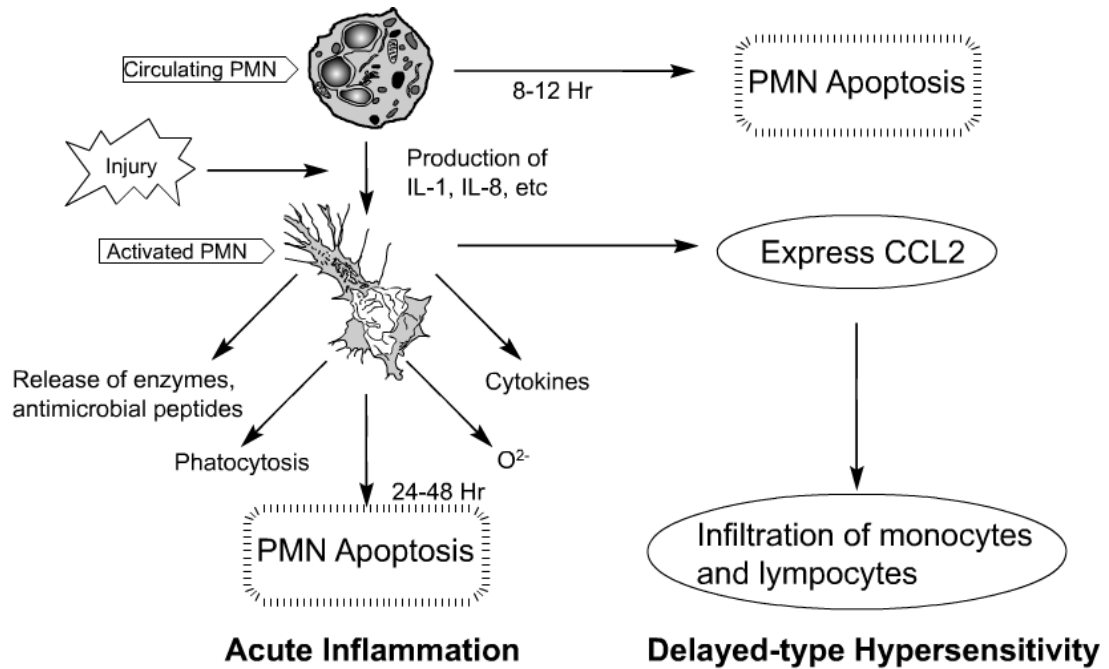
Figure 3 – Acute inflammation

Circulating neutrophils have a life span of 8-12 hours after which they undergo

apoptosis and are replenished by new cells from the bone marrow. Recruited

neutrophils become activated during extravasation with an extended life span. By

releasing the contents of their granules and by phagocytosis, they clear acute

inflammatory sites of invading pathogens. In addition, the expression of CCL2

recruits monocytes and lymphocytes, thereby activating the adaptive immune system

[2].

Diapedesis and extravasation

In 1841 William Addison first proposed that leukocytes get to tissues by diapedesis [7]. The term "diapedesis" strictly refers to the movement of blood cells, primarily leukocytes, through the intact walls of blood vessels whereas "extravasation" is a more general term referring to leakage or movement out of a container, but when used to describe the movement of leucocytes it encompasses the events leading up to and including diapedesis.

In order for neutrophils to extravasate several steps are required for them to overcome high hemodynamic shear forces and make their way into the extravascular tissues. With the initiation of an inflammatory response an intricate cascade of events begins and continues for an extended period of time. Pro-inflammatory signaling activates the vascular endothelium near the site of insult. This initiates the recruitment of leukocytes, primarily neutrophils, from the systemic circulation. Neutrophil extravasation which has been thoroughly studied and well characterized, requires at least two major types of adhesion molecules. Selectins which are expressed on activated vascular endothelium (E-selectin, P-selectin) and neutrophil (L-selectin) provide a means of slowing the passage of neutrophils, causing them to roll along the vascular endothelium and potentially becoming firmly adherent via leukocyte integrins (β1 and β2) and endothelial ligands (ICAM-1 and VCAM-1) [23-25]. After becoming firmly adherent they transmigrate the vascular wall with the aid of endothelial intercellular adhesion molecules (ICAMs) interaction as well as platelet endothelial cell adhesion molecule (PECAM-1), into the extravascular tissue, becoming activated in the process [26]. Margination, the crowding of leukocytes at the outer margin of vessels, and subsequent transmigration of leukocytes into extravascular tissues, was first reported by von Haller in 1756 [27].

19

Phagocytosis and degranulation

Early in the 20th century neutrophils were classified, along with monocytes/macrophages, as "professional phagocytes" [1] and phagocytosis has long been considered their primary function. Once neutrophils have arrived at the site of inflammation they are engaged in phagocytosis and releasing granule contents; in this way killing invading micro-organisms and clearing residual debris. Activated neutrophils become polarized with a pseudopodium in the front of the cell and a knoblike uropod at the rear [12, 28, 29]. During phagocytosis the pseudopodium of the activated neutrophil flows around the particle and forms a phagosome. The granule membranes fuse with the phagosomes and release their antimicrobial proteins and enzymes. Neutrophils also release reactive oxygen species and cytokines outside the cells, through exocytosis, in order to kill extracellular micro-organisms. This release of granule contents is also pro-inflammatory and recruits additional leukocytes to the site [7].

Immuno-modulation and resolution of inflammation

As previously mentioned, neutrophils have classically been described as primarily phagocytic cells. Not only do activated neutrophils phagocytize pathogens and cellular debris, they are also involved in activation of both the innate and adaptive immune response. They play a role in immuno-modulation by producing pro-inflammatory cytokines and chemokines (e.g. IL-1β and TNF-α) [1, 3]. Recent evidence suggests they also produce anti-inflammatory molecules and other factors that help resolve inflammation. In addition, they block and scavenge chemokines and cytokines, and also contribute to the systhesis of resolvins, thereby contributing to the resolution of

inflammation [4]. Ultimately neutrophils undergo apoptosis (presumably) and thereafter are cleared by scavenger macrophages [21]. This also helps to resolve inflammation and stimulates macrophage transformation to the anti-inflammatory M2 phenotype, contributing to the resolution of inflammation and also promoting tissue repair [1, 4, 21, 30].

The whole process of inflammation and its resolution is complex and involves interactions of inflammatory cells, the surrounding tissue, and chemical mediators. Each of these may be affected by environmental or genetic factors.

A recent study of neutrophil migration in the zebra fish embryo challenges many of the previous notions of neutrophil migration [31]. It showed repeat forward and reverse migration between the wound and blood vessels in the first 4-6 hours. Some, but not all, neutrophils returned back into the vessel lumen (intravasation) after leaving the wound. After returning to circulation they dispersed to diverse tissues which may explain how local tissue insult produces systemic inflammation. The number of neutrophils returning to the wound was shown to decrease with time, contributing to the resolution of inflammation. Surprisingly they did not detect any neutrophil apoptosis. This study suggests some drastically different concepts in the inflammatory process, but as the authors pointed out, these findings may or may not generalize to mammals.

Interaction with other leukocytes

Not surprisingly, due to their common progenitor cells, neutrophils and macrophages have many common characteristics such as being avid phagocytes, containing a large array of antimicrobials (although much more so in neutrophils), secreting common cytokines and chemokines, and expressing overlapping cell surface receptors. Recent

research has shown significant cooperation between the two types of immune cells in

numerous ways including innate and adaptive immune responses [1]. Macrophages have

been shown to recruit/attract neutrophils as well as control their lifespan and activity [3,

4] while neutrophils are a major source of pro-inflammatory cytokines that can induce

pro-inflammatory M1 differentiation of macrophages [32]. Macrophages are resident in

tissues [33, 34] and contain fewer cytotoxic anti-microbial molecules. They are therefore

less likely to cause damage to surrounding tissues. Neutrophils on the other hand are

recruited into the tissues only when needed and contain large amounts of potent

molecules. It has been shown that neutrophils may transfer their anti-microbial molecules

to macrophages by phagocytosis of apoptotic or even viable neutrophils [1, 35]. In

addition there are bi-directional interactions with immune cells other than macrophages

such as, dendritic cells, natural killer cells, B and T cells [4]. It has also been shown that

neutrophils can function as antigen presenting cells [4] and even have anti-tumor

properties in certain human tumors [3].

Migration – general

Even though there has been rather extensive research emphasis on the extravasation of

neutrophils, the process of migration from the site of extravasation to the site of injury,

which has received less emphasis, is just as critical. Because neutrophils are not tissue

resident but are the first cell responders to the wound site, their migration from the site of

extravasation to the site of injury is prerequisite to their engagement in the inflammatory

response. As such, the mechanism(s) used by neutrophils for locomotion is (are)

important to understand. This understanding would help in knowing when and how to

modulate inflammation for optimal healing as well as how alterations in the physical or molecular tissue environment affect healing.

The activated and transformed neutrophils must provide intrinsic locomotion through the interstitium which is avascular and quite variable depending on the type and location of the tissue. Neutrophils are stimulated and guided during the migration by chemotaxis (along a chemo-attractant gradient in solution) and/or haptotaxis (along a gradient bound to the substrate). Figure 4 shows an example of numerous neutrophils migrating through the avascular corneal stroma. In this particular example they are responding to a scratch wound that was inoculated with *Aspergillus* fungus 12 hours prior. Neutrophils preferentially migrate in the anterior stroma for unknown reasons [36]. However, in my experience with mice, in the presence of overwhelming invasion of pathogens, neutrophils are also found in the posterior stroma and even between the endothelium and Descemet's membrane. Although not confirmed, it is possible that some neutrophils may immigrate into the posterior stroma from the anterior chamber.
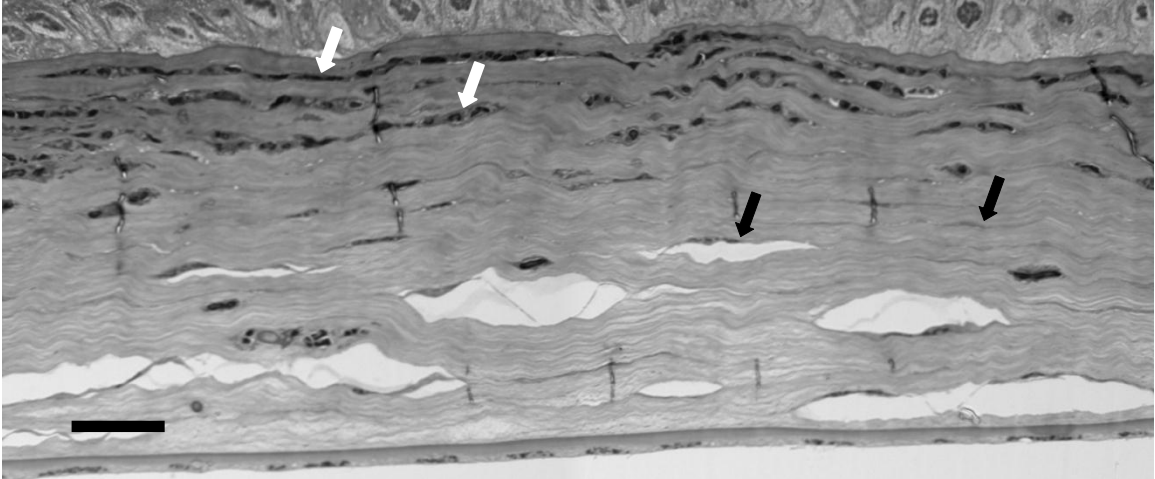
Figure 4– Anterior migration preference

12Hr after aspergillus infection – note anterior migration preference.

Infiltrating neutrophils are seen "training" through the anterior stroma (white arrows).

Keratocytes are seen between the lamellae (black arrows). Separations between the

lamellae are seen in the posterior stroma, which was more prevalent than anterior.

Scale bar = 10µm.

1.2 - Cell motility

Neutrophils are one of the fastest moving cells in the body and are recruited to sites of inflammation in large numbers. This makes them ideal candidates for studying cell motility. Motile cells have common mechanisms of locomotion and therefore an increased understanding of neutrophil motility would likely apply to other cell types as well. *In vitro* studies have provided potential mechanisms of neutrophil motility and elucidated some of the modulating factors. However, there is a need for additional understanding of *in vivo* migration and its regulation.

1.2.1 Cell Locomotion

Once activated, neutrophils become polarized and highly motile, undergoing frequent shape changes. Their means of locomotion has been described as "amoeboid" where the anterior pseudopod protrudes followed by contraction of the posterior uropod, achieving average speeds of 7+ μm/min up to 30+ μm/min [12, 37, 38]. Locomotion by cell protrusion depends on tissue geometry and follows paths of least resistance, a process known as contact guidance [37, 39].   Leukocytes are particularly prone to using other cell surfaces for guided migration [12]. Mandeville described neutrophil motility as being similar to a balloon being squeezed through a hole and demonstrated that this squeezing can stretch the matrix to a certain degree in order to accommodate the cell, thus demonstrating exertion of mechanical force by the cell on the ECM [39]. This is an important consideration in regards to neutrophils migrating through the corneal stroma where they have to squeeze between the lamellae. Electron micrographs clearly show a displacement of the surrounding collagen fibrils to make room for the infiltrating

neutrophil [39]. Mandeville went on to propose that neutrophils migrate through a 3-D

matrix by a combination of chemical and mechanical interactions, the relative

contribution of which is determined by the features of the extracellular matrix and the

adhesiveness of the cells. Tan, et al 2001 showed that maximum cell migration may be

facilitated by the proper combination of both chemical (angstrom-scale) and mechanical

(micron-scale) features (Figure 5) [40].
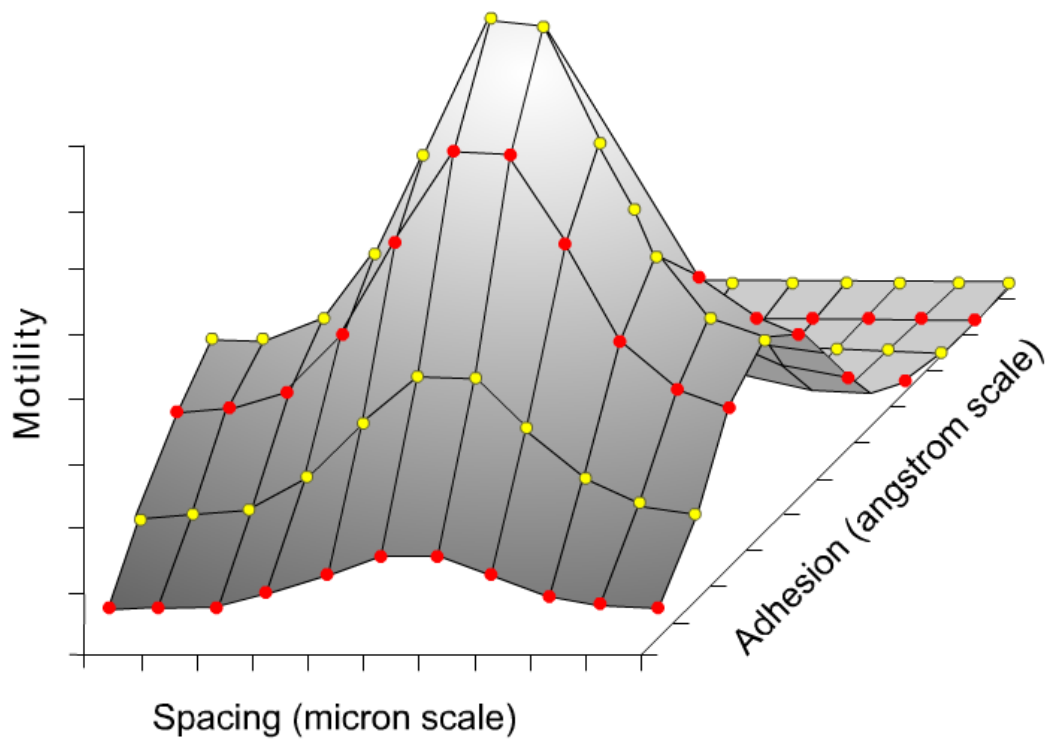
(Adapted from Tan, *et al.* 2001) [40]

Figure 5 – Adherence vs. friction

This 3-D plot illustrates that the maximum speed of motility is achieved with the proper combination of adherence of the cell to the substrate and the frictional forces due to the spacing of the elements of the matrix through which it is migrating.

There seems to be no disagreement that neutrophil migration in 2-D *in vitro* models requires integrin adhesion [12] [41]. These models have been used primarily to study isolated characteristics of cell motility and chemokinesis/haptokinesis. By adding another dimension, 3-D matrices provide some insight into how confinement by the surrounding environment may affect motility. Most 3-D migration studies have concluded that neutrophils are largely, if not completely, capable of migration through a 3-D collagen matrix without the benefit of integrin binding, being mediated instead by actin flow, shape change and squeezing [12, 37, 41].

Since neutrophil locomotion has been described as amoeboid it would therefore not be expected to follow a straight path. Several *in vitro* 2-D studies of neutrophil migration have concluded that neutrophils follow a pattern of random walk [38, 42, 43]. Random walk is a path consisting of a series of steps (either fixed or variable step size), whose direction is chosen at random. If a large sample of cells moved in a pattern of random walk, the resultant displacement of the group would be expected to be zero. When a chemoattractant is added neutrophils take a tortuous path described as a biased random walk, with frequent deviations from straight line and frequent stops. In this case the resultant displacement would have a magnitude and direction, with the direction presumably toward the chemoattractant. Interestingly, in 2-D assays, neutrophils were shown to choose the shortest route, avoid paths occupied by other neutrophils and tended to turn opposite to the direction of their previous turn [38, 43]. These events cannot be explained as purely stochastic. In 3-D migration assays the pattern of motility is much more complex and influenced by the physical characteristics of the matrix. This pattern of locomotion which is directed by variation in the physical space surrounding a cell

(anisotropy) is described as contact guidance (Figure 6). While the cellular environment affects locomotion, stochastic events and biochemical factors still play a varying role in contact guided motility. Figure 7 and 8 show examples of migration patterns of cells that are not drawn by chemoattractants and ultimately result in random displacement from the point or origin. By contrast Figure 9 shows the effects of a cell's response to guidance signals which could be induced from chemoattractants, topographical characteristics of the substrate, or cell polarity.
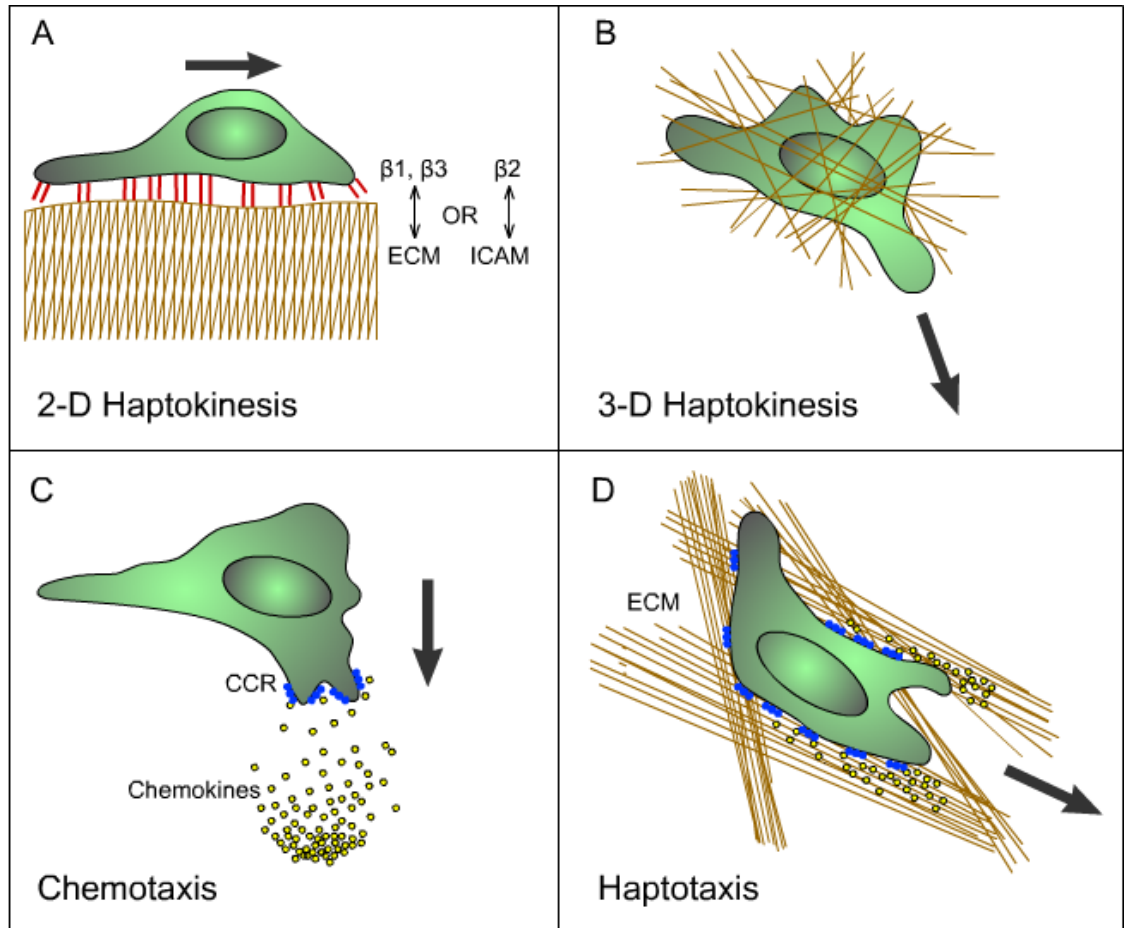
(Adapted from Friedl, *et al*. 2008) [12]

Figure 6 – 2-D and 3-D migration

Migration on 2-D surfaces (A) depends on integrin binding while within 3-D matrixes

(B) neutrophils are able to locomote using mechanical forces alone and thus integrin-

independent. Chemotaxis (C) is directed movement due a gradient of chemokines in

solution whereas haptotaxis (D) is directed movement along substrate-bound

chemokines.
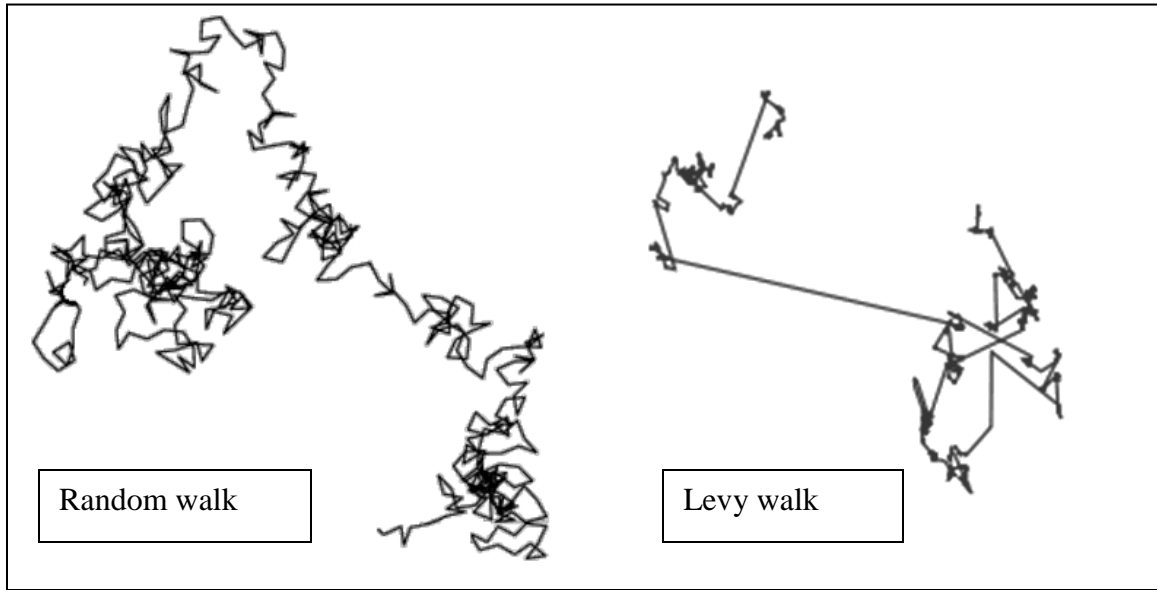
Figure 7 – Migration patterns

Shown here are two examples of possible cell migration patterns on uniform substrate without exogenous tactic stimuli. The random walk movement is totally random with orientation and step size normally distributed. It is characteristic of biological activity. The levy walk pattern is a modified form of Brownian movement where there is a relatively constant persistence of motion in a single direction before the next turn. The Levy walk pattern has been used to describe many types of cell migration patterns.
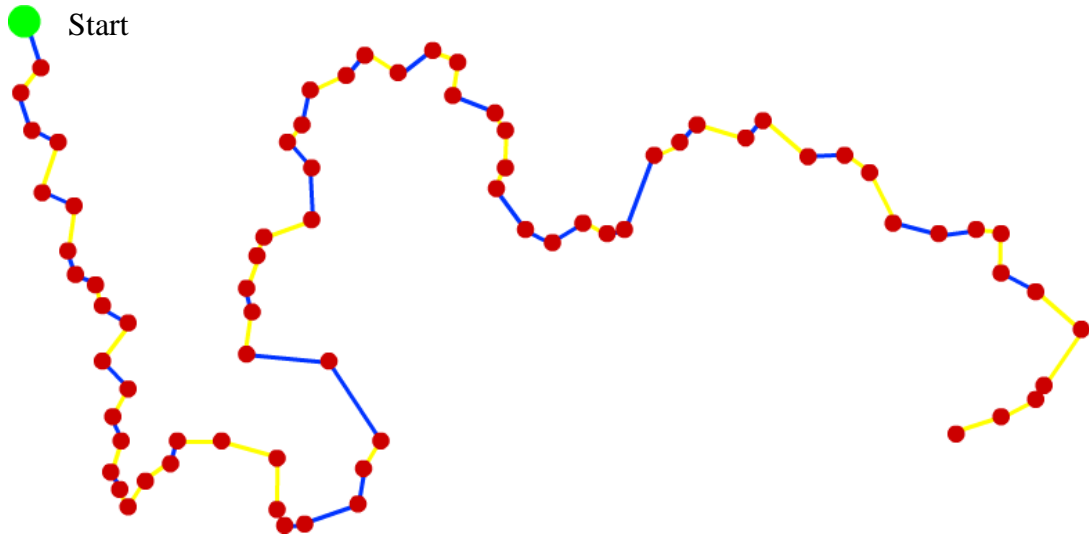
Figure 8 – Searching pattern

This example shows the migration pattern typical for many eukaryotic cell types. In this case, the cells move in a zig-zag pattern with alternating right and left changes in direction. The duration of movement between turns and the amplitude of change in direction are both exponentially distributed. This is considered to be an efficient form of cell movement when searching for a target, i.e. in the absence of a chemoattractant
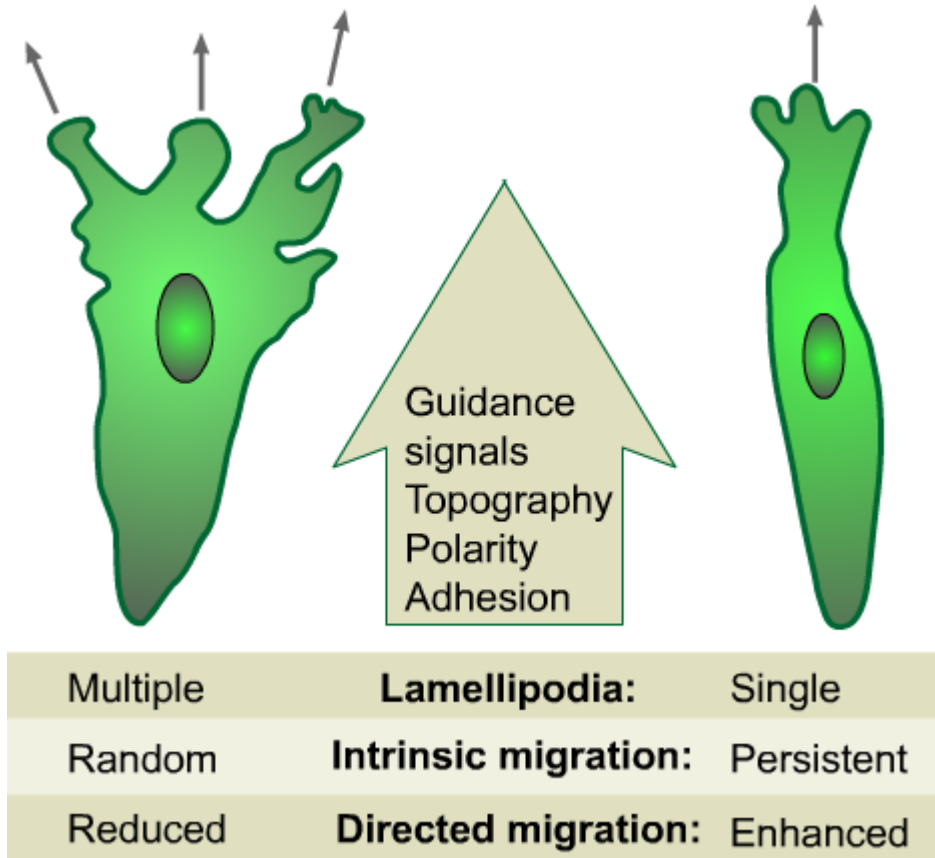
Figure 9 – Amoeboid locomotion

Migrating neutrophils are guided to the site of inflammation rather than randomly searching. Morphologically they would resemble the cell on the right, showing a single lamellipodia.

<u>1.2.2 Adhesion molecules</u>

Cell adhesion molecules (CAMs) are cell surface proteins that bind a cell to other cells or to the extracellular matrix. There are four main families of CAMs which include the immunoglobulin superfamily (IgSF), cadherins, selectins, and integrins. As mentioned previously, selectins and integrins are involved with neutrophil trafficking along with members of the IgSF. As neutrophils extravasate they shed selectins and up-regulate integrins.

Integrins are transmembrane heterodimer proteins composed of an alpha and beta subunit. Their main functions are cell-cell and cell-ECM attachment, cell migration, and cell signaling (both outside-in and inside-out). They are involved in embryogenesis, wound repair, immunological responses, and tumor invasion. There are more than 20 different alpha subunits and 9 beta subunits. Neutrophils infiltrating the cornea have been shown to express $\beta 1$ (CD29), $\beta 2$ (CD18), and $\beta 3$ (CD61) families of integrins, of which $\beta 2$ is exclusively found on neutrophils. Keratocytes express $\beta 1$ (CD29) and $\beta 3$ (CD61) as well as ICAM-1, a ligand for neutrophil $\beta 2$ (CD18) (Table 2 summarizes the stromal integrins). There are possibly other adhesion molecules which could be involved in neutrophil migration, such as CD44 however there are currently no studies linking them to acute neutrophil interstitial migration. The scope of experiments included in this dissertation is therefore confined to the function of the integrins expressed on migrating neutrophils as a result of acute inflammation.

Table 2– Integrins in the inflamed stroma [1-4]

Family	Sub units	Ligands	Keratocytes *in situ*	Fibroblasts *in vitro*	Neutrophils
CD29 β1	α2	CN, LN	✓	✓	
	α3	CN, LN, FN	✓	✓	
	α4	FN		✓	✓
	α5	CN, LN, FN		✓	✓
	α6	CN, LN, FN	✓	✓	
	α9	FN, TNC, vWF, FBN, TG, VEGF			✓
CD18 β2	αX	ICAMs, FBN			✓
	αM	iC3b			✓
	αL	ICAMs,			✓
CD51 αV	β1	LN, FN	✓	✓	
	β3	FN, VN, Fbn, vWF, Tsp	✓	✓	

CN – collagen	TG – transglutamine
FN – fibronectin	Tsp – thrombospondin
Fbn – fibrinogen	VEGF-C
LN – laminin	VN – vitronectin
TNC – tenascin-C	vWF – von Willebrand Factor

1.3 - Cornea

The experiments described in this dissertation are related to the migration of neutrophils within the corneal stroma. This chapter will describe some general features of the human cornea, with occasional reference to the mouse cornea, in order to provide the context for migration. In a later chapter the anatomical differences between human and mouse cornea will be described in detail.
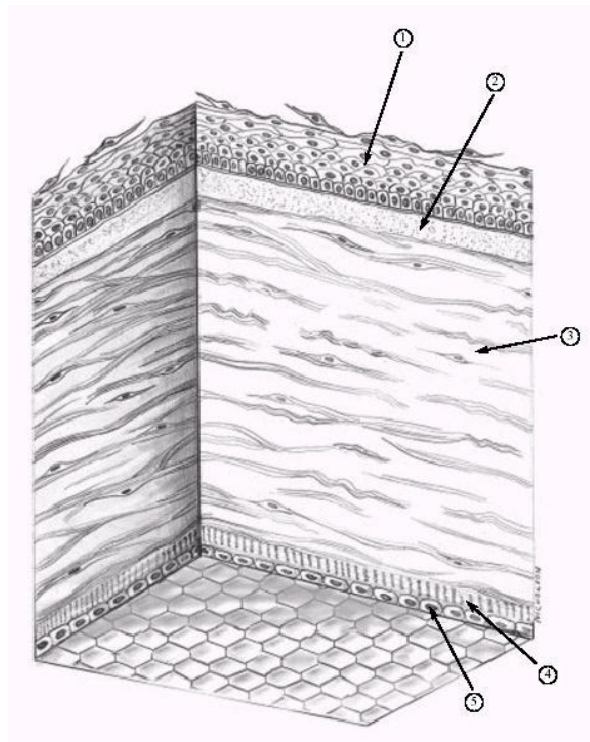
(telemedicine.orbis.org, public domain)

Figure 10 – Diagram of human cornea

A simplified diagram of the five major layers of the human cornea; (1) stratified epithelium, (2) Bowman's layer, (3) stroma, (4) Descemet's membrane, (5) endothelial monolayer.

<u>1.3.1 Cornea anatomy review</u>

Epithelium

The cornea consists of 5 distinctly different layers (Figure 10). The external layer is composed of 5-7 sub-layers of epithelial cells sitting on a basement membrane. Superficially there are the flattened non-keratinized squamous cells that form tight junctions with one another [44]. These cells not only serve as a fluid barrier but also serve as an effective physical barrier to protect the underlying tissues from microbial or other harmful agents. There is a single sub-layer of columnar basal cells attached to a basement membrane. These cells are still mitotically active and important in replacing epithelial cells lost from apoptosis or injury [45]. Between the basal cells and the superficial cells there are sub-layers of terminally differentiated wing cells. The epithelium in humans is approximately 50μm thick, roughly 10% of the total corneal thickness. Primarily the epithelium serves as a barrier while providing a minimal role in tensile strength as shown by the fact that its removal causes little or no change in the anterior corneal curvature [46].

Epithelial wounding produces an array of pro-inflammatory signals which engage the innate immune system and recruit neutrophils to the site [47]. In addition, a break in the tight epithelial barrier may allow pro-inflammatory cytokines from the tears to diffuse into the stroma and thereby initiating an inflammatory response [48]. The normal turn-over rate for epithelial cells is between 1-2 weeks, but after epithelial injury, by way of cell proliferation and migration, the epithelium is repaired typically within 48-72 hours [49].

Bowman's

Immediately beneath the epithelium is Bowman's layer (also referred to as anterior

limiting lamina) an 8 to 12-µm-thick acellular condensation of stroma which consists

primarily of randomly oriented type I collagen fibers [50]. This layer contributes to the

anchoring of the epithelial cells and may provide some rigidity (strength) to the dome-

shaped cornea although there is still controversy as to the role of Bowman's layer and

whether or not it contributes to the mechanical properties of the cornea [48, 51].

Stroma

The stroma, located beneath Bowman's layer, constitutes the bulk of the cornea (roughly

90% of the total thickness). On a weight basis, the stroma is approximately 78% water,

15% collagen and 7% non-collagenous proteins, proteoglycans and salts. It consists of

200-300 lamellae which are composed of mainly type I collagen fibrils of uniform

diameter (approximately 30-35 nm), regularly spaced (approximately 50 nm center-to-

center) with proteoglycans surrounding them. The lamellae are 1.15 to 2.0 µm thick and

9-260 µm wide (Histology of the human eye: an atlas and textbook by Michael J. Hogan,

Jorge A. Alvarado, Joan E. Weddell; Saunders, 1971), laid down in criss-cross fashion in

layers largely parallel with the corneal surface (Figure 11). Their orientation is somewhat

more random in the anterior stroma where significantly more oblique branching and

interweaving are noted [50]. Interlamellar (vertical) branching is also more extensive in

the corneal periphery than in its center and varies among species [52, 53]. Interweaving

of collagen bundles between neighboring lamellae provides an important structural

foundation for shear (sliding) resistance [54] and transfer of tensile loads between

lamellae [55].
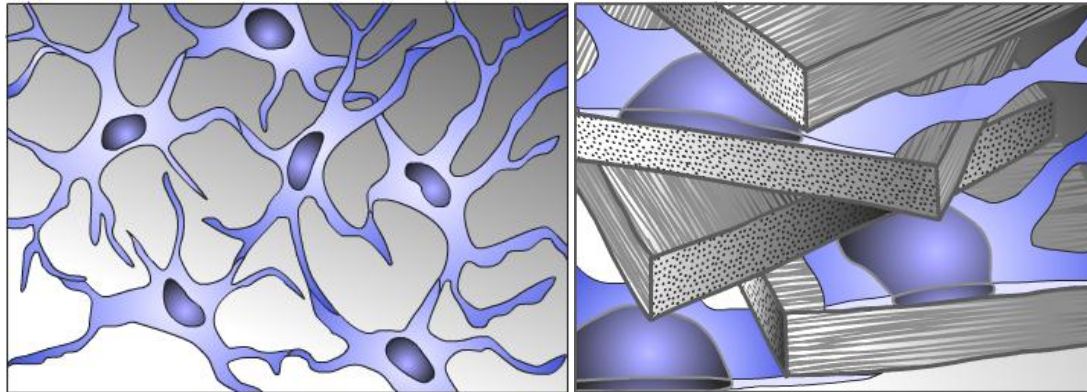
(Adapted from *Hogan, et al – Histology of the human eye, 1971*)

Figure 11 – Illustration of keratocytes and lamellae

The drawing on the left illustrates the interconnected network of keratocytes and the

one on the right shows the keratocytes interspersed between the layers (lamellae) of

criss-crossed collagen fibrils.

During embryogenesis the anterior and posterior stroma develop separately and not surprisingly in the mature cornea, there are physical and biochemical differences. The posterior stoma differs from the anterior by having somewhat more organized and orthogonal orientation of lamellae, less dense and larger keratocytes, and slightly larger collagen fibrils. There is also a variation in the types of keratan sulfate proteoglycans (KSPGs) comparing anterior to posterior. In the adult mouse, for example, there is a high expression of lumican KSPG within the posterior stroma [56]. It has been proposed that the posterior stroma contains chains that are longer or more over-sulfated and the anterior stroma has more chains but shorter and/or less sulfated [57].

KSPGs consist of a horseshoe-shaped core protein with protruding glycosaminoglycan (GAG) side chains [56, 58, 59]. The shape of the core protein, along with type V collagen, is critical in controlling fibril diameter while the sulfated GAGs regulate fibril spacing [57, 60-62]. The sulfated side chain GAGs produce a stiffer macromolecule which interconnects neighboring fibrils at regular intervals and provides resistance to compression [58, 60]. Loss of KSPG expression during scarring and its replacement with larger chondroitin sulfate PGs produces larger fibrils and increased spacing [56]. Core protein interactions have a variety of functions including epithelial-mesenchymal transition, cell proliferation and apoptosis [63]. During mouse embryological development, lumican core protein is synthesized by keratocytes as a glycoprotein not a KSPG [64, 65].

A common feature of all primates, including humans and mice, is an annulus of highly aligned collagen surrounding the cornea at the limbus. The pattern of collagen is important for biomechanics of the cornea and maintenance of its shape [66-69]. In

addition to type I collagen there are lesser amounts of types IV, V, and VI which provide secondary support and aid in the uniformity of the collagen I fibrils.

Unlike the interstitium of many other tissues, the corneal stroma is tightly compact with no pre-existing channels or spaces for the migration of infiltrating cells. Thus the physical framework of the stroma may have a significant impact on cell migration.

Descemet's

Descemet's membrane, the basement membrane for the corneal endothelium, and also the thickest basement membrane in the body, is located immediately posterior to the stroma and plays a passive role in permeability. It is composed of type IV, VIII and XVII collagen and continually thickens throughout the life of the individual [70]. The extensibility and low stiffness of Descemet's membrane help to ensure that it remains pliable over a broad range of intraocular pressures (IOP) and may serve to prevent transmission of stromal stresses to the endothelium [71].

Endothelium

The endothelium, the innermost layer of the cornea, consists of a mono-layer of cuboidal hexagonal squamous cells. Endothelial cells are terminally differentiated and normally considered to be non-proliferating and their numbers decline with age, disease, and/or trauma [72]. They contain many mitochondria and dense endoplasmic reticulum, evidence of high metabolic activity. Primarily the endothelium serves to preserve corneal transparency by controlling the balance of fluids within the stroma. Junctions between cells allows some passage of fluid from the anterior chamber into the stroma due to

hydrostatic pressure imposed by the intraocular pressure as well as the osmotic pressure due to the concentration of GAGs in the stroma. To overcome the influx of fluid, the endothelial cells actively transport fluid from the stroma into the anterior chamber [73].

Figure 12 shows some representative electron micrographs of stromal details. As noted in panel (A) there are specialized structures called hemidesosomes which securely anchor the epithelium to the stroma. Panel B shows cross sections of the alternately oriented bundles (lamellae) that constitute the bulk of the cornea. At the posterior border of the stroma is Descemet's membrane.

In examining the intricate details of the cornea, one must keep in mind that the cornea is uniquely transparent.
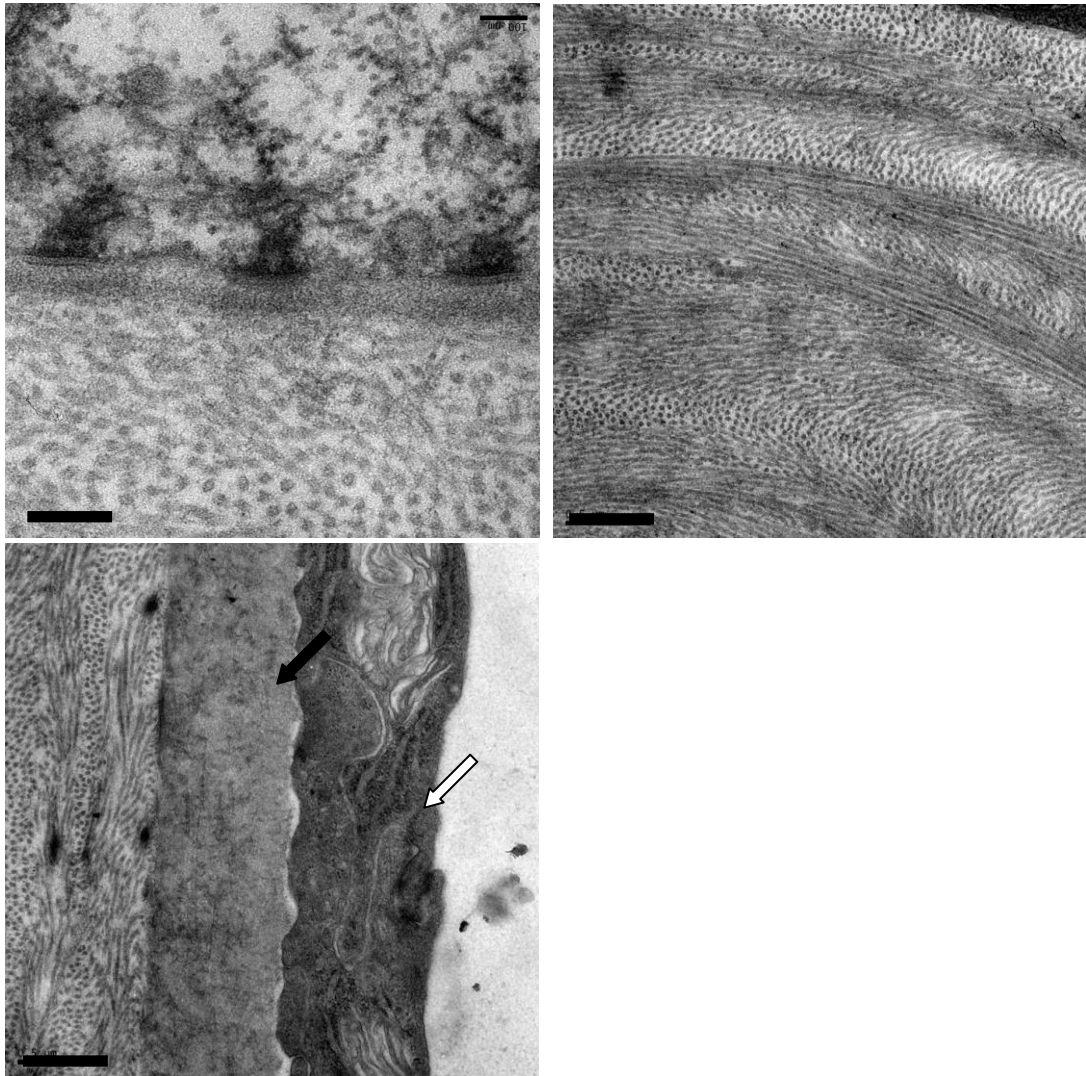
Figure 12 – EM stromal details

Upper left image (A) showing hemidesmosomes which help to secure the epithelium to the basement membrane and stroma (arrows). Upper right image (B) of stromal lamellae with closely packed, orthogonally arranged collagen fibrils. Lower left image (C) of posterior stroma, Descemet's membrane (black arrow), and endothelium (white arrow).

Corneal nerves

The cornea is extensively innervated with sensory nerve fibers (the densest tissue of the body) from the ophthalmic division of the trigeminal nerve via the anterior ciliary nerves. Shortly after entering the cornea in a radial pattern, the nerves lose their myelin sheath and divide into anterior and posterior groups which form the sub-epithelial and sub-basal plexi, respectively. Nerves are found in the anterior and mid stroma but not in the posterior stroma [74]. Corneal neurons have been shown to be functionally heterogenous and expressing variable amounts of calcitonin-gene-related-peptide (CGRP) and substance P [75]. About 20% of sensory fibers respond to mechanical forces only (mechano-nociceptors) and 70% respond to mechanical as well as heat and chemical irritants (polymodal nociceptors). The remaining fibers are cold sensitive [76, 77]. Corneal nerves are important in regulating epithelial integrity, cell proliferation, and wound healing [78]. There are also autonomic sympathetic nerve fibers within the cornea which may serve to modulate epithelial Cl^- transport and other cellular processes [79]

Deturgescence

The corneal stroma has a natural tendency to imbibe water but is maintained in a state of relative deturgescence by the active transport of water molecules by the corneal endothelium. The swelling pressure of the rabbit stroma *in vivo* has been measured at 40-50 mmHg [80]. When the intraocular pressure produces a hydrostatic pressure that exceeds the ability of the endothelial pump there is significant corneal edema and loss of transparency. The maintenance of stromal hydration is a delicate balance between numerous factors, alteration of any of which may result in corneal edema. Edema results

from excess accumulation of water within the stroma resulting in increased separation between stromal lamellae, and it affects the inter-fibrillar collagen spacing [81].

1.3.2 Resident stromal cells

Historically the cornea was thought of as being essentially isomorphic and isotropic. However research through the years has shown it to be a highly structured cellular tissue. Keratocytes are by far the most prominent resident cells in the stroma and are the key to maintaining homeostasis as well as instrumental in wound repair. They have been termed "quiescent" but evidence suggests that they are active even at the status quo. However they can become highly activated and may phenotypically transform into fibroblasts and myofibroblasts [82-84]. Keratocytes are flattened, stellate cells with long cytoplasmic processes generally tightly interspersed between the lamellae and make up 2.5-5% of the stromal volume (Figure 13). At their thickest point, the location of the nucleus, they are approximately 2 μm thick. Keratocytes connect with one another forming a network essentially parallel with the surface and with occasional vertical connections between keratocyte layers (Figure 14). This extensive network potentially serves at least 3 purposes: 1) may provide some tethering of lamellae to help maintain structural regularity; 2) establishes a communication network; 3) serves as a "cellular highway" for neutrophil contact-guided migration. In Figure 15 details of a keratocyte can be seen. Even though keratocytes are described as quiescent, they have extensive rough endoplastic reticulum and many mitochrondria which suggests that they are quite active. In addition to keratocytes, macrophages and dendritic cells are also resident in the corneal

stroma [33, 34]. However, neutrophils are generally not found in the central cornea in the

absence of inflammation.
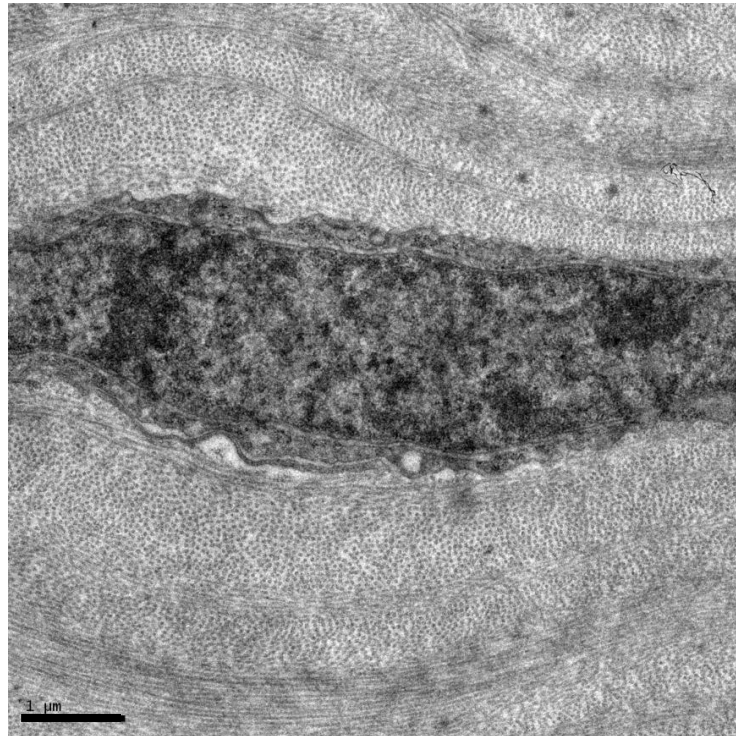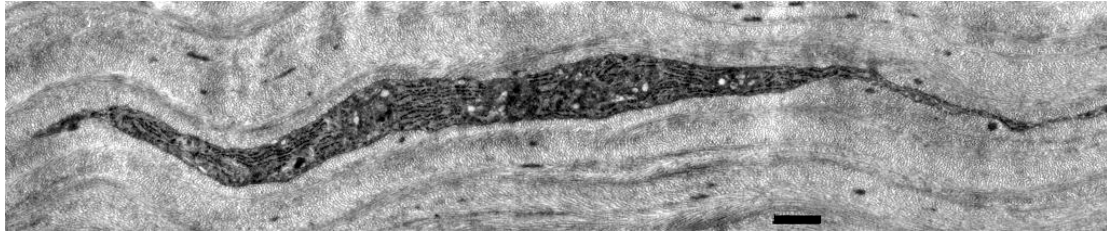
Figure 13 – EM keratocytes

EM images of mouse keratocytes tightly interspersed between the collagen lamellae. In both images the scale bars are 1μm.
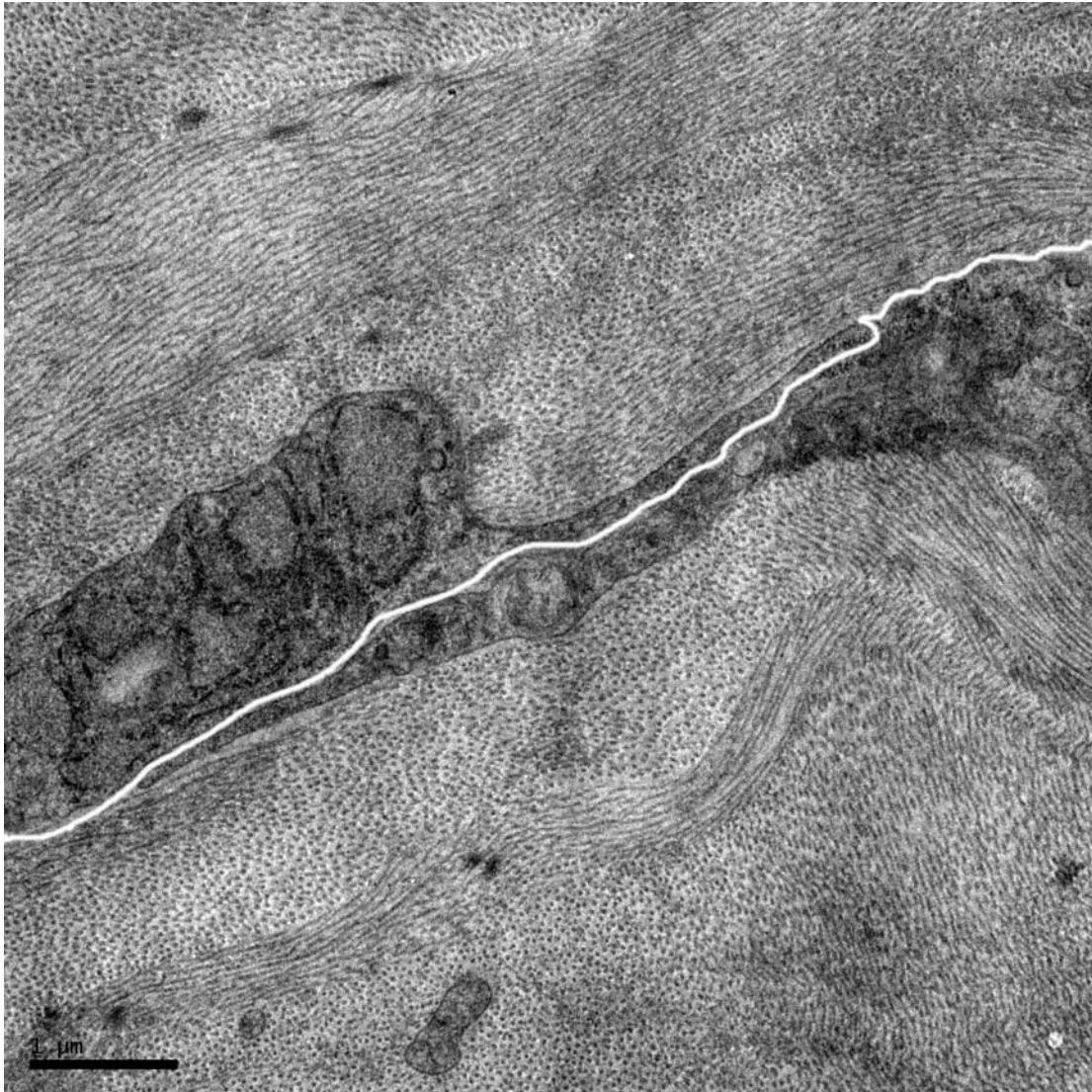
Figure 14 – EM showing coupled keratocytes

White line (added) separates two murine keratocytes which are part of a continuous

network (note mitochrondia in the lower one, arrows). Mitochrondia and rough

endoplasmic reticulum (arrow heads) are commonly seen in keratocytes, suggesting they

are quite active. Scale bar = 1µm.
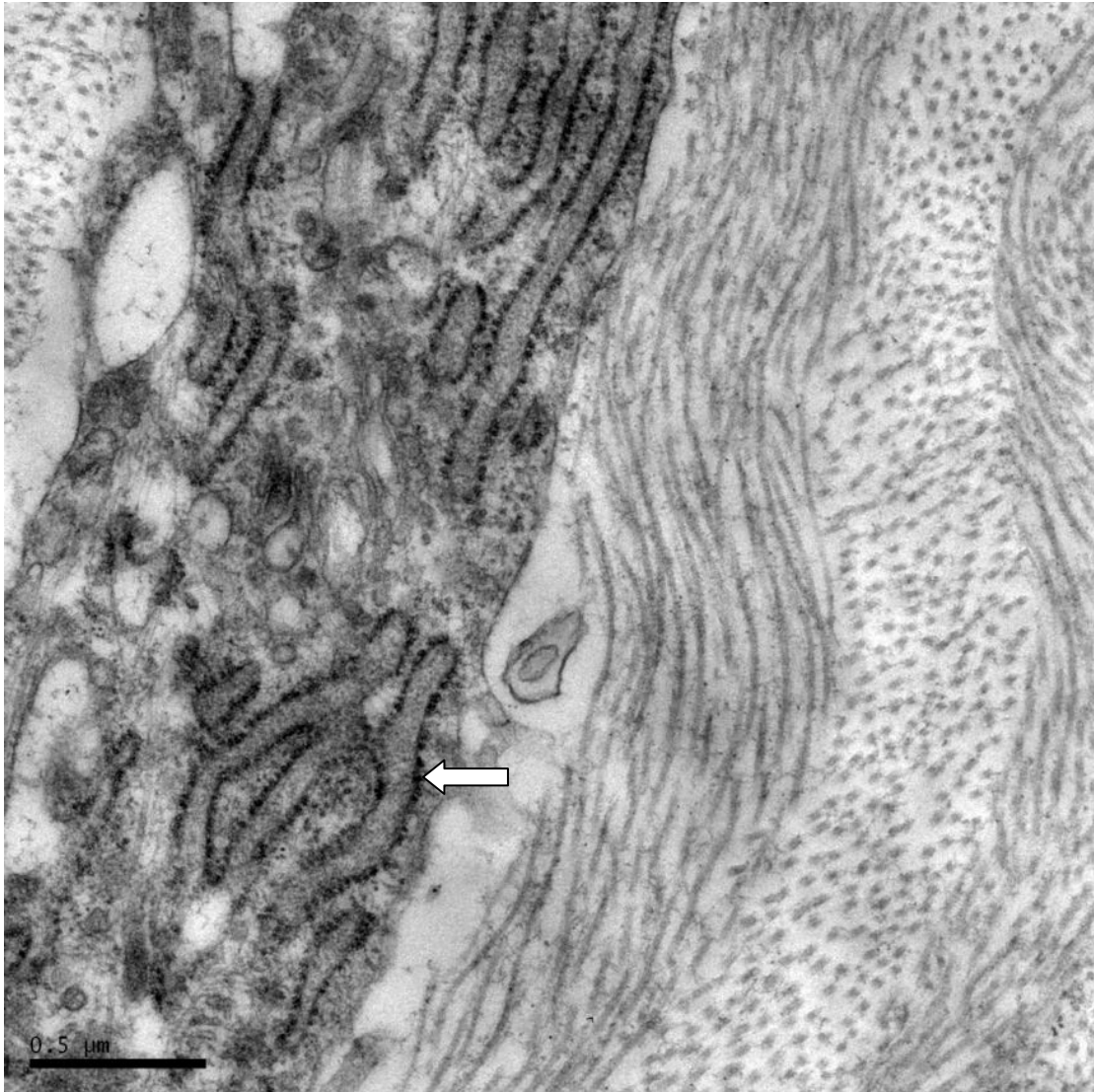
Figure 15 – EM keratocyte details

A mouse keratocyte between collagen lamellae shows extensive rough endoplasmic

reticulum (white arrow). Orientation of collagen fibrils within lamellae alternate between

parallel and perpendicular to the cross-sectional plane. Scale bar = 0.5μm

Keratocyte cell death

Keratocyte apoptosis is an exceedingly rare event in the normal uninjured cornea,

however immediately following an epithelial injury stromal keratocytes beneath the

injury begin to die due to apoptosis and/or necrosis [85, 86]. The early apoptosis serves

as an initial defense against posterior extension of infectious organisms [87, 88].

Keratocyte apoptosis is triggered by soluble mediators released from injured corneal

epithelial cells [86] and/or from the tears [89], but does not require the removal of the

epithelium. Direct mechanical trauma such as epithelial removal used in many wound

models, has also been shown to contribute to keratocyte death beneath the wound [88,

90].

1.3.3 Optical properties of the cornea

Being the sensory organ for sight, the eye is not unlike a camera. It must have the means

to transmit and refract light onto the retina located at its focal plane. The cornea has two

critical roles in the optics of the eye. In order to transmit a clear image onto the retina the

cornea must be highly transparent, which is a unique tissue quality. Secondly the shape of

the cornea must maintain the correct curvature to provide the dioptric power needed to

focus in-coming light rays with minimal distortion. In order to maintain shape and

transparency, it must precisely regulate the state of hydration and architecture of its

stromal elements. The tight epithelial barrier function and the endothelial pumping action

are critical to maintaining the cornea in a relatively dehydrated state, while the small,

uniform size, spacing and orientation of the fibrils comprising the stromal matrix assure

its transparency and strength. These qualities must be maintained, and restored when

50

necessary, throughout the lifespan of the animal. Because sight is critical for survival of most animal species, wound healing in the cornea is generally quite rapid.

1.3.4 KSPGs and corneal inflammation

The KSPGs have been found to have functions beyond structural, including regulating cellular functions and contributing to wound healing [65, 91, 92]. For example, lumican is involved in cell migration and proliferation during embryonic development; it facilitates keratocyte migration, and its absence retards neutrophil migration in inflammation. Only in the cornea do the core proteins of KSPGs become sulfated and assume the character of proteoglycans. The changes that occur in KSPG sulfation during wounding may help to localize inflammatory cells at sites of injury [93].

The significant role of KSPGs in the sequence of events in corneal inflammation has recently been outlined by Carlson, *et al*. 2010 [94]:

1. Exposure to microbes or microbial products such as LPS induces TLR signaling in resident macrophages and DCs, resulting in production of CXC chemokines, including CXCL1(KC)

2. Chemokines bind to proteoglycans creating a haptotactic gradient

3. Neutrophils are recruited from limbal vessels and migrate along the gradient

4. At the site of inflammation neutrophils secrete matrix metalloproteinases **(**MMPs) or stimulate endogenous MMPs

5. Keratocan and lumican are cleaved and the lower molecular weight KSPG products and CXCL1(KC) then diffuse into the anterior chamber thereby contributing to the resolution of inflammatory response

1.4 - The mouse as animal model

The mouse has been a leading mammal for genetic research for the past century and has been a valuable model for human physiology and disease [95]. With both the human and mouse genomes sequenced there was found to be a 99% overlap [96]. Not surprisingly the mouse has been used extensively for corneal research. However similar the two species are genetically, they are not the same. Whenever research is conducted using an animal model and the results extrapolated to humans, there is a caveat. Even subtle differences can have a significant impact on experimental results. None the less, animal models such as the mouse are invaluable for scientific research.

1.4.1 Mouse compared to human

A mouse cornea is obviously smaller than a human's but it is not uniformly down-scaled (Figure 16). The corneal epithelium in the mouse is nearly the same average thickness as a human's (40μm vs. 50 μm) while the stroma is a fraction of the human thickness (65 μm vs. 500 μm) (Figure 17). Even though the stroma is so much thinner, the size and organization of the collagen fibrils is quite similar but the arrangement of lamellae is somewhat different. In the mouse the stroma thins towards the limbus whereas in humans it thickens. Instruments such as optical coherence tomographers (OCTs) allow visualization of *in vivo* anatomical structures as seen in Figure 18. Figure 19 shows the mouse cornea diameter is nearly equal to the diameter of the entire globe, unlike human eyes where there is considerable sclera seen surrounding the cornea. In addition, the lens occupies a large portion of the mouse posterior chamber and causes bulging forward of

the iris, as seen in the gonioscopic view in Figure 19. The anatomical differences between human and murine corneas are summarized in Table 3.

There are biochemical differences as well. The type, relative distribution (anterior/posterior), and amount of sulfation of keratan sulfate proteoglycancs KSPGs is somewhat different between the species [97, 98]. There are differences in cytokines, chemokines, and growth factors as well, but by-and-large the mouse stroma provides a physical and molecular environment about as close to the human as possible in an animal model.
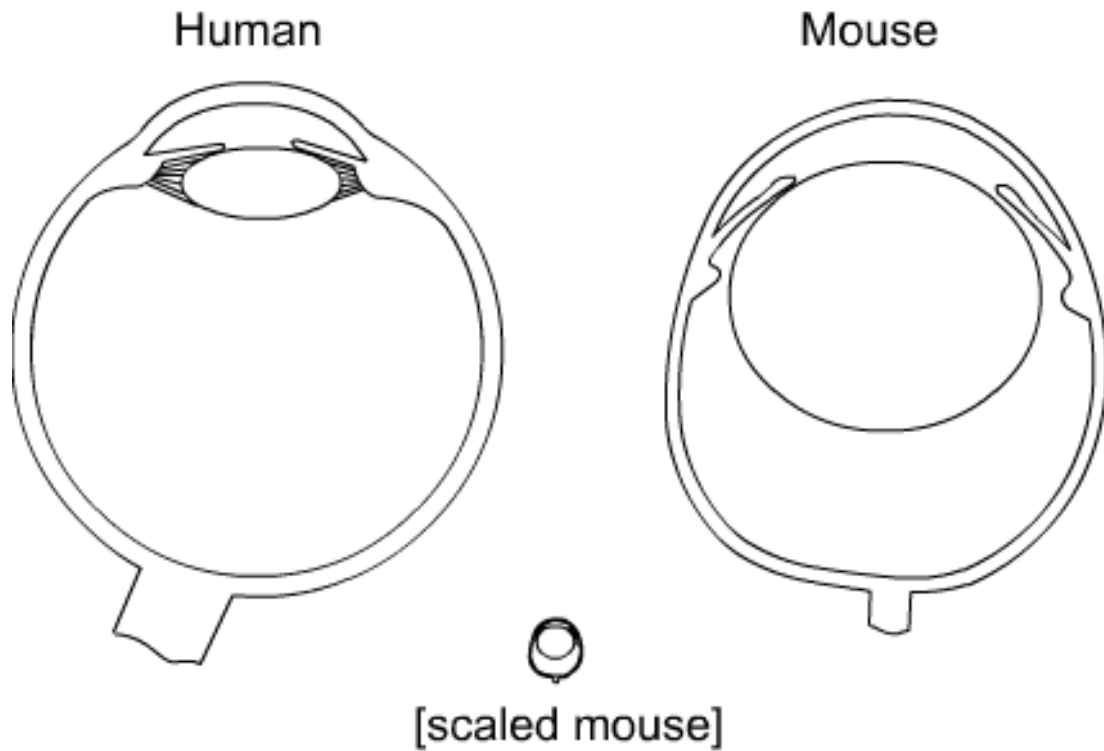
Figure 16 – Human vs. mouse schematic

Schematic representation of the differences in eye anatomy comparing the mouse to

human. The most obvious differences being the relative difference in size of the lens

and the diameter of the cornea. The scaled mouse eye illustrates the overall size

difference.
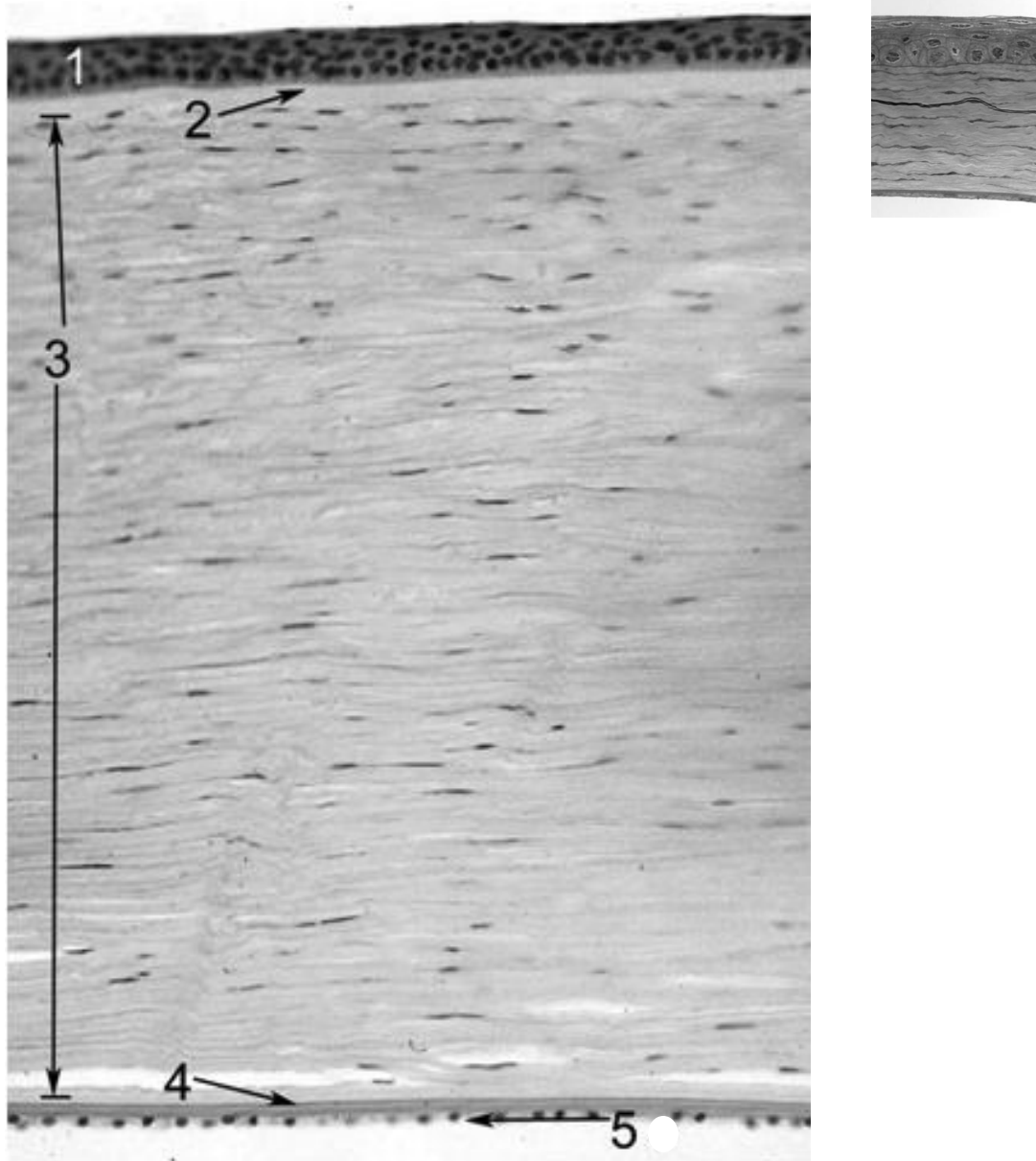
Figure 17 – LM human vs. mouse

The image on the left shows a cross section of human cornea while the small image on the right shows a mouse cornea at the same magnification. The epithelium (1) is only slightly thicker in the human as is Descemet's membrane (4) and the endothelium (5). Bowman's layer (2) does not exist as a distinct layer. The bulk of the difference in thickness is the stroma (3).
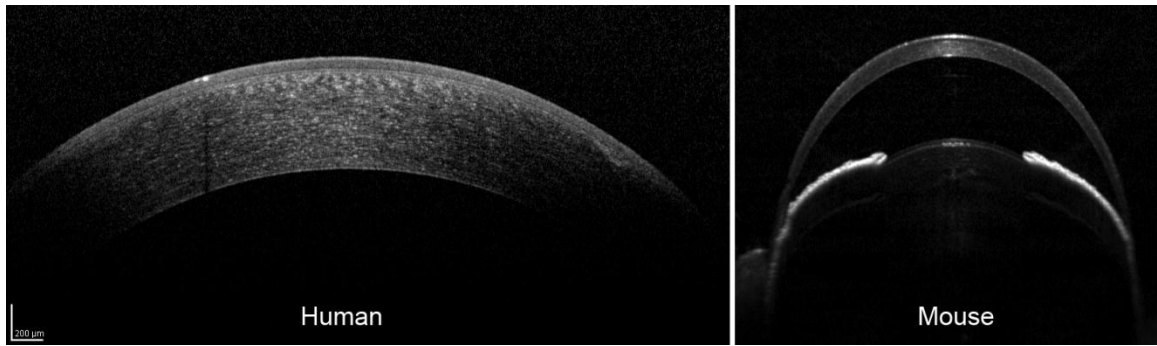
Figure 18 – OCT human vs. mouse

Corneal x-section views obtained with the Spectralis SD-OCT. Details obtained with this

in vivo imaging are nearly equivalent to low magnification light microscopy of

histological specimens. Only a small part of the central human cornea is able to be

scanned at one time while the entire mouse cornea and anterior chamber is contained

within one scanned image. Note the peripheral corneal thinning in the mouse. Images are

roughly to scale.

Table 3 – Summary Human vs. mouse

	Human	**Mouse**
1. Epithelium	50 µm (5-7 layers)	40 µm (6-9 layers)
2. Bowman's	8 µm	?
3. Stroma	500 µm	70 µm
4. Descemet's	3-20 µm	1-4 µm
5. Endothelium	5 µm (Single layer) $2500/mm^2$	2-4 µm (Single layer) $2500/mm^2$
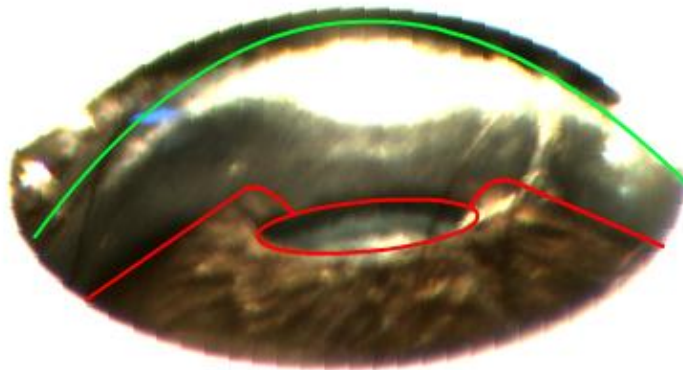
Figure 19 – Mouse eye images

The top image shows that the corneal diameter, unlike the human eye, is nearly the same diameter as the entire eye. The bottom image is a gonioscopic view where the green line outlines the cornea and the red line the iris and pupil. The plane of the iris in human eyes is nearly flat as compared to the convex iris of the mouse.

1.4.2 Mouse cornea development

Embryonic

Corneal development essentially consists of differentiation of cells from surface ectoderm and migration of mesenchymal cells of neural crest origin. The surface ectoderm produces the epithelium (cornea and conjunctiva) by E12. The primary stroma is then formed by components synthesized by the corneal epithelium. Two waves of mesenchymal cell migration occur. The first forms the endothelium and the second wave of cells becomes keratocytes which then produce the secondary stroma present in adult vertebrates. However, in mice there is only a single migration of mesenchymal cells into the primary stroma and these cells differentiate into either endothelium or keratocytes by E17 [99-101]. The gestational period for mice is 19-21 days.

Postnatal

   Mice are essentially born premature with eyelids remaining closed until P12. Figure 20 shows a developmental series of images obtained with SD-OCT and shows the development of the anterior chamber and changes in the thickness of the cornea up to P10, a couple of days prior to eyelid opening. While the epithelial thickness gradually increases from P0 to P30, the stromal thickness shows a rapid increase from P8-P12, a gradual decrease after eyelid opening and then a gradual increase to adult thickness at P30. The peak stromal thickness that occurs at P12, at the time of eyelid opening, is probably due to the increase in KSPG which increases water retention at a time when the endothelial pump is not yet fully functional [56]. Lumican is evenly distributed anterior and posterior at P10 and then by P45 it is almost exclusively in the posterior stroma. With

58

a higher level of lumican in the posterior stroma, there is also a higher concentration of keratocan sulfate and therefore a greater water retention capability [102].

At the time of lid opening (P12-14) the epithelium increases proliferation while keratocytes and endothelial cells cease proliferation. Keratocytes exit into G0 phase and are not terminally differentiated while endothelial cells are arrested in G1 phase and cannot be readily stimulated to proliferate [103]. The number of stromal cells rapidly decreases from P1-P12 and continues to decrease through P30 [56]. The electron micrographs in Figure 21 illustrate the differences in keratocyte density between the newborn and adult. Table 4 provides data from Song, *et al.* 2003 showing the decrease in density with development. This decrease in stromal cell density and the up-regulation of soluble proteins such as aldehyde dehydrogenase 3 (ALDH3) and transketolase (TKT) help reduce light scattering and increase transparency [56, 104, 105]. The epithelial cells continue a high rate of proliferation until P21 [103].
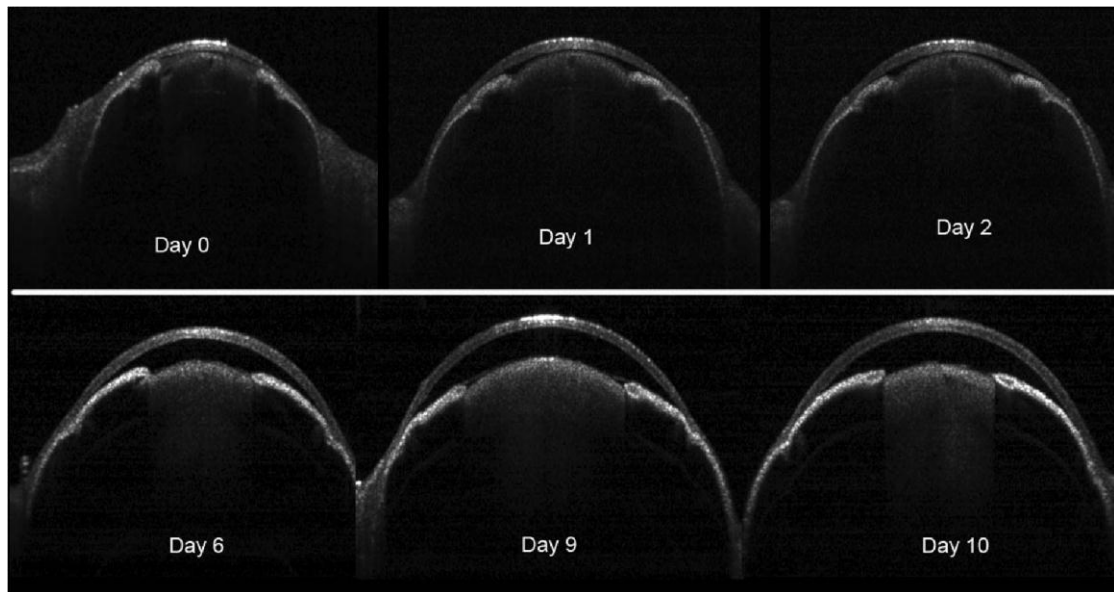
Figure 20 – Postnatal OCT

Pre-eyelid opening (P1-10) images with SD-OCT showing the development of the
anterior chamber and changes in corneal thickness. The corneal thickness reaches a
peak just before eyelid opening (P12-14) and decreases immediately after opening.
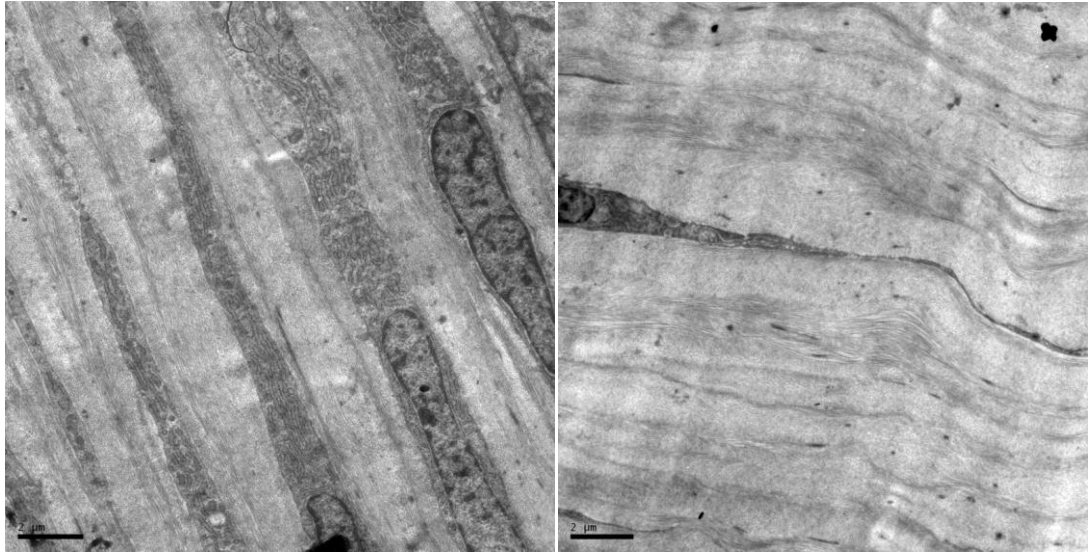
One day old   10 week old

Figure 21 – EM newborn vs. adult

Electron micrographs showing the differences in keratocyte (arrows) density in the

newborn compared to adult cornea. Scale bar = 2 µm.

Table 4 – Keratocyte density

Age (weeks)	n	K (cell/mm3)	SD
1	5	163,639	12,265
2	5	92,063	11,671
3	5	75,868	9,228
4	5	65,967	12,032
8	5	64,496	7.371
12	5	48,382	16,574

(Song, et al 2003) [56]

1.5 – Direction and relevance

Inflammation is critical to host survival with neutrophils playing a key role in this complex process. Neutrophils are the initial and primary cell-mediated innate immune response and therefore understanding their migration mechanisms is essential. While much has been gained in our understanding of this process, many gaps, and perhaps misunderstandings, remain. With tools and methods constantly evolving, gaps will be filled-in and processes clarified in the years to come. Gaps in our knowledge are especially evident when it comes to extravascular migration of neutrophils. Cell motility and locomotion have been extensively researched as they are vital for so many life functions, but there are many unanswered questions.

The management of corneal inflammation (now including dry eye syndrome) is a common task for ophthalmic practitioners. By and large it involves suppressing the immune response. However, inflammation is a necessary step in healing. Our understanding of neutrophil interstitial migration is important in order to know when and how to best modulate the innate immune response. In addition, we need to know the effect that medical and surgical intervention (e.g., LASIK, collagen cross-linking, dry eye treatment) have on neutrophil migration. Understanding the events involved in corneal inflammation is important for developing potential therapeutic interventions for corneal healing, but will also provide a more generalized understanding of inflammation. For example, many systemic conditions such as insulin resistance, now known to have inflammatory components, would potentially have an effect on wound healing and neutrophil migration.

In addition to potentially improving our management of inflammation, there are other reasons why information gained from these experiments may be useful. The mechanisms of neutrophil locomotion and guidance are likely to be applicable to other types of cells. For example, understanding cell migration details may help suppress invasion of tumor cells. An individual's age, presence of disease, degeneration, or scarring (even contact lens wear) alter the corneal interstitium and *in vivo* studies are the only way to assess their effect on the ability of neutrophils to respond to inflammation. Understanding the mechanics of cell migration also benefits the attempts to create artificial scaffolds for cornea tissue engineering where host cells are required to infiltrate the scaffold.

Until recently we have not had the means to non-invasively observe *in vivo* neutrophil migration. We have had to rely on *in vitro* studies or surgically manipulated tissues *in vivo*, not including the cornea. The corneal stroma is a very complex environment that is in a state of dynamic balance that can change rapidly in response to many factors. However, the simplistic cellular environment that has typically been used for research in this area bypasses many of the physiological events that occur *in vivo*.

The overall intent of this dissertation research was to investigate neutrophil migration within the corneal stroma using *in vivo* methods and to examine histological evidence to provide additional explanation for migration mechanisms. In order to do this it was first necessary to establish the optimal minimal mouse age to use for these studies in order to avoid effects on migration that could be attributed to a changing developmental environment. The significance of *in vivo* experiments lies in their ability to represent the unperturbed, naïve state of the animal/tissue. A second prerequisite was to establish a method that produced accurate, representative histological specimens which would reveal

evidence of physical changes, which might help to explain functional alterations observed with *in vivo* experiments.

The *in vivo* environment includes numerous types of molecular constituents including integrins. Integrins serve multiple purposes including cell migration. It has been clearly demonstrated that neutrophils express β_2 integrins which are required for extravasation and mediate neutrophil/keratocyte surface contact [36]. β_1 integrins are expressed on numerous cells including neutrophils where they are up-regulated upon cell activation. It has also been shown that $\alpha V \beta_3$ integrin is found on both neutrophils and keratocytes in the inflamed cornea [106]. Therefore integrins seem likely to be involved in neutrophil migration within the corneal stroma. However there is still some question of whether or not they are necessary for neutrophil locomotion.

Research Question

What is the mechanism(s) of neutrophil locomotion during interstitial migration?
Specifically - Is the interstitial migration of neutrophils in the murine cornea integrin dependent?

<u>Aim 1 – Age of stromal maturity</u>

<u>Determine accurate central corneal stroma thickness of mouse cornea from birth to maturity</u>

Wild type C57BL/6 mice are widely used in corneal research, but there is a surprising lack of information regarding postnatal corneal development and apparently no consensus as to when their cornea is fully developed. A biometric parameter commonly reported in the literature is the central corneal thickness (CCT) which may be used to evaluate normal corneal development. Measuring the corneal thickness in a mouse, which is roughly one-fifth the thickness and diameter of the human cornea, presents a challenge and many of the human measurement techniques are not applicable. Published biometric data show a wide-range of values for corneal thickness [107]. Since the CCT is an important consideration in determining the maturation level of the cornea, accurate measurement of corneal thickness is desirable. Clearly, there is a need to develop a simple method for accurately measuring the CCT in the mouse as a means of monitoring postnatal development of the cornea through to adulthood. A recent example demonstrating the importance of corneal maturation showed that conditional fibroblast (keratocyte) knock out of β1 (CD29) integrins had a profound effect on the stroma when deleted before reaching maturity (<40 days of age) but negligible afterwards [108].

Hypothesis 1.1 – *Spectral Domain-Optical Coherence Tomography (SD-OCT) can be used to accurately determine in vivo corneal thickness*

   Significance – Because of the small size and thinness of the mouse cornea, measuring the central corneal thickness *in vivo* is difficult and the various methods reported are

inconsistent. The SD-OCT does not make contact with the cornea and has high axial resolution, making it a good choice for thickness measurements. Accurate *in vivo* measurement of the central corneal thickness can then be used as a benchmark with which to compare histological specimen measurement.

Hypothesis 1.2 – *Lamellar separation commonly seen with histological sections is an artifact that erroneously adds to the stroma thickness measurements*

  Significance – Many published studies of the cornea show corneal cross-sections with large separations between stromal lamellae and not surprisingly there has been a large variation in reported central corneal thickness measurements. The *in vivo* measurements from hypothesis 1 serve as a benchmark to show that these separations are artifactual and should not be considered in thickness measurements.

Hypothesis 1.3 – *It is possible to produce histological sections with minimal artifacts that yield the same corneal thickness as in vivo (retaining ultrastructural dimensions)*

  Significance –Being able to prepare histology specimens that are true representations of anatomical *in vivo* structure is important for evaluation of potential alterations in the ECM that may affect neutrophil migration during inflammation elicited by corneal epithelial abrasion.

Hypothesis 1.4 – *The mouse cornea continues to undergo significant developmental changes for some time after birth.*

Significance – The mouse cornea undergoes rapid post-natal developmental changes in corneal thickness and cellularity. Knowing the age at which the stroma reaches adult thickness is an indicator of overall corneal maturity. Corneal maturation is an important consideration for evaluating wound healing parameters in mice. Using mice with mature corneas provides a level of standardization that removes the confounding influence of unfinished post-natal developmental changes.

Aim 2 – Characterizing and Quantifying *in vivo* migration

Characterize neutrophil motility in the corneal stroma using *in vivo* confocal microscopy

The cornea, being an externally visible transparent structure that requires leukocytes to travel a considerable distance from the point of extravasation to the remote central cornea, lends itself to *in vivo* studies of leukocyte interstitial migration of inflammatory cells *in situ* without tissue manipulation. *In vivo* confocal microscopy using instruments such as the HRTIII-RCM provide a novel approach to studying interstitial migration in the cornea.

   After transendothelial migration, the activated and transformed neutrophils must traverse avascular stromal tissue consisting of a dense matrix of near-orthogonally crossed layers of parallel collagen fibrils with interconnected keratocytes interspersed between these collagen lamellae. However keratocyte death directly beneath an epithelial abrasion begins shortly after wounding, even though the epithelial basement membrane remains intact [86, 88]. Infiltrating neutrophils then must migrate through regions with intact keratocytes as well as those with dead keratocytes; two distinctly different environments. *In vivo* time lapse HRT-RCM sequences provided the means, for the first time, to quantify speed and directionality of cellular movement while observing neutrophil interaction with stromal keratocytes in the living eye.

Hypothesis 2.1 – *Neutrophils preferentially migrate along the keratocyte network*

  Significance – Following a central corneal epithelial abrasion, previous ultrastructural studies showed close contacts exist between neutrophils and keratocytes, suggesting the migrating neutrophils were using the keratocytes as a "cellular highway," a

classic structure/function relationship [36]. Live imaging of neutrophils migrating

along stromal keratocytes has never been documented. *In vivo* confocal microscopy

is a novel tool for examining the relative contribution of the keratocyte network to

leukocyte migration within the corneal stroma. Preferential migration along the

keratocyte network is suggestive that integrin binding between neutrophil β2

(CD18) integrin and ligands on keratocytes is involved.

Hypothesis 2.2– *Neutrophil migration motility is altered beneath the wound area where keratocytes have died*

Significance – Keratocytes die in the anterior stroma directly beneath the site of

epithelial injury. Neutrophils that enter this region migrate without the presumed

benefit of an intact keratocyte network. Observation and comparison of locomotion

parameters in regions with and without viable keratocytes will provide additional

data on how neutrophil locomotion is affected by the absence of a keratocyte

network.

<u>Aim 3 – Role of integrins in neutrophil migration</u>

<u>Determine the role of the β1 (CD29), β2 (CD18) and β3 (CD61) integrin families in</u>

<u>neutrophil locomotion within the corneal stroma using *in vivo* confocal microscopy</u>

Even though it has been shown that neutrophils can migrate through 3-D matrices

without integrin binding, the question of whether or not integrin binding affects

neutrophil migration *in vivo* has not been definitively answered previously. Leukocyte

motility has been previously studied primarily on two-dimensional surfaces and in three-

dimensional cultures. From 3-D *in vitro* experiments it appears that integrin-independent

neutrophil migration is possible and is accomplished by contact guidance, following

paths of least resistance and using mechanical force to squeeze through the matrix.[12,

39, 109] The corneal stroma, for example has an organized architecture, contains cells

and an assortment of proteoglycans, all of which may interact with migrating leukocytes.

In vivo data obtained using HRT-RCM time lapse sequences, coupled with integrin-

targeted antibody blockade, provide the means, for the first time, to quantify speed and

directionality of cellular movement to determine the relative contribution of β1 (CD29),

β2 (CD18) and β3 (CD61) integrins to neutrophil locomotion in the inflamed murine

cornea.

Hypothesis 3.1 – *Neutrophil locomotion within the mouse corneal stroma is modulated*

by integrin binding

  Significance – The timing of neutrophil arrival and departure as well as their signaling

    roles undoubtedly involves integrins, but our understanding is far from complete.

    Integrin surface expression on neutrophils is up-regulated upon activation and if

they are not required for locomotion then it can be implied that they are important

for other functions.

Chapter 1 References

1.   Silva, M.T. (2009) When two is better than one: macrophages and neutrophils work in concert in innate immunity as complementary and cooperative partners of a myeloid phagocyte system. *J Leukoc Biol*.

2.   Yamashiro, S., Kamohara, H., Wang, J.M., Yang, D., Gong, W.H., Yoshimura, T. (2001) Phenotypic and functional change of cytokine-activated neutrophils: inflammatory neutrophils are heterogeneous and enhance adaptive immune responses. *J Leukoc Biol* 69, 698-704.

3.   Kumar, V., Sharma, A. (2010) Neutrophils: Cinderella of innate immune system. *Int Immunopharmacol* 10, 1325-34.

4.   Mantovani, A., Cassatella, M.A., Costantini, C., Jaillon, S. (2011) Neutrophils in the activation and regulation of innate and adaptive immunity. *Nat Rev Immunol* 11, 519-31.

5.   Burns, A.R., Smith, C.W., Walker, D.C. (2003) Unique structural features that influence neutrophil emigration into the lung. *Physiol Rev* 83, 309-36.

6.   Li, Z., Rumbaut, R.E., Burns, A.R., Smith, C.W. (2006) Platelet response to corneal abrasion is necessary for acute inflammation and efficient re-epithelialization. *Invest Ophthalmol Vis Sci* 47, 4794-802.

7.   Dale, D.C., Boxer, L., Liles, W.C. (2008) The phagocytes: neutrophils and monocytes. *Blood* 112, 935-45.

8.   Nathan, C., Ding, A. (2010) Nonresolving inflammation. *Cell* 140, 871-82.

9.   Gronert, K. (2010) Resolution, the grail for healthy ocular inflammation. *Exp Eye Res* 91, 478-85.

10. Edwards, A.O., Malek, G. (2007) Molecular genetics of AMD and current animal models. *Angiogenesis* 10, 119-32.

11. Raisler, B.J., Nozaki, M., Baffi, J., Hauswirth, W.W., Ambati, J. (2008) Toward a higher fidelity model of AMD. *Adv Exp Med Biol* 613, 185-92.

12. Friedl, P., Weigelin, B. (2008) Interstitial leukocyte migration and immune function. *Nat Immunol* 9, 960-9.

13. Rhen, T., Cidlowski, J.A. (2005) Antiinflammatory action of glucocorticoids-- new mechanisms for old drugs. *N Engl J Med* 353, 1711-23.

14. Song, I.H., Gold, R., Straub, R.H., Burmester, G.R., Buttgereit, F. (2005) New Glucocorticoids on the Horizon: Repress, Don't Activate! *J Rheumatol* 32, 1199- 1207.

15. Klein, N.C., Go, C.H., Cunha, B.A. (2001) Infections associated with steroid use. *Infect Dis Clin North Am* 15, 423-32, viii.

16. Lawrence, T., Willoughby, D.A., Gilroy, D.W. (2002) Anti-inflammatory lipid mediators and insights into the resolution of inflammation. *Nat Rev Immunol* 2, 787-95.

17. Gilroy, D.W., Lawrence, T., Perretti, M., Rossi, A.G. (2004) Inflammatory resolution: new opportunities for drug discovery. *Nat Rev Drug Discov* 3, 401-16.

18. Serhan, C.N., Savill, J. (2005) Resolution of inflammation: the beginning programs the end. *Nat Immunol* 6, 1191-7.

19. Gronert, K. (2008) Lipid autacoids in inflammation and injury responses: a matter of privilege. *Mol Interv* 8, 28-35.

20. Chiang, N., Serhan, C.N., Dahlen, S.E., Drazen, J.M., Hay, D.W., Rovati, G.E., Shimizu, T., Yokomizo, T., Brink, C. (2006) The lipoxin receptor ALX: potent ligand-specific and stereoselective actions in vivo. *Pharmacol Rev* 58, 463-87.

21. Savill, J., Haslett, C. (1995) Granulocyte clearance by apoptosis in the resolution of inflammation. *Semin Cell Biol* 6, 385-93.

22. Christenson, K., Bjorkman, L., Karlsson, J., Sundqvist, M., Movitz, C., Speert, D.P., Dahlgren, C., Bylund, J. (2011) In vivo-transmigrated human neutrophils are resistant to antiapoptotic stimulation. *J Leukoc Biol* 90, 1055-63.

23. Nourshargh, S., Hordijk, P.L., Sixt, M. (2010) Breaching multiple barriers: leukocyte motility through venular walls and the interstitium. *Nat Rev Mol Cell Biol* 11, 366-78.

24. Ley, K., Laudanna, C., Cybulsky, M.I., Nourshargh, S. (2007) Getting to the site of inflammation: the leukocyte adhesion cascade updated. *Nat Rev Immunol* 7, 678-89.

25. Smith, C.W., Marlin, S.D., Rothlein, R., Toman, C., Anderson, D.C. (1989) Cooperative interactions of LFA-1 and Mac-1 with intercellular adhesion molecule-1 in facilitating adherence and transendothelial migration of human neutrophils in vitro. *J Clin Invest* 83, 2008-17.

26. Muller, W.A., Weigl, S.A., Deng, X., Phillips, D.M. (1993) PECAM-1 is required for transendothelial migration of leukocytes. *J Exp Med* 178, 449-60.

27. Burns, A.R.a.R., R.E. (2005) Mechanisms of neutrophil migration. In *The Neutrophils: New outlook for old cells* (D. I. Gabrilovich, ed) Imperial College Press, London.

28. Fais, S., Malorni, W. (2003) Leukocyte uropod formation and membrane/cytoskeleton linkage in immune interactions. *J Leukoc Biol* 73, 556-63.

29. Downey, G.P. (1994) Mechanisms of leukocyte motility and chemotaxis. *Curr Opin Immunol* 6, 113-24.

30. Asai-Coakwell, M., Backhouse, C., Casey, R.J., Gage, P.J., Lehmann, O.J. (2006) Reduced human and murine corneal thickness in an Axenfeld-Rieger syndrome subtype. *Invest Ophthalmol Vis Sci* 47, 4905-9.

31. Yoo, S.K., Huttenlocher, A. (2011) Spatiotemporal photolabeling of neutrophil trafficking during inflammation in live zebrafish. *J Leukoc Biol* 89, 661-7.

32. Mahdavian Delavary, B., van der Veer, W.M., van Egmond, M., Niessen, F.B., Beelen, R.H. (2011) Macrophages in skin injury and repair. *Immunobiology* 216, 753-62.

33. Chinnery, H.R., Humphries, T., Clare, A., Dixon, A.E., Howes, K., Moran, C.B., Scott, D., Zakrzewski, M., Pearlman, E., McMenamin, P.G. (2008) Turnover of bone marrow-derived cells in the irradiated mouse cornea. *Immunology* 125, 541-8.

34. Hamrah, P., Huq, S.O., Liu, Y., Zhang, Q., Dana, M.R. (2003) Corneal immunity is mediated by heterogeneous population of antigen-presenting cells. *J Leukoc Biol* 74, 172-8.

35. Tan, B.H., Meinken, C., Bastian, M., Bruns, H., Legaspi, A., Ochoa, M.T., Krutzik, S.R., Bloom, B.R., Ganz, T., Modlin, R.L., Stenger, S. (2006)

Macrophages acquire neutrophil granules for antimicrobial activity against intracellular pathogens. *J Immunol* 177, 1864-71.

36.   Petrescu, M.S., Larry, C.L., Bowden, R.A., Williams, G.W., Gagen, D., Li, Z., Smith, C.W., Burns, A.R. (2007) Neutrophil interactions with keratocytes during corneal epithelial wound healing: a role for CD18 integrins. *Invest Ophthalmol Vis Sci* 48, 5023-9.

37.   Friedl, P., Brocker, E.B. (2000) The biology of cell locomotion within three-dimensional extracellular matrix. *Cell Mol Life Sci* 57, 41-64.

38.   Li, L., Norrelykke, S.F., Cox, E.C. (2008) Persistent cell motion in the absence of external signals: a search strategy for eukaryotic cells. *PLoS One* 3, e2093.

39.   Mandeville, J.T., Lawson, M.A., Maxfield, F.R. (1997) Dynamic imaging of neutrophil migration in three dimensions: mechanical interactions between cells and matrix. *J Leukoc Biol* 61, 188-200.

40.   Tan, J., Shen, H., Saltzman, W.M. (2001) Micron-scale positioning of features influences the rate of polymorphonuclear leukocyte migration. *Biophys J* 81, 2569-79.

41.   Khandoga, A.G., Khandoga, A., Reichel, C.A., Bihari, P., Rehberg, M., Krombach, F. (2009) In vivo imaging and quantitative analysis of leukocyte directional migration and polarization in inflamed tissue. *PLoS One* 4, e4693.

42.   Planck, S.R., Becker, M.D., Crespo, S., Choi, D., Galster, K., Garman, K.L., Nobiling, R., Rosenbaum, J.T. (2008) Characterizing extravascular neutrophil migration in vivo in the iris. *Inflammation* 31, 105-11.

43. Ambravaneswaran, V., Wong, I.Y., Aranyosi, A.J., Toner, M., Irimia, D. (2010) Directional decisions during neutrophil chemotaxis inside bifurcating channels. *Integr Biol (Camb)* 2, 639-47.

44. Ban, Y., Dota, A., Cooper, L.J., Fullwood, N.J., Nakamura, T., Tsuzuki, M., Mochida, C., Kinoshita, S. (2003) Tight junction-related protein expression and distribution in human corneal epithelium. *Exp Eye Res* 76, 663-9.

45. Zagon, I.S., Sassani, J.W., Ruth, T.B., McLaughlin, P.J. (2000) Cellular dynamics of corneal wound re-epithelialization in the rat. III. Mitotic activity. *Brain Res* 882, 169-79.

46. Litwin, K.L., Moreira, H., Ohadi, C., McDonnell, P.J. (1991) Changes in corneal curvature at different excimer laser ablative depths. *Am J Ophthalmol* 111, 382-4.

47. Ebihara, T., Matsumoto, M., Seya, T. (2008) HCV and innate immunity. *Uirusu* 58, 19-26.

48. Wilson, S.E., Mohan, R.R., Ambrosio, R., Jr., Hong, J., Lee, J. (2001) The corneal wound healing response: cytokine-mediated interaction of the epithelium, stroma, and inflammatory cells. *Prog Retin Eye Res* 20, 625-37.

49. Hanna, C., Bicknell, D.S., O'Brien, J.E. (1961) Cell turnover in the adult human eye. *Arch Ophthalmol* 65, 695-8.

50. Komai, Y., Ushiki, T. (1991) The three-dimensional organization of collagen fibrils in the human cornea and sclera. *Invest Ophthalmol Vis Sci* 32, 2244-58.

51. Seiler, T., Wollensak, J. (1991) Myopic photorefractive keratectomy with the excimer laser. One-year follow-up. *Ophthalmology* 98, 1156-63.

52. Polack, F.M. (1961) Morphology of the cornea. I. Study with silver stains. *Am J Ophthalmol* 51, 1051-6.

53. Smolek, M.K., McCarey, B.E. (1990) Interlamellar adhesive strength in human eyebank corneas. *Invest Ophthalmol Vis Sci* 31, 1087-95.

54. Ehlers, N. (1966) Studies on the hydration of the cornea with special reference to the acid hydration. *Acta Ophthalmol (Copenh)* 44, 924-31.

55. Dupps, W.J., Jr., Wilson, S.E. (2006) Biomechanics and wound healing in the cornea. *Exp Eye Res* 83, 709-20.

56. Song, J., Lee, Y.G., Houston, J., Petroll, W.M., Chakravarti, S., Cavanagh, H.D., Jester, J.V. (2003) Neonatal corneal stromal development in the normal and lumican-deficient mouse. *Invest Ophthalmol Vis Sci* 44, 548-57.

57. Akhtar, S., Kerr, B.C., Hayes, A.J., Hughes, C.E., Meek, K.M., Caterson, B. (2008) Immunochemical localization of keratan sulfate proteoglycans in cornea, sclera, and limbus using a keratanase-generated neoepitope monoclonal antibody. *Invest Ophthalmol Vis Sci* 49, 2424-31.

58. Cornuet, P.K., Blochberger, T.C., Hassell, J.R. (1994) Molecular polymorphism of lumican during corneal development. *Invest Ophthalmol Vis Sci* 35, 870-7.

59. Weber, I.T., Harrison, R.W., Iozzo, R.V. (1996) Model structure of decorin and implications for collagen fibrillogenesis. *J Biol Chem* 271, 31767-70.

60. Miyagawa, A., Kobayashi, M., Fujita, Y., Hamdy, O., Hirano, K., Nakamura, M., Miyake, Y. (2001) Surface ultrastructure of collagen fibrils and their association with proteoglycans in human cornea and sclera by atomic force microscopy and energy-filtering transmission electron microscopy. *Cornea* 20, 651-6.

61.   Chakravarti, S., Magnuson, T., Lass, J.H., Jepsen, K.J., LaMantia, C., Carroll, H. (1998) Lumican regulates collagen fibril assembly: skin fragility and corneal opacity in the absence of lumican. *J Cell Biol* 141, 1277-86.

62.   Rada, J.A., Cornuet, P.K., Hassell, J.R. (1993) Regulation of corneal collagen fibrillogenesis in vitro by corneal proteoglycan (lumican and decorin) core proteins. *Exp Eye Res* 56, 635-48.

63.   Saika, S., Miyamoto, T., Tanaka, S., Tanaka, T., Ishida, I., Ohnishi, Y., Ooshima, A., Ishiwata, T., Asano, G., Chikama, T., Shiraishi, A., Liu, C.Y., Kao, C.W., Kao, W.W. (2003) Response of lens epithelial cells to injury: role of lumican in epithelial-mesenchymal transition. *Invest Ophthalmol Vis Sci* 44, 2094-102.

64.   Ying, S., Shiraishi, A., Kao, C.W., Converse, R.L., Funderburgh, J.L., Swiergiel, J., Roth, M.R., Conrad, G.W., Kao, W.W. (1997) Characterization and expression of the mouse lumican gene. *J Biol Chem* 272, 30306-13.

65.   Saika, S., Shiraishi, A., Liu, C.Y., Funderburgh, J.L., Kao, C.W., Converse, R.L., Kao, W.W. (2000) Role of lumican in the corneal epithelium during wound healing. *J Biol Chem* 275, 2607-12.

66.   Aghamohammadzadeh, H., Newton, R.H., Meek, K.M. (2004) X-ray scattering used to map the preferred collagen orientation in the human cornea and limbus. *Structure* 12, 249-56.

67.   Boote, C., Dennis, S., Meek, K. (2004) Spatial mapping of collagen fibril organisation in primate cornea-an X-ray diffraction investigation. *J Struct Biol* 146, 359-67.

68. Hayes, S., Boote, C., Lewis, J., Sheppard, J., Abahussin, M., Quantock, A.J., Purslow, C., Votruba, M., Meek, K.M. (2007) Comparative study of fibrillar collagen arrangement in the corneas of primates and other mammals. *Anat Rec (Hoboken)* 290, 1542-50.

69. Meek, K.M., Newton, R.H. (1999) Organization of collagen fibrils in the corneal stroma in relation to mechanical properties and surgical practice. *J Refract Surg* 15, 695-9.

70. Jun, A.S., Chakravarti, S., Edelhauser, H.F., Kimos, M. (2006) Aging changes of mouse corneal endothelium and Descemet's membrane. *Exp Eye Res* 83, 890-6.

71. Jue, B., Maurice, D.M. (1986) The mechanical properties of the rabbit and human cornea. *J Biomech* 19, 847-53.

72. Worner, C.H., Olguin, A., Ruiz-Garcia, J.L., Garzon-Jimenez, N. (2011) Cell pattern in adult human corneal endothelium. *PLoS One* 6, e19483.

73. Maurice, D.M. (1972) The location of the fluid pump in the cornea. *J Physiol* 221, 43-54.

74. Marfurt, C.F., Cox, J., Deek, S., Dvorscak, L. (2010) Anatomy of the human corneal innervation. *Exp Eye Res* 90, 478-92.

75. Muller, L.J., Marfurt, C.F., Kruse, F., Tervo, T.M. (2003) Corneal nerves: structure, contents and function. *Exp Eye Res* 76, 521-42.

76. Gallar, J., Pozo, M.A., Tuckett, R.P., Belmonte, C. (1993) Response of sensory units with unmyelinated fibres to mechanical, thermal and chemical stimulation of the cat's cornea. *J Physiol* 468, 609-22.

77.   Belmonte, C., Acosta, M.C., Gallar, J. (2004) Neural basis of sensation in intact and injured corneas. *Exp Eye Res* 78, 513-25.

78.   Patel, D.V., McGhee, C.N. (2005) Mapping of the normal human corneal sub-Basal nerve plexus by in vivo laser scanning confocal microscopy. *Invest Ophthalmol Vis Sci* 46, 4485-8.

79.   Klyce, S.D., Beuerman, R.W., Crosson, C.E. (1985) Alteration of corneal epithelial ion transport by sympathectomy. *Invest Ophthalmol Vis Sci* 26, 434-42.

80.   Dohlman, C.H., Hedbys, B.O., Mishima, S. (1962) The swelling pressure of the corneal stroma. *Invest Ophthalmol* 1, 158-62.

81.   Meek, K.M., Leonard, D.W., Connon, C.J., Dennis, S., Khan, S. (2003) Transparency, swelling and scarring in the corneal stroma. *Eye (Lond)* 17, 927-36.

82.   Zieske, J.D., Guimaraes, S.R., Hutcheon, A.E. (2001) Kinetics of keratocyte proliferation in response to epithelial debridement. *Exp Eye Res* 72, 33-9.

83.   Fini, M.E. (1999) Keratocyte and fibroblast phenotypes in the repairing cornea. *Prog Retin Eye Res* 18, 529-51.

84.   Funderburgh, J.L., Mann, M.M., Funderburgh, M.L. (2003) Keratocyte phenotype mediates proteoglycan structure: a role for fibroblasts in corneal fibrosis. *J Biol Chem* 278, 45629-37.

85.   Gao, J., Gelber-Schwalb, T.A., Addeo, J.V., Stern, M.E. (1997) Apoptosis in the rabbit cornea after photorefractive keratectomy. *Cornea* 16, 200-8.

86.   Wilson, S.E., Kim, W.J. (1998) Keratocyte apoptosis: implications on corneal wound healing, tissue organization, and disease. *Invest Ophthalmol Vis Sci* 39, 220-6.

87. Wilson, S.E., Chaurasia, S.S., Medeiros, F.W. (2007) Apoptosis in the initiation, modulation and termination of the corneal wound healing response. *Exp Eye Res* 85, 305-11.

88. Zhao, J., Nagasaki, T. (2004) Mechanical damage to corneal stromal cells by epithelial scraping. *Cornea* 23, 497-502.

89. Zhao, J., Nagasaki, T., Maurice, D.M. (2001) Role of tears in keratocyte loss after epithelial removal in mouse cornea. *Invest Ophthalmol Vis Sci* 42, 1743-9.

90. Pal-Ghosh, S., Pajoohesh-Ganji, A., Tadvalkar, G., Stepp, M.A. (2011) Removal of the basement membrane enhances corneal wound healing. *Exp Eye Res* 93, 927-36.

91. Kao, W.W., Funderburgh, J.L., Xia, Y., Liu, C.Y., Conrad, G.W. (2006) Focus on molecules: lumican. *Exp Eye Res* 82, 3-4.

92. Vij, N., Roberts, L., Joyce, S., Chakravarti, S. (2005) Lumican regulates corneal inflammatory responses by modulating Fas-Fas ligand signaling. *Invest Ophthalmol Vis Sci* 46, 88-95.

93. Funderburgh, J.L., Mitschler, R.R., Funderburgh, M.L., Roth, M.R., Chapes, S.K., Conrad, G.W. (1997) Macrophage receptors for lumican. A corneal keratan sulfate proteoglycan. *Invest Ophthalmol Vis Sci* 38, 1159-67.

94. Carlson, E.C., Sun, Y., Auletta, J., Kao, W.W., Liu, C.Y., Perez, V.L., Pearlman, E. (2010) Regulation of corneal inflammation by neutrophil-dependent cleavage of keratan sulfate proteoglycans as a model for breakdown of the chemokine gradient. *J Leukoc Biol* 88, 517-22.

95. Ecoiffier, T., Yuen, D., Chen, L. (2009) Differential distribution of blood and lymphatic vessels in the murine cornea. *Invest Ophthalmol Vis Sci* 51, 2436-40.

96. Waterston, R.H., Lindblad-Toh, K., Birney, E., Rogers, J., Abril, J.F., Agarwal, P., Agarwala, R., Ainscough, R., Alexandersson, M., An, P., Antonarakis, S.E., Attwood, J., Baertsch, R., Bailey, J., Barlow, K., Beck, S., Berry, E., Birren, B., Bloom, T., Bork, P., Botcherby, M., Bray, N., Brent, M.R., Brown, D.G., Brown, S.D., Bult, C., Burton, J., Butler, J., Campbell, R.D., Carninci, P., Cawley, S., Chiaromonte, F., Chinwalla, A.T., Church, D.M., Clamp, M., Clee, C., Collins, F.S., Cook, L.L., Copley, R.R., Coulson, A., Couronne, O., Cuff, J., Curwen, V., Cutts, T., Daly, M., David, R., Davies, J., Delehaunty, K.D., Deri, J., Dermitzakis, E.T., Dewey, C., Dickens, N.J., Diekhans, M., Dodge, S., Dubchak, I., Dunn, D.M., Eddy, S.R., Elnitski, L., Emes, R.D., Eswara, P., Eyras, E., Felsenfeld, A., Fewell, G.A., Flicek, P., Foley, K., Frankel, W.N., Fulton, L.A., Fulton, R.S., Furey, T.S., Gage, D., Gibbs, R.A., Glusman, G., Gnerre, S., Goldman, N., Goodstadt, L., Grafham, D., Graves, T.A., Green, E.D., Gregory, S., Guigo, R., Guyer, M., Hardison, R.C., Haussler, D., Hayashizaki, Y., Hillier, L.W., Hinrichs, A., Hlavina, W., Holzer, T., Hsu, F., Hua, A., Hubbard, T., Hunt, A., Jackson, I., Jaffe, D.B., Johnson, L.S., Jones, M., Jones, T.A., Joy, A., Kamal, M., Karlsson, E.K., et al. (2002) Initial sequencing and comparative analysis of the mouse genome. *Nature* 420, 520-62.

97. Young, R.D., Akama, T.O., Liskova, P., Ebenezer, N.D., Allan, B., Kerr, B., Caterson, B., Fukuda, M.N., Quantock, A.J. (2007) Differential immunogold localisation of sulphated and unsulphated keratan sulphate proteoglycans in

normal and macular dystrophy cornea using sulphation motif-specific antibodies. *Histochem Cell Biol* 127, 115-20.

98.   Quantock, A.J., Meek, K.M., Brittain, P., Ridgway, A.E., Thonar, E.J. (1991) Alteration of the stromal architecture and depletion of keratan sulphate proteoglycans in oedematous human corneas: histological, immunochemical and X-ray diffraction evidence. *Tissue Cell* 23, 593-606.

99.   Saika, S., Liu, C.Y., Azhar, M., Sanford, L.P., Doetschman, T., Gendron, R.L., Kao, C.W., Kao, W.W. (2001) TGFbeta2 in corneal morphogenesis during mouse embryonic development. *Dev Biol* 240, 419-32.

100.   Tanifuji-Terai, N., Terai, K., Hayashi, Y., Chikama, T., Kao, W.W. (2006) Expression of keratin 12 and maturation of corneal epithelium during development and postnatal growth. *Invest Ophthalmol Vis Sci* 47, 545-51.

101.   Bard, J.B., Bansal, M.K., Ross, A.S. (1988) The extracellular matrix of the developing cornea: diversity, deposition and function. *Development* 103 Suppl, 195-205.

102.   Chakravarti, S., Petroll, W.M., Hassell, J.R., Jester, J.V., Lass, J.H., Paul, J., Birk, D.E. (2000) Corneal opacity in lumican-null mice: defects in collagen fibril structure and packing in the posterior stroma. *Invest Ophthalmol Vis Sci* 41, 3365-73.

103.   Zieske, J.D. (2004) Corneal development associated with eyelid opening. *Int J Dev Biol* 48, 903-11.

104.   Norman, B., Davis, J., Piatigorsky, J. (2004) Postnatal gene expression in the normal mouse cornea by SAGE. *Invest Ophthalmol Vis Sci* 45, 429-40.

105. Quantock, A.J., Meek, K.M., Chakravarti, S. (2001) An x-ray diffraction investigation of corneal structure in lumican-deficient mice. *Invest Ophthalmol Vis Sci* 42, 1750-6.

106. Stepp, M.A. (2006) Corneal integrins and their functions. *Exp Eye Res* 83, 3-15.

107. Hanlon, S.D., Patel, N.B., Burns, A.R. (2011) Assessment of postnatal corneal development in the C57BL/6 mouse using spectral domain optical coherence tomography and microwave-assisted histology. *Exp Eye Res* 93, 363-70.

108. Parapuram, S.K., Huh, K., Liu, S., Leask, A. (2011) Integrin beta1 is necessary for the maintenance of corneal structural integrity. *Invest Ophthalmol Vis Sci* 52, 7799-806.

109. Koenderman, L., van der Linden, J.A., Honing, H., Ulfman, L.H. (2010) Integrins on neutrophils are dispensable for migration into three-dimensional fibrin gels. *Thromb Haemost* 104, 599-608.

CHAPTER 2 – MATERIALS AND METHODS

2.1 Animals

As mentioned previously, the mouse model is commonly used for corneal research. There are some notable differences between mouse and human corneas however, the structural elements of the stroma and adhesion molecules expressed in the two species are quite similar. These similarities, in addition to the practical (breeding and handling) advantages, were the reasoning behind choosing the mouse for these experiments.

All animals used in these studies were C57BL/6 strain obtained from an established inbred colony bred and housed at the College of Optometry. Mice used for interstitial migration experiments were between the ages of 8-14 weeks. All animals were treated according to the guidelines described in the Association for Research in Vision and Ophthalmology Statement for the Use of Animals in Vision and Ophthalmic Research and University of Houston animal handling guidelines. Each animal was euthanized with CO_2 asphyxiation followed by cervical dislocation for those more than 2 weeks old, and by isoflurane overdose for younger mice.

2.2 Bench-processed histology

After observing initial obvious processing artifacts, several modifications to our protocol were investigated and the data presented were obtained with the method that consistently produced the best results. From our experience, removing corneas *in situ* could not be accomplished without altering the corneal shape even when the eyes were pre-fixed with topical application of glutaraldehyde fixative prior to removing the cornea. Therefore

whole right and left eyes were immediately harvested from euthanized male and female mice (n = 39) briefly fixed (10 minutes, RT) in 0.1M sodium cacodylate buffer (pH 7.2) containing 2.5% glutaraldehyde, the corneas were then removed and placed in the same fixative for another 2 hours Corneas were post fixed in 2% osmium tetroxide in 0.1M sodium cacodylate buffer, dehydrated in an increasing series of acetone (30, 50, 70, 90, 100, 100%; 15 minutes each), and embedded in Embed 812 resin (Electron Microscopy Sciences, Hatfield, PA). Transverse microscope sections (0.5 µm) through the center of the cornea were cut with an ultramicrotome (RMC, MT7000) and stained with Toluidine blue.

Initial light microscopic tissue processing produced stromal artifacts and subsequently the fixative solution was changed to 2.0% glutaraldehyde in 0.08M sodium cacodylate as recommended by Doughty, *et al*. (1997)[1]. However, the incidence and severity of artifacts and amount of swelling remained the same hence CCT data from both fixative solutions were combined for analysis.

Using a 20x objective (N.A. 0.75) a limbus-to-limbus digital montage was created (Sony Coolsnap camera) for each corneal transverse section using a DeltaVision Core deconvolution microscope system running SoftWorx software (Applied Precision, Isaquah, WA). A grid of three parallel lines spaced 50µm apart was over-laid on the montage at the geometric center and the total, epithelial, and stromal corneal thickness measured at each line with ImageJ software (NIH). The pixel to µm conversion factor was determined by measuring the full width of the image in µm using the SoftWorx software measuring tool and dividing the image size (1024 pixels) by this amount.

2.3 Ex vivo fixation effects

To evaluate conventional fixation-induced artifacts (shrinkage, swelling and general distortion) eyes complete with extraocular muscles were removed from euthanized mice (n=9, >8 weeks of age) and a plastic clip was attached to the extraocular tissue. This allowed the eye to be held without any force being applied to the globe (Figure 22). The suspended eyes were then immersed in fixative in a plastic chamber with a glass coverslip observation window glued in-place to optimize scanning. The chamber was then placed in front of the Visante (Carl Zeiss Meditec, Dublin, CA) OCT such that the axis of the OCT was perpendicular to the iris plane and centered on the pupil. Scans were obtained every 5 minutes up to 60 minutes of total time in fixative. Three different fixatives were used in an attempt to determine the optimum solution as well as varying the fixation time and tissue harvesting methods. Over one hundred eyes were sampled during the course of this investigation.
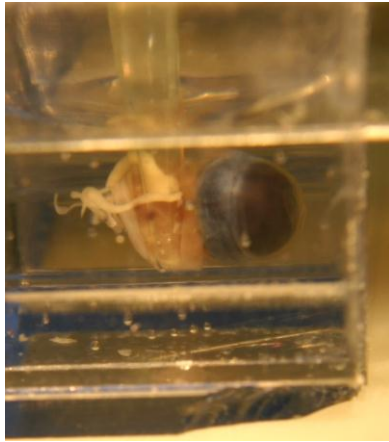
Figure 22 – Ex vivo eye holder

Whole eyes were removed and held by their muscle cone in a fluid-filled chamber for

Visante OCT imaging.

2.4 SD-OCT imaging and CCT

To achieve the highest resolution and thus a more accurate CCT measurement, the Spectralis (Heidelberg Engineering, Dossenheim, Germany) Spectral Domain Optical Coherence Tomography (SD-OCT) instrument was used for *in vivo* and *in situ* measurements. It is designed for retinal imaging and therefore required optical modification for corneal scanning. To achieve focus on the cornea, a 30 diopter aspheric lens was attached to the front of the instrument (Figure 23). The optimum focal power and reference arm setting for image acquisition were determined and the same settings were used for all subsequent scans. The accuracy of the SD-OCT axial thickness determination was assessed using two approaches. In the first, a number 1.5 microscope glass coverslip was imaged by SD-OCT and the thickness was compared to that obtained using digital calipers (accuracy of 0.01mm) and that obtained by through-focus imaging on an Olympus IX70 inverted microscope equipped with a 40x objective lens (N.A. 1.4). In a similar manner, miniature polymethyl-methacrylate (PMMA) contact lenses of 1.4mm radius of curvature were scanned for center thickness with the SD-OCT and compared with the thickness estimate provided by through-focus imaging on an IX70 Olympus inverted microscope. In each case, for the SD-OCT, appropriate compensation was made for the difference in index of refraction between glass, PMMA, and mouse cornea (1.523, 1.495 and 1.4015, respectively).

For SD-OCT corneal imaging, euthanized male and female mice (n=36) were immediately secured in a 50ml plastic tube (VWR Lab Shop, Batavia, IL) with a cutout for the nose and mouth as well as openings for the eyes (Figure 24). Very young mice were attached to a wooden tongue depressor for support. The corneas were scanned in a

series producing a sequence of horizontal cross-sectional views encompassing the entire cornea. Additionally, a series of radial scans was performed covering 360 degrees. When imaging neonates prior to lid opening ($\leq$ 14 days), the animals were euthanized and lids were carefully removed before scanning. Eyes were kept moist by occasional misting with ophthalmic irrigating solution (OCuSOFT, Inc., Rosenberg, TX). Mice greater than 4 weeks of age (n = 15) were anesthetized with ketamine/xylazine intraperitoneal injection (100/10 mg/kg) and scanned with SD-OCT in the same manner as the euthanized animals. The same animals were subsequently sacrificed, fixed and processed for histological sectioning.

Three scans were taken for each eye and the CCT was measured at the geometric center of the corneal cross sections. Each cross section measured was obtained by selecting the scan which passed through the center of the pupil and with the iris plane perpendicular to the scanning beam. Three measurements were made for each scan, one at the center and one 50 μm on either side of center. ImageJ software was used to create a "profile plot" (linear plot of image reflectivity). Peaks on the profile representing the anterior and posterior corneal surfaces were selected for measurements. The measurements were obtained in pixels and the appropriate pixel to μm conversion factor was applied.
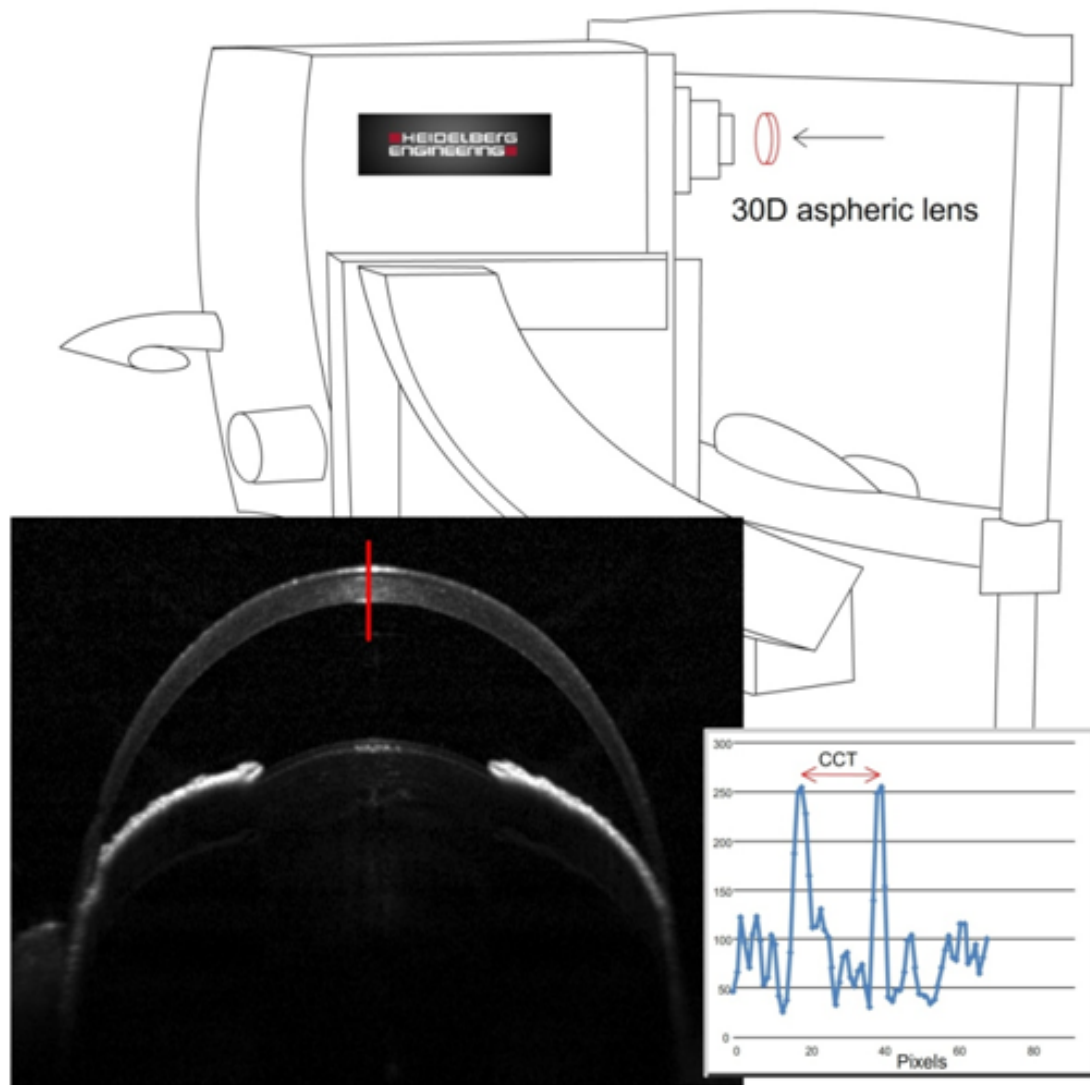
Figure 23 – Cornea imaging with SD-OCT

The background line drawing shows the Spectralis SD-OCT with the addition of a 30D

aspheric lens to allow focus on the cornea. The image in the lower left is a representative

mouse cornea with the red line indicating the location where the central corneal thickness

was measured. Thickness was determined from the distance between peaks in the profile

plot shown in the lower right.
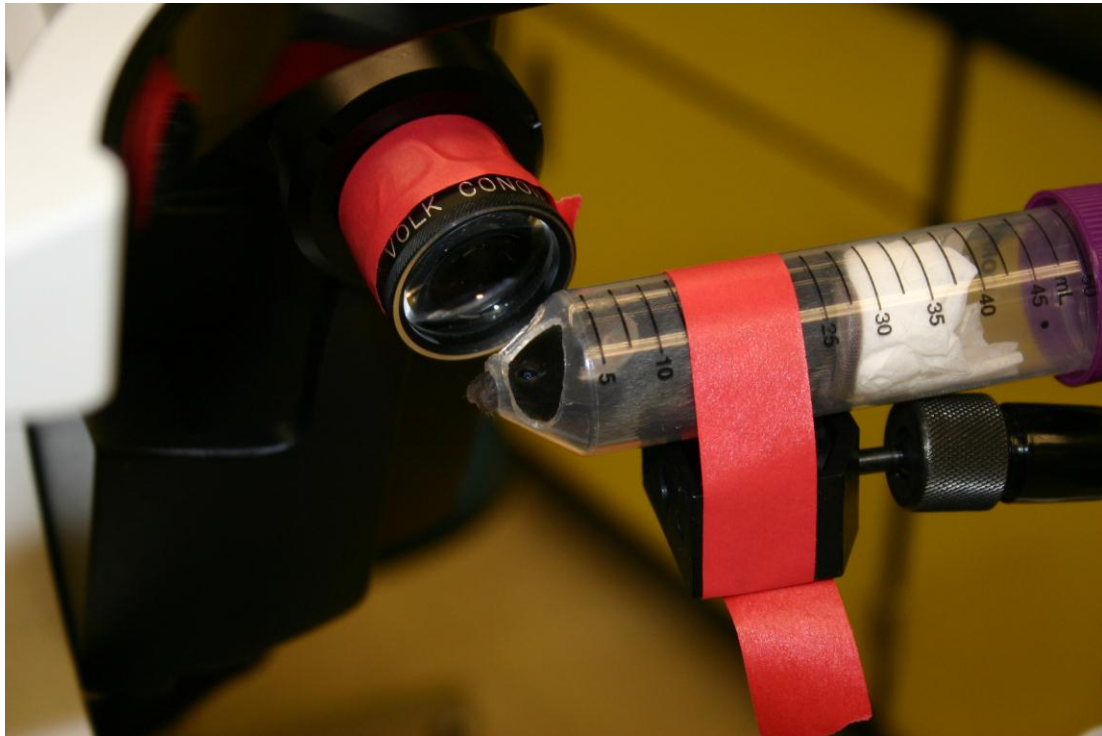
Figure 24 – SD-OCT imaging apparatus

The 30D aspheric lens is shown taped to the front of the SD-OCT and the anesthetized

mouse is held in the plastic tube.

2.5 Microwave-processed histology

In an attempt to improve the fixation conditions and avoid distortion artifacts, eyes from mice (n = 24) at various ages were processed using a vacuum-assisted PELCO Biomicrowave (Ted Pella, Inc., Redding, CA) (Figure 25). Even though whole eyes could be processed using the recommended protocol from the microwave manufacturer without gross morphological distortion and minimal interlamellar separations, there was microscopic evidence of inadequate fixation. Subsequently, modifications to the protocol were investigated to optimize the protocol used in this study. Whole eyes were removed from euthanized mice, placed in fixative (2.5% glutaraldehyde in 0.1M sodium cacodylate buffer, pH 7.2), and immediately processed in the microwave under vacuum, as follows: The eyes received microwave radiation for 1 minute on-1 minute off-1 minute on, at 150 watts. The whole eyes were then removed from the microwave, placed on a bed of paraffin, and the cornea removed by a single cut with a thin double-edged razor blade. The cornea was placed back in fixative and the 3 minute microwave fixation cycle was repeated. The remainder of the protocol was as recommended by the microwave manufacturer which included the same post-fixation processes as with conventional fixation only performed with the microwave (Table 5). With microwave processing, the eyes were only exposed to glutaraldehyde fixative solution for 8-10 minutes and the entire fixation process up to resin polymerization was completed in approximately 75 minutes as compared to 72 hours, or more, in conventional processing. CCT values of microwave fixed samples were obtained in the same fashion as with conventional histology specimens.

Figure 25 – The biomicrowave apparatus

The plastic container in the microwave holds the tissue being processed and is air tight to provide a vacuum as indicated in the protocol. Beneath the plastic container is a heat-sink water container to prevent heating of the tissue.

Table 5 – Microwave processing protocol

Step	Description	Time	Watts	Vacuum
1	Glutaraldehyde ON (2.5% /0.1M NaCac)	1:00	150	ON
2	Glutaraldehyde OFF	1:00	0	ON
3	Glutaraldehyde ON	1:00	150	ON
4	Remove posterior shell			
5	Glutaraldehyde ON (2.5% /0.1M)	1:00	150	ON
6	Glutaraldehyde OFF	1:00	0	ON
7	Glutaraldehyde ON	1:00	150	ON
8	Buffer Rinse	0:40	150	Off
9	Buffer Rinse	0:40	150	Off
10	Osmium ON (1% /0.1M)	2:00	100	ON
11	Osmium OFF	2:00	0	ON
12	Osmium ON	2:00	100	ON
13	Osmium OFF	2:00	0	ON
14	Osmium ON	2:00	100	ON
15	Nanopure Water Rinse	0:40	150	Off
16	Cut corneas in half			
17	Dehydration 50% Acetone	0:40	150	Off
18	Dehydration 70% Acetone	0:40	150	Off
19	Dehydration 90% Acetone	0:40	150	Off
20	Dehydration 100% Acetone	0:40	150	Off
21	Dehydration 100% Acetone	0:40	150	Off
22	Dehydration 100% Acetone	0:40	150	Off
23	Resin Infiltration 1- 1:1 Acetone:Resin	3:00	350	ON
24	Resin Infiltration 2- 100% Resin	3:00	350	ON
25	Resin Infilitration 3- 100% Resin	3:00	350	ON

Ultrastructural morphology

Representative tissue blocks from adult mice (8-12 weeks) prepared using conventional processing and ones prepared using microwave processing were sectioned transversely with an ultramicrotome (RMC, MT 7000) at a thickness of 80-100nm and stained with uranyl acetate and lead citrate. Images were obtained using an FEI Tecnai 12 transmission electron microscope equipped with an Ultrascan 1000 digital camera. Collagen fibril diameter and interfibril spacing were measured as previously described [2]. Briefly, using cross-sectional views, individual fibril diameters were measured and the center to center distances measured to the surrounding 6-7 fibrils (Figure 26). Images were captured at 49,000x magnification and measured using ImageJ.
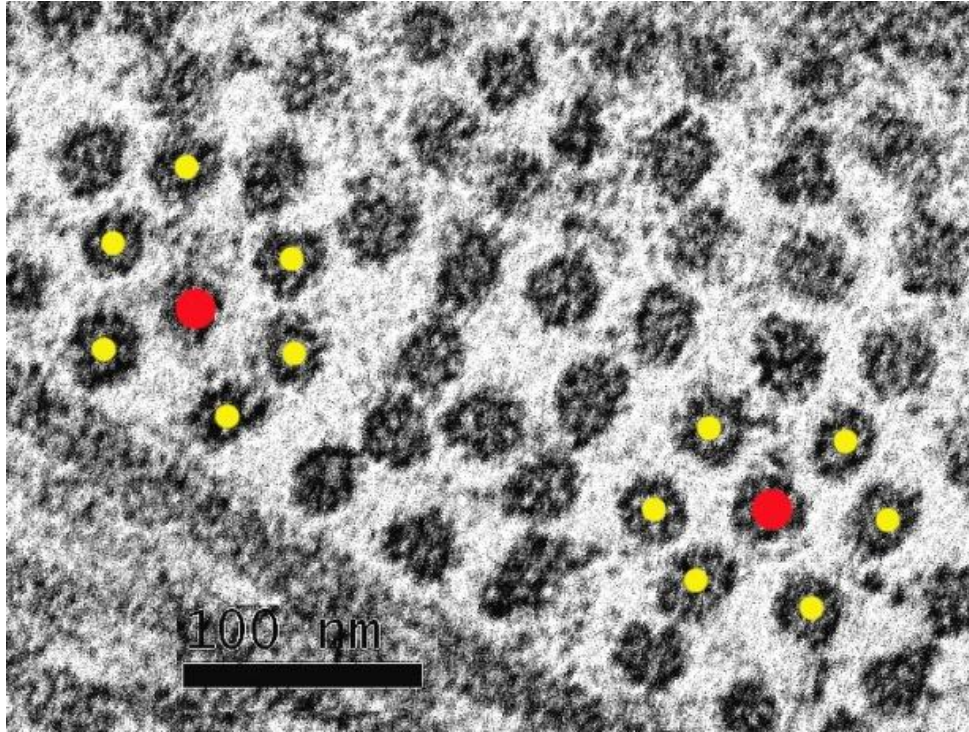
Figure 26 – Collagen fibril spacing

Collagen fibrils arranged in a pseudo-hexagonal pattern with central fibril. The Bragg

distance is the distance between fibril centers measured between central red and each

of the surrounding yellow fibrils

2.6 Wounding

Animals were anesthetized between 0730 and 0830 hours with an intraperitoneal (IP) injection of ketamine (75mg/kg body weight) and xylazine (7.5mg/kg body weight). Each cornea was inspected, using a dissecting microscope, for signs of pre-existing corneal abrasion or infection and excluded if present. With the aid of a stereo dissecting microscope the eyelashes were trimmed to prevent their interfering with imaging. The corneal epithelium was removed in a single vertical stripe approximately 0.5mm wide and extending to within 0.5mm of the inferior and superior limbus using an Algerbrush with 0.5mm burr (Alger Equipment Co., Inc., Lago Vista, TX)
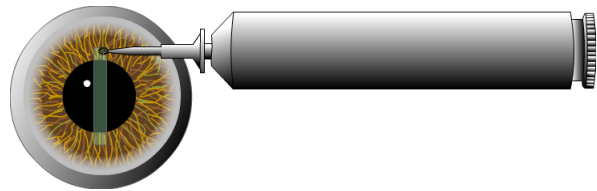
Figure 27 – Alger brush wounding

held tangent to the corneal surface. The wound was initiated in the upper cornea (superior or inferior, depending on the orientation of the mouse) moving toward the lower limbus. The mouse was then rotated 180° and the Algerbrush again applied moving from upper to lower cornea. This method provided the most consistent results, well defined vertical edges, and minimal effect on the basement membrane as shown later. The vertical stripe was used rather than a central circular wound in order to provide ample parawound area for imaging yet produce a wound roughly the size of a 1.5mm circular wound with a similar degree of inflammatory reaction. The parawound was selected as our region of interest for analysis of neutrophil migration where the keratocytes and ECM are minimally disturbed and therefore allow neutrophil interaction in a relatively normal physical environment. Mice were kept on an isothermal heating pad while under

anesthesia and then placed in an isolation cage for the duration of the 8 hours before

imaging to minimize the possibility of additional corneal injury.

2.7 HRT in vivo confocal microscopy

In vivo leukocyte cell motility was recorded after 8 hours using the HRT-RCM. At that

time each mouse was anesthetized with IP ketamine (100mg/kg body weight) and

xylazine (10mg/kg body weight) and placed in a heated holding device consisting of a

50ml centrifuge tube (VWR Lab Shop, Batavia, IL) with the bottom cut out to allow the

mouse head to protrude for imaging, The tube was wrapped with a rheostat-controlled

heating cable and insulating foam (Figure 28). Body temperature was monitored by rectal

probe and maintained between 36.5 and 37.0^{o}C (Microtherma 2, ETI Ltd. UK). As we

observed in previous experiments, and as others have reported [3], cell speed is heavily

dependent on body temperature below this range. Corneal temperature was initially

measured before and after imaging using an infrared thermistor (Vario-Therm 6000L,

Everest Interscience, Inc., Tucson AZ) and found to be nearly constant (33-34°C) as long

as the body temperature was maintained within the indicated range.

   The 8 hour time point was selected for imaging as it is before the peak influx of

neutrophils [4], when they are making their way toward the wound. At this time there is

minimal congestion of cell traffic that might affect individual cell speed but late enough

that at least 12 cells would be typically observed in a single plane within the 400x400µm

image frame.
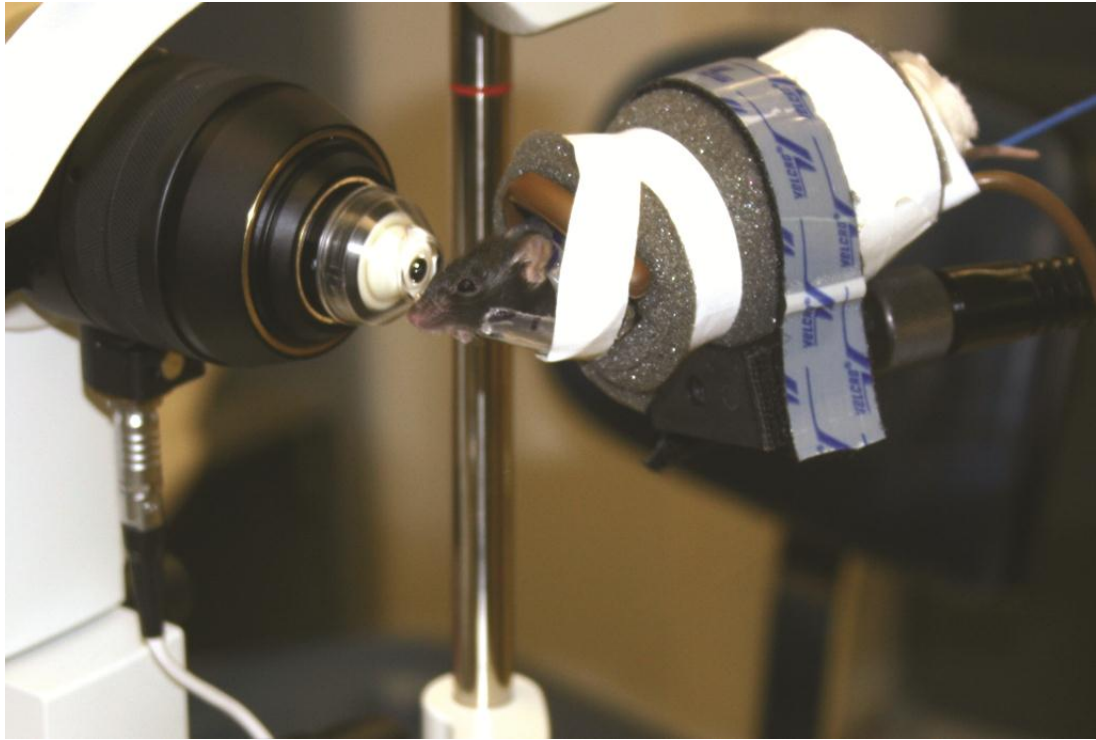
Figure 28 – HRT imaging apparatus

The Heidelberg Retinal Tomographer III (HRT) is shown on the left with the Rostock

Cornea Module (RCM). The mouse being imaged is held in the tube on the right. A

heating cable (brown wire) is connected to a rheostat and a blue wire connects the rectal

probe to the temperature display. The insulated holding tube is supported by a gooseneck

clamp attached to an I.V. stand.

Eyes were applanated and scanned using the Heidelberg Retinal Tomographer III with Rostock Corneal Module (HRT-RCM) (400umx400um resolution). The mouse holding tube was attached to a gooseneck clamp and was positioned such that the cap of the HRT-RCM objective was parallel to the mouse facial plane (Figure 28). The cornea was applanated with enough force to maintain a stable image. During protocol development it was shown that even maximum force had no effect on cell speed. Six 100-second scan sequences at 1 frame per second (the slowest capture rate on the instrument) were obtained in the nasal or temporal parawound area. Depth of the scans was 10-20 μm beneath the basement membrane where the keratocyte network was clearly visible but still within the anterior stroma where the vast majority of neutrophils are found, even though motility parameters were found not to vary significantly for various depths within the cornea. For comparing neutrophil motility parameters beneath the wound as compared to the parawound area, 10 minute sequences were obtained in each of the two areas. For assessing the effects of antibody blocking only the parawound area was imaged. In each case the parawound area selected was at least 100μm from the edge of the wound to assure viable keratocytes were present. Areas selected for scanning had at least 12 inflammatory cells (neutrophils). After the sequence scans were completed, volume scans of the same location were obtained in order to determine the stromal thickness. Immediately after scanning the animals were sacrificed by CO_2 asphyxiation and cervical dislocation. Harvested corneas were then processed for immunohistochemistry and prepared as corneal whole-mounts or microwave processed for light microscopy and/or transmission electron microscopy.

For neutrophil motility assessment every attempt was made to eliminate or at least standardize any confounding variables. Table 6 summarizes the methods to control potential confounding variables. The inter-cornea coefficient of variation was slightly less than intra-cornea (between cells), thus suggesting that uncontrolled variables were not influencing our results.

Table 6 – Controlling motility variables

Variable	Control
Age of mouse	8 to 14 weeks for all experiments
Gender	female, non-pregnant
Temperature	body temperature monitored and regulated
Time of day	wound was done between 0730 and 0830
Time after	cell tracking was done 8 hours after wounding
Applanation force	moderate applanation force
Depth of scan	10 to 20 μm beneath epithelium
Nature of wound	same shape, size, and method by same person

2.8 Application of blocking antibodies

In order to assess the effect of functionally blocking CD18 , CD29, or CD61, at the time of wounding 5µl of blocking antibody (GAME-46 anti-CD18, BD Pharmingen; HMβ1-1 anti-CD29, BioLegend; HMβ3-1 anti-CD61, BioLegend), non-immune IgG antibody (25µg/ml diluted in normal saline), or normal saline alone, was applied topically to the wounded cornea and allowed to penetrate for 5 minutes. The excess solution was then wicked off the cornea along with any cellular debris and a second application of the antibody/saline was applied and allowed to penetrate until the animal recovered from anesthesia (typically 10-15 minutes without blinking). Left undisturbed, the droplet of solution could still be seen after 15 minutes and covered the entire cornea. In some experiments a cocktail of the three blocking antibodies (25µg/ml of each in normal saline) was applied.

2.9 Immunohistochemistry

Diffusion of the blocking antibodies was confirmed by indirect immunolabeling using the appropriate conjugated secondary antibody. Immediately after mice were sacrificed whole eyes were removed and placed in 2% paraformaldehyde fixative for 10 minutes at room temperature. At that time the posterior sclera shell and crystalline lens were removed from each eye and remaining cornea with sclera rim returned to fixative for another 50 minutes. Corneas were then thoroughly rinsed with PBS and placed in blocking buffer (2%BSA+ 10% mouse serum) with Fc block, overnight at 4°C. Next they were transferred to permeabilizing solution containing 0.1% Triton-X for 30 minutes at 4°C after which they were transferred to permeabilizing solution containing the

fluorophore-conjugated secondary antibody with DAPI and left over night in the dark at 4°C. The whole corneas were then rinsed in PBS and whole-mounted on microscope slides using ProLong Gold mounting medium (Invitrogen, Grand Island NY). Labeling of neutrophils was accomplished in a similar manner using a primary conjugated Ly-6G antibody.

2.10 Image processing

To assess inflammatory cell motility, the six image sequences were combined into a single 10 minute sequence and post-stabilized using a custom MatLab (MathWorks, Natick MA) program. Cell tracking was accomplished using a second custom MatLab program which semi-automatically tracked 12 randomly selected cells from each stabilized movie sequence. Since automatic cell trackers frequently need manual corrections, we chose to manually mark the cell location by selecting the centroid of the cells' visible area. Cells that were non-motile (displaced < 10 µm in 10 minutes) were not included. Likewise, ones that were so close to the edge that they moved out of view during the image sequence were not included. Twelve was the typical minimum number of cells per imaging field although on rare occasions 12 cells were not visible (the fewest was 10 cells). The X,Y coordinates for the centroid of each cell was marked every 20 frames (seconds) and the distance and direction of movement calculated for each time interval.

2.11 Motility parameters and cell tracking

Several motility parameters (Table 7) were considered in analyzing our data. Cell speed (CS) is a commonly reported parameter regarding cell motility [5] and is simply determined by dividing the total distance a cell traveled by the amount of time that it took to travel that distance. It is therefore an average speed and does not show bursts of speed or periods of relative inactivity. Cell velocity (CV), on the other hand, is the straight-line displacement of a cell from the initial location to the final location divided by the measured time period. Unless a cell travels in a straight-line the velocity will always be less than the speed, likewise velocity divided by speed will be between 0 -1 and gives an indication of how straight a cell moves. This value has been given several names including directionality [6-8], chemotactic index [9], McCutcheon index [10], and confinement ratio [5, 11]. We have chosen to use the term confinement ratio (CR) since chemotaxis would be an assumption that a chemoattractant gradient existed and directionality may be confusing when describing direction of migration for a group of cells. These parameters for single cell analysis were used to describe motility for an "average" cell. However when studying effects on cell migration it is also desirable to consider parameters describing the population of cells. One such parameter, commonly reported, is mean displacement (MD) which refers to the mean displacement for all cells tracked at each time interval. The mean displacement plot (MDP) displays the mean displacement vs. square root of the elapsed time and its shape is characteristic for directed, random walk, or confined motility, for long tracking times. However MDP cannot distinguish between migration affected by multiple local attractors and a true

random walk [5]. For a tracking time of only 10 minutes as in our experiments, the MDP is essentially linear and its slope is defined as the motility coefficient (MC)[3, 5, 12, 13].

The population migration velocity (MV) and migration angle (direction of migration) (MA) parameters take into consideration the direction that cells move when computing the average, whereas the average of individual cell CV's does not. For example, two cells moving in opposite directions at the same velocity would have a net result of zero MV. MV is calculated by determining the resultant vector using the average total x displacement (+ or -) and average total y displacement (+ or -) for the group of cells. This describes the velocity and direction a group of 12 cells is moving which we then compared to the location of the wound for describing a tactic response. Dividing MV by the average of individual cell CV's defines the Tactic Index (TI) where a value of 1.00 indicates that all cells moved in the same direction. MA for each cornea cell group was compared to the direction of the wound from the cell. The group movement was considered toward the wound if the MA was within $\pm 75^{o}$ of horizontal, parallel if within $\pm 15^{o}$ of the vertical and away from the wound if $>105^{o}$ or $< -105^{o}$.

Table 7 – Parameters assessed

Cell Speed (CS)

$$\frac{\sum_{i=1}^{n-1} \sqrt{(x_{i+1} - x_i)^2 + (y_{i+1} - y_i)^2}}{time}$$

The total distance traveled divided by the elapsed time.

Cell Velocity (CV)

$$\frac{\sqrt{(x_n - x_1)^2 + (y_n - y_1)^2}}{time}$$

The displacement from origin divided by the elapsed time.

Confinement Ratio (CR)

$$\frac{CV}{CS}$$

The ratio of cell velocity to cell speed. Gives an indication the straightness of a cell path. Values between 0 and 1.

Mean Displacement (MD)

$$\sqrt{\langle|\Delta x(t)|\rangle^2 + \langle|\Delta y(t)|\rangle^2}$$

The mean total displacement from the origin determined by the mean x-axis displacement and y-axis displacement for the time interval.

Motility Coefficient (MC)

$$\frac{\Delta MD}{\Delta \sqrt{t}}$$

The slope of mean displacement plotted against square root of elapsed time. Is a function of cell speed as well as the straightness of the path.

Migration Velocity (MV)

$$\frac{\sqrt{\langle\Delta x\rangle^2 + \langle\Delta y\rangle^2}}{time}$$

For a group of cells the total displacement is determined using the mean x-axis displacement and y-axis displacement for the entire time. The result is divided by time.

Migration Angle (MA)

$$arctan2(\langle\Delta y\rangle, \langle\Delta x\rangle)$$

For a group of cells the mean x-axis displacement and y-axis displacement define the resultant vector where MA is the polar angle of the vector.

Tactic Index (TI)

$$\frac{MV}{\langle CV \rangle}$$

The migration velocity divided by the mean cell velocity. If all cells were traveling in the same direction TI would equal 1.

2.12 Inter/Intra-observer comparison

Five representative movies were analyzed by two independent observers and their summary data were compared for tracking of 12 cells. In the first instance the second observer used the identical same set of cells as the first observer and in the second instance each observer chose the set of cells randomly. Additionally, summary data were compared from the same eyes which were analyzed twice by the same observer.

2.13 Statistical analysis

Statistical analyses were made using Student's t-test for two groups and ANOVA with Tukey post-test for multiple comparisons were used for comparisons among three groups in comparing the corneal thicknesses. For motility parameter comparisons ANOVA followed by Bonferroni post-hoc correction were used. In each case a p value of < 0.05 was considered significant. Developmental growth curves were generated using the exponential rise to maximum equation. All data are shown as mean $\pm$ SEM.

Chapter 2 References

1.   Doughty, M.J., Bergmanson, J.P., Blocker, Y. (1997) Shrinkage and distortion of
        the rabbit corneal endothelial cell mosaic caused by a high osmolality
        glutaraldehyde-formaldehyde fixative compared to glutaraldehyde. *Tissue Cell*
        29, 533-47.

2.   Petrescu, M.S., Larry, C.L., Bowden, R.A., Williams, G.W., Gagen, D., Li, Z.,
        Smith, C.W., Burns, A.R. (2007) Neutrophil interactions with keratocytes during
        corneal epithelial wound healing: a role for CD18 integrins. *Invest Ophthalmol
        Vis Sci* **48**, 5023-9.

3.   Miller, M.J., Wei, S.H., Parker, I., Cahalan, M.D. (2002) Two-photon imaging of
        lymphocyte motility and antigen response in intact lymph node. *Science* **296**,
        1869-73.

4.   Li, Z., Burns, A.R., Smith, C.W. (2006) Two waves of neutrophil emigration in
        response to corneal epithelial abrasion: distinct adhesion molecule requirements.
        Invest Ophthalmol Vis Sci **47**, 1947-55.

5.   Beltman, J.B., Maree, A.F., de Boer, R.J. (2009) Analysing immune cell
        migration. *Nat Rev Immunol* **9**, 789-98.

6.   Khandoga, A.G., Khandoga, A., Reichel, C.A., Bihari, P., Rehberg, M.,
        Krombach, F. (2009) In vivo imaging and quantitative analysis of leukocyte
        directional migration and polarization in inflamed tissue. *PLoS One* **4**, e4693.

7.   Petrie, R.J., Doyle, A.D., Yamada, K.M. (2009) Random versus directionally
        persistent cell migration. *Nat Rev Mol Cell Biol* **10**, 538-49.

8.   Koenderman, L., van der Linden, J.A., Honing, H., Ulfman, L.H. (2010) Integrins on neutrophils are dispensable for migration into three-dimensional fibrin gels. *Thromb Haemost* **104**, 599-608.

9.   Heit, B., Colarusso, P., Kubes, P. (2005) Fundamentally different roles for LFA-1, Mac-1 and alpha4-integrin in neutrophil chemotaxis. *J Cell Sci* **118**, 5205-20.

10.   Bultmann, B.D., Gruler, H. (1983) Analysis of the directed and nondirected movement of human granulocytes: influence of temperature and ECHO 9 virus on N-formylmethionylleucylphenylalanine-induced chemokinesis and chemotaxis. *J Cell Biol* **96**, 1708-16.

11.   Hugues, S., Fetler, L., Bonifaz, L., Helft, J., Amblard, F., Amigorena, S. (2004) Distinct T cell dynamics in lymph nodes during the induction of tolerance and immunity. *Nat Immunol* **5**, 1235-42.

12.   Sumen, C., Mempel, T.R., Mazo, I.B., von Andrian, U.H. (2004) Intravital microscopy: visualizing immunity in context. *Immunity* **21**, 315-29.

13.   Gail, M.H., Boone, C.W. (1970) The locomotion of mouse fibroblasts in tissue culture. *Biophys J* **10**, 980-93.

CHAPTER 3 – RESULTS

3.1 – Age of Stromal Maturation

3.1.1 Introduction

It has been accepted as a matter of course that histological specimens of the cornea will many times include separations between the stromal lamellae. Many research articles and text books include figures displaying the cornea with many significant separations between lamellae. In some cases these (presumed) artifacts may not affect the study. However, when determining stromal or total corneal thickness these separations cannot be ignored and may explain why there is such a wide range of values reported for normal corneal thickness of mice (Figure 29). In addition, when investigators are looking at interactions between stromal cells and surrounding collagen, the separations may obscure the actual physical juxtapositions. So it seems to be a reasonable and necessary objective to propose a method of tissue fixation that will minimize lamellar separation within the corneal stroma and to show that these separations are indeed artifacts and not present *in vivo*. In this way stromal thickness can be determined separate from the total corneal thickness. As pointed out in a previous chapter, there are substantial changes taking place during the postnatal period [1-7]. Subsequent *in vivo* experiments require some indication, such as stromal thickness, that maturational changes are minimal.

Wild type C57BL/6 mice are widely used to study normal corneal structure [8], while mutant C57BL/6 mice with targeted deletions in cell adhesion molecules [9] , chemokines [10] and proteoglycans [11-14] have contributed much to our understanding of how the cornea responds to injury and infection. Despite their widespread use in corneal research,

there is a surprising lack of information regarding postnatal corneal development and apparently no consensus as to when the cornea is fully developed in the C57BL/6 mouse.

A biometric parameter commonly reported in the literature is the central corneal thickness (CCT) which may be used to evaluate normal corneal development and to diagnose a variety of ocular/corneal pathologies [15-20] as well as pre- and post-surgical conditions [21]. It is also a consideration in contact lens fitting and continuing care for contact lens wearers [22, 23]. The CCT in humans has been measured using several *in vivo* modalities including, optical pachymetry, ultrasound pachymetry, specular microscopy, confocal microscopy, and optical low-coherence interferometry. Measuring the corneal thickness in a mouse, which is roughly one-fifth the thickness and diameter of the human cornea, presents a challenge and many of the human measurement techniques are not applicable to the mouse. Since the CCT is one consideration in determining the maturation level of the cornea, accurate measurement of corneal thickness is desirable.

In the past, histology was the only method for determining murine corneal thickness, and is still a frequently reported method although it produces a large range of CCT values even for the same age, sex and mouse strain. Published biometric data show a wide-range of values for corneal thickness (Figure 30). Recently, for example, one study reported a mean CCT for C57BL/6 adult mice as 74.7±8.6 μm [24] and another reported 137.0±14.0 μm [25]. Both were measurements from histological sections. Histological artifacts including shrinking, swelling and distortion, which occur frequently, undoubtedly affect the native thickness of the cornea.
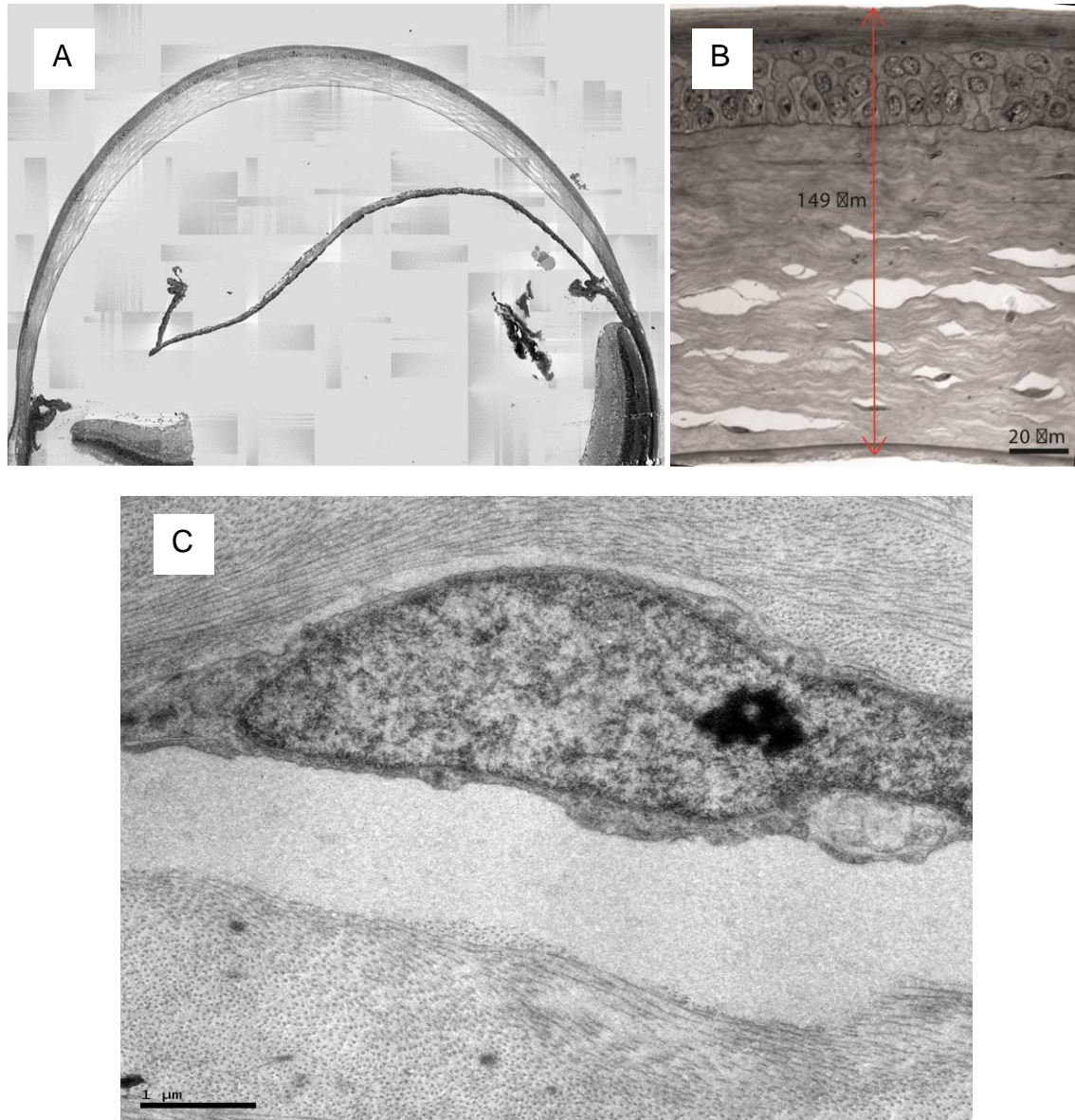
Figure 29 – Examples of lamellar separations

Montage of the entire cornea cross-section (A) and a close up of the central cornea (B) as

seen with DeltaVision bright field microscopy shows extensive separations between

lamellae (*), predominantly in the central and posterior stroma. Transmission electron

microscopy (C) shows details of separation between a keratocyte and the collagen (*).
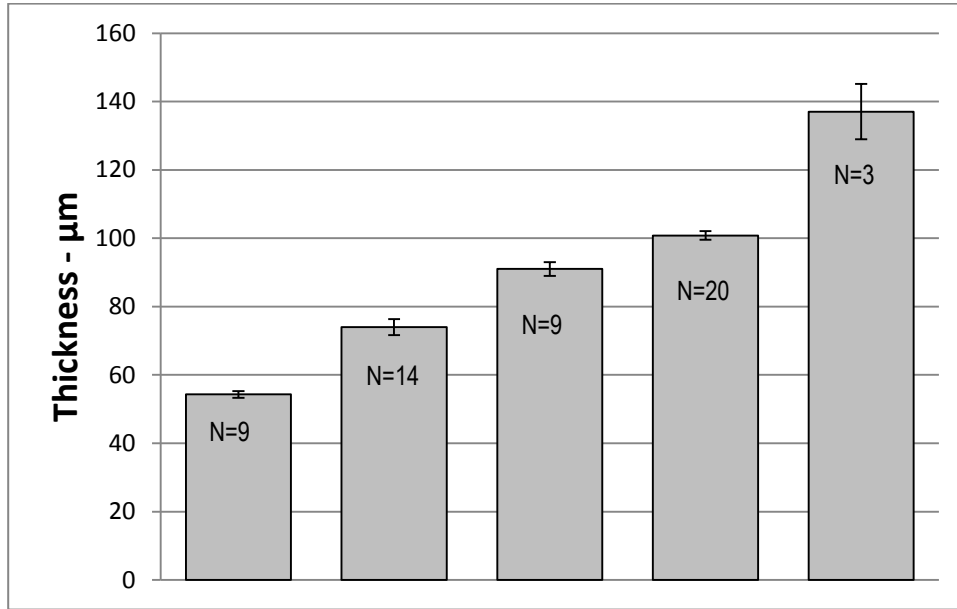
1 – Lluch[8]; 2 – Haddadin[9]; 3 – Schmucker[12];
4 – Lively[13]; 5 – Henriksson[14]

Figure 30 – Various CCT values reported

Central corneal thickness values reported in the literature are quite variable even within

the same adult mouse strain (C57BL/6).

Not only is there a large variability in adult CCT values reported, but there is also apparently no published data on the CCT of C57BL/6 mice beginning from birth. One study reports the CCT for CD1 mice from birth to 12 weeks [1] and measurements were made using confocal microscopy through-focus. Schmucker and Schaeffel [26] reported early corneal thickness changes for C57BL/6 mice from P25-P53 using frozen sections and optical low coherence interferometry and Zhou and colleagues [27] measured corneas using a custom built optical coherence tomography instrument (from mice age P22 -P102).

Clearly, there is a need to develop a simple method for accurately measuring the CCT in the mouse as a means of monitoring postnatal development of the mouse cornea through to adulthood. This information would accomplish several goals. First, it would define the growth kinetics of the cornea and define the age at which the cornea reaches its adult thickness. Second, it would provide a baseline with which to determine if artifacts (shrinkage, swelling) exist in corneas prepared for histological analysis. Finally, if routinely-fixed histological artifacts are detected, it should be possible to modify the fixation protocol to yield artifact-free corneal tissue sections that preserve the true biometric dimensions of the mouse cornea and preserve ultrastructural details.

The purpose of this study was to evaluate postnatal corneal growth and development in C57BL/6 mice by obtaining accurate CCT values. Using spectral domain optical coherence tomography (SD-OCT), we show CCT data can be obtained and used to monitor postnatal corneal development. Moreover, the CCT information is a useful benchmark for evaluating corneal histology and correcting histological artifacts.

The purpose of fixation of biological specimens is to permanently preserve the structural/anatomical integrity of the specimen in a way that is as close as possible to *in vivo* conditions and which prevents autolysis or degradation over time. There have been many proposed optimal chemical fixatives but there does not appear to be any consensus, largely due to the fact that each tissue responds to fixatives differently. As many authors have pointed out, histology specimens are subjected to harsh fixative and preparatory procedures which potentially have a significant effect. Many of the artifacts that occur during fixation are caused by physical contraction and compression as a result of the changes in osmolarity that occur during fixation or subsequent processing [28]. In studies reporting corneal thickness, various methods for histological specimen preparation have been described and they produce somewhat different results. As one looks at the biometric data published, it is noted that there is a wide-range of values, especially for corneal thickness which is most likely due to differences in tissue processing.

In the research conducted in support of this dissertation optimum tissue fixation was important for the following reasons: 1) establishing the age at which the stroma has reached mature thickness; 2) providing evidence for structural changes beneath the wound areas that might alter migration speed; 3) providing clues for structural changes induced by integrin-blocking antibodies.

3.1.2 Results

Accuracy of SD-OCT measurements

Accuracy of thickness measurements obtained by the optically modified Spectralis SD-OCT instrument was first assessed by measuring a flat glass coverslip whose thickness

was determined using digital calipers (170±0μm) and microscopic through focus

(174±4μm). Employing the default μm/pixel used by Spectralis software for thickness

measurements and after the adjustment for index of refraction (1.523 compared to 1.4015

for the mouse cornea), the SD-OCT measurements of the glass coverslip (176±2 μm)

were not significantly different from those obtained by digital calipers or through-focus.

Secondly, in order to assess the effect of curvature, a PMMA contact lens with a radius of

curvature similar to a mouse cornea (1.4mm) was measured. The contact lens thickness

measured 272±3 μm with through-focus imaging on the Olympus IX70 and 270±0 μm

with SD-OCT (Table 8). The shape of the cornea is somewhat distorted with Spectralis

(increased convexity) as it is designed to image the concave retina and not the convex

surface of the cornea (Figure 31). The glass cover slip image produced a curved

(concave) image that could be mathematically corrected. Even though lateral dimensions

were affected, the transverse (anterior/posterior) dimensions measured were accurate and

consistent. Collectively, these calibration measurements confirm the accuracy of the SD-

OCT for axial thickness measurements.
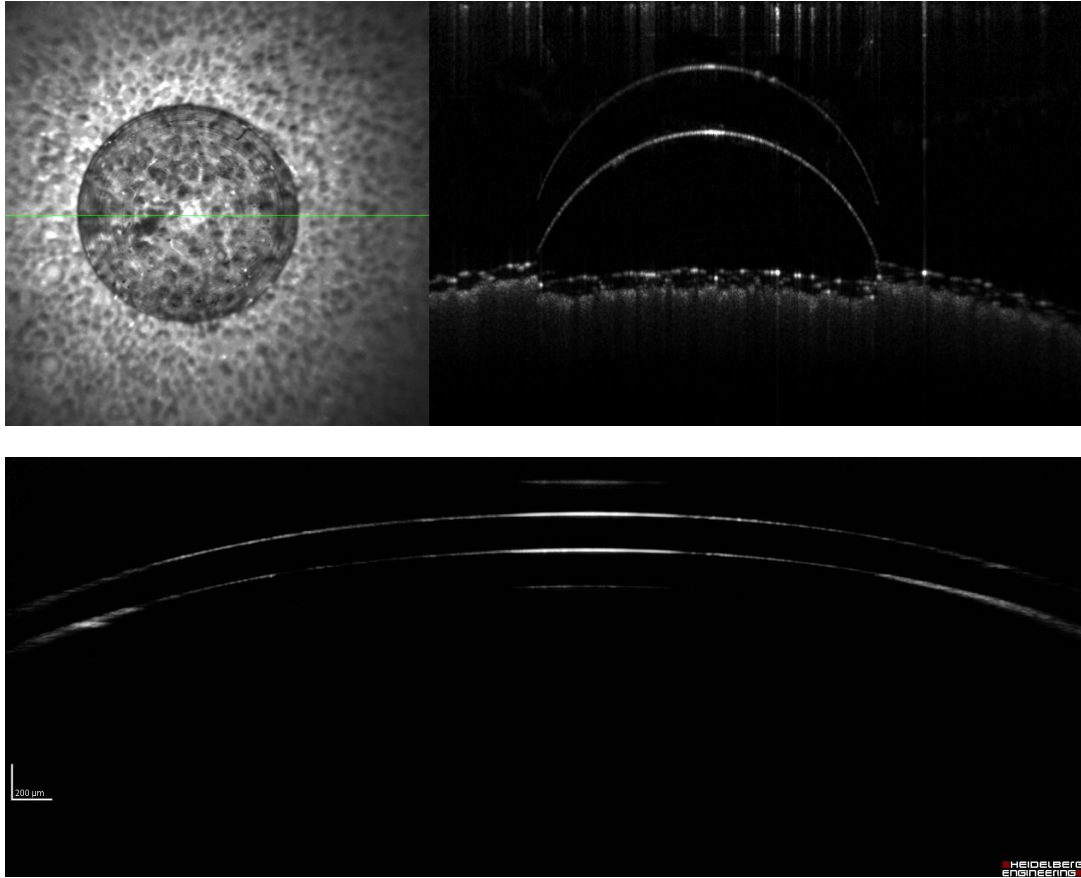
Figure 31 – OCT thickness calibration

The contact lens (radius 1.4mm) was held by tape (A, Spectralis infra-red frontal view of

contact lens) and imaged with the Spectralis OCT (B, cross section view). A microscope

slide cover slip was also imaged (C). Both (B) and (C) show curvature of the image that

did not affect the central thickness measurements.

Table 8 – Calibration data

	DV	SD	OCT	SD
Contact Lens	272.1	±2.8	269.9	±0.0
Cover slip	168.5	±1.7	175.9	±1.7

(The OCT px/um = 3.8673)

Figure 32 – Sample OCT image of mouse cornea

The modified Spectralis OCT provided excellent images of the mouse anterior segment.

C- Cornea; I – Iris; L – Lens

CCT growth curve determined by SD-OCT measurements

SD-OCT produced images with a resolution (approximately 4μm) approaching that of low powered light microscopy (Figure). Although individual lamellar layers are not discernible, there is evidence of a horizontal organization to the stroma. The images cover limbus to limbus, provide excellent visualization of the iris and show the anterior portion of the crystalline lens.

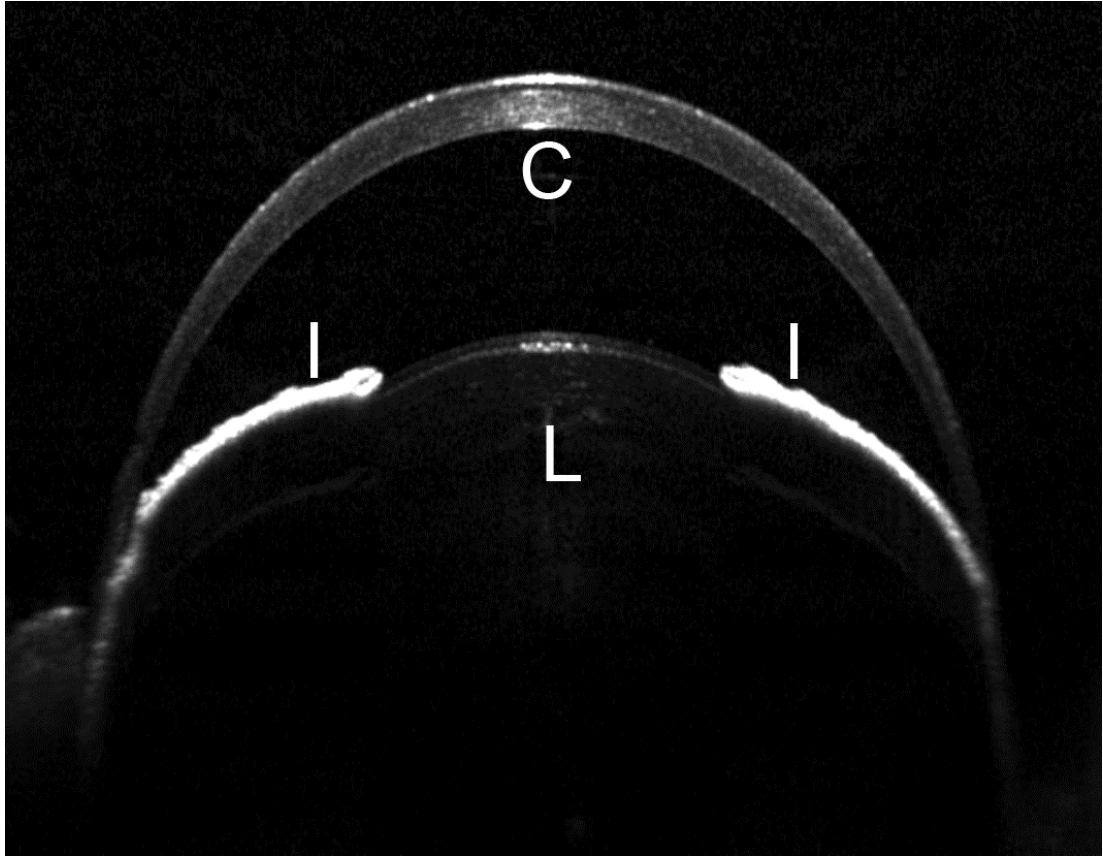In order to characterize the rate of growth of the central cornea, after confirming the accuracy of SD-OCT thickness measurements, CCT data were obtained for mice ranging in ages from P0 to P250. There was no significant difference found between anesthetized and euthanized animals, nor between males and females (data not shown), therefore CCT data presented in Figure 33 include data from all mice. The data show that during the first few weeks postnatal there is a rapid increase in central corneal thickness and by P55 it has achieved 95% of its maximum value, after which it begins to level off. The maximum CCT predicted from fitting the exponential rise to maximum equation to the data (r^2=0.84) is 106μm. The average of the measured values for greater than 55 days of age was 103±2μm. In summary, thickness measurements obtained by SD-OCT were shown to be accurate, and when applied to the murine cornea, to provide accurate CCT measurements representative of the native cornea. The epithelial thickness is also shown in Figure 33. The epithelium achieves a stable thickness about a week before the CCT indicating that the stroma does not reach adult thickness until P55.
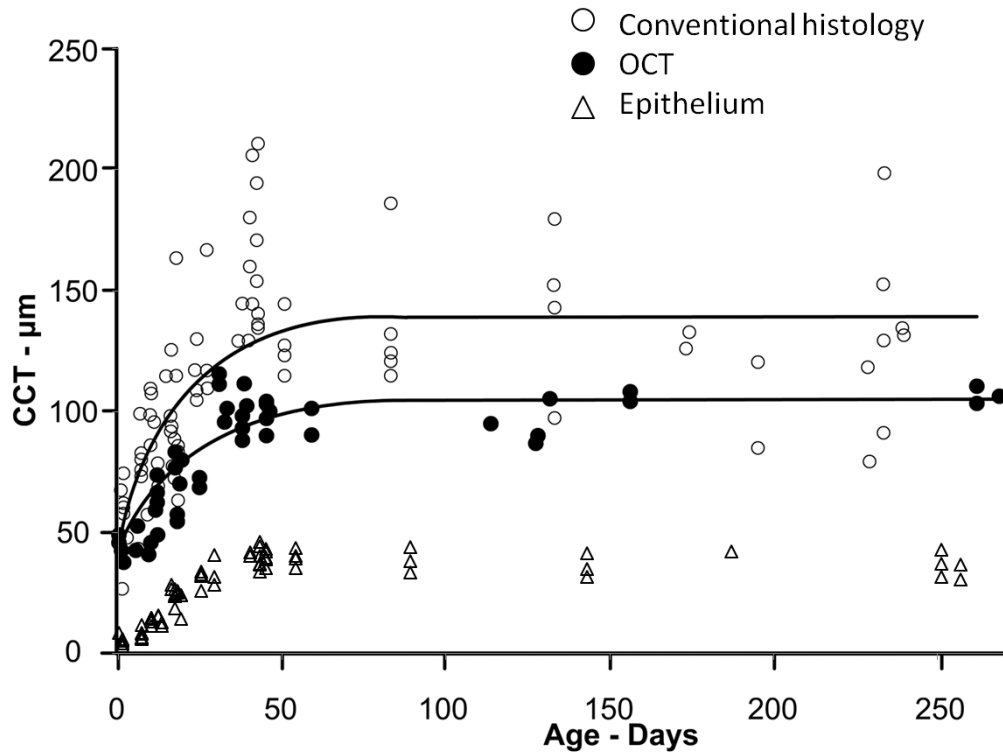
Figure 33 – Thickness exponential rise to maximum

Central corneal thickness measurements from the day of birth to 250 days postnatal

using *in vivo* OCT and conventional histology. There was a rapid increase in CCT which

leveled off about 8 weeks of age (P56). The epithelial thickness leveled off

approximately 1 week earlier (no significant difference between methods). Histology

measurements were significantly higher and more variable for CCT.

Limitations of conventional histology CCT measurements

Measuring the CCT using conventional histology sections produced considerable variation in values and some of the corneal transverse sections were distorted in shape and many had separations between the stromal lamellae some of which were quite large (Figure 38, Panel A). Separations were more evident in the posterior stroma, but occasionally included the anterior stroma as well. In a few cases the whole stroma appeared obviously thickened, without large lamellar separations. It was of interest to note that the very young corneas (prior to lid opening) were more resistant to separations (data not shown). As mentioned in the methods, the central corneal measurements were made by randomly placing three lines in the geometric center. In many cases measurements were made in areas where there were separations between lamellae. This resulted in a large variation in the measured thickness and a high mean value as compared to SD-OCT (Figure 33). The initial, P0 CCT was similar to the SD-OCT value of approximately 50μm and rose to about 140μm (>2.5 fold increase) before beginning to level off at 50 days (95% of maximum) of age after which it remained constant. The maximum CCT predicted from fitting the exponential rise to maximum equation to the data (r^2=0.56) was 141μm while the average of the measured values for greater than 50 days was 138±5μm or approximately 33% thicker than what was found with SD-OCT and with greater variability.

    The epithelium is only 1-2 cell layers thick at birth with an average thickness of 5-6 μm and rapidly increases in number of layers and thickness during P0-P50 after which it levels off. The percentage of the total corneal thickness attributed to the epithelium increases (approximately 10% - 30%) during the same time period before leveling off. It

is readily apparent from Figure 33 that most of the histological variability in CCT is due to variations in stromal thickness rather than epithelial thickness.

Our results show that conventional histological processing of mouse corneas produced CCT values that were not representative of *in vivo* values as shown by SD-OCT. Clearly, the stroma is prone to artifactual separations between lamellae and generalized thickening beyond what can be explained by these separations. Hence, in order to collect meaningful morphological and ultrastructural details, a method of tissue preparation that minimizes artifacts induced by processing is desirable.

Fixative induced distortions

The primary fixative utilized for our conventional histology was glutaraldehyde, which would be expected to penetrate a 100 µm cornea in approximately 30 minutes [29] and crosslink resident proteins. Post-fixation with osmium tetroxide enhances the process by stabilizing cell membrane lipids. Cells are killed while tissues stabilize during primary fixation and this seems the most likely step in processing to induce artifacts. In order to assess the overall effects of glutaraldehyde, whole eyes were imaged by OCT during fixation in real-time.

Ex vivo scanning revealed distortion of the shape and swelling of the cornea with exposure to glutaraldehyde. With a concentration of 2.5%, the distortion began after about 10-15 minutes and after 30 minutes it was severe, sometimes ultimately resulting in total loss of the anterior chamber. During this time the CCT increased by 25-35%. When the concentration of glutaraldehyde was reduced to 2.0% the distortion took longer to occur, however the CCT increased by the same amount after 60 minutes (approximately

40-45% as shown in Figure 35). Figure 37 shows an example of a whole eye in 2.5% glutaraldehyde initially (Panel A) and then after 30 minutes (Panel B). The same eye processed for microscopy showed large lamellar separations.

Figure 36 illustrates the effect of fixation time on the amount of swelling and therefore, in order to produce histological specimens with minimal artifacts, it seemed imperative that the exposure time to glutaraldehyde be minimized while at the same time providing adequate preservation of the tissue.
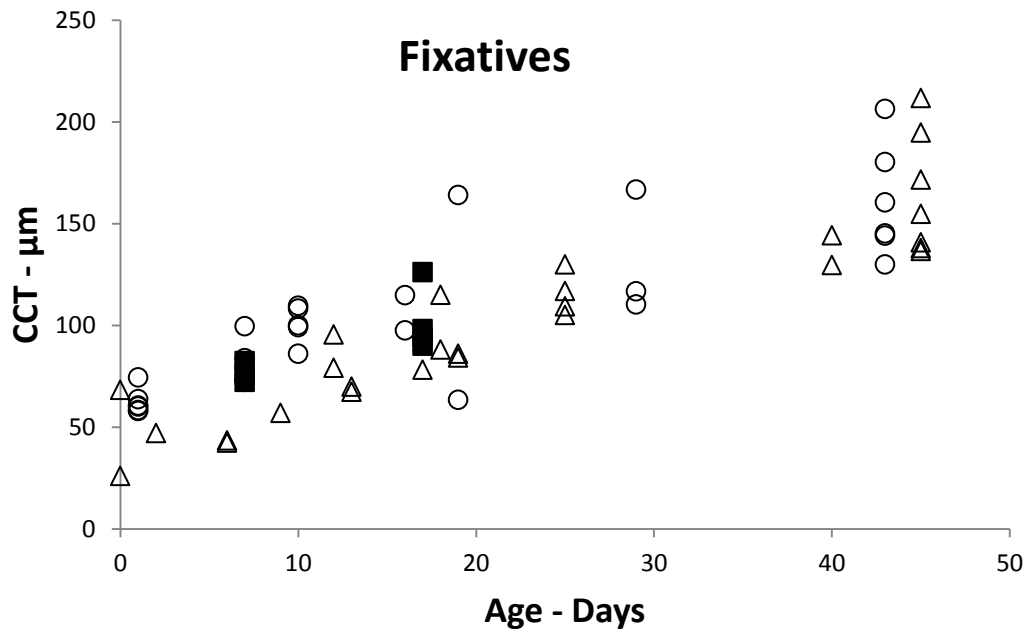
Figure 34 – Fixative solution effect on CCT

There was no significant difference in CCT for the three different fixative solutions.

Fixative A (circle) = 2.5% glutaraldehyde/0.1M NaCac

Fixative B (filled square) = 2.0% glutaraldehyde/0.05M NaCac

Fixative Berg (triangle) = 2.0% glutaraldehyde/0.08 NaCac
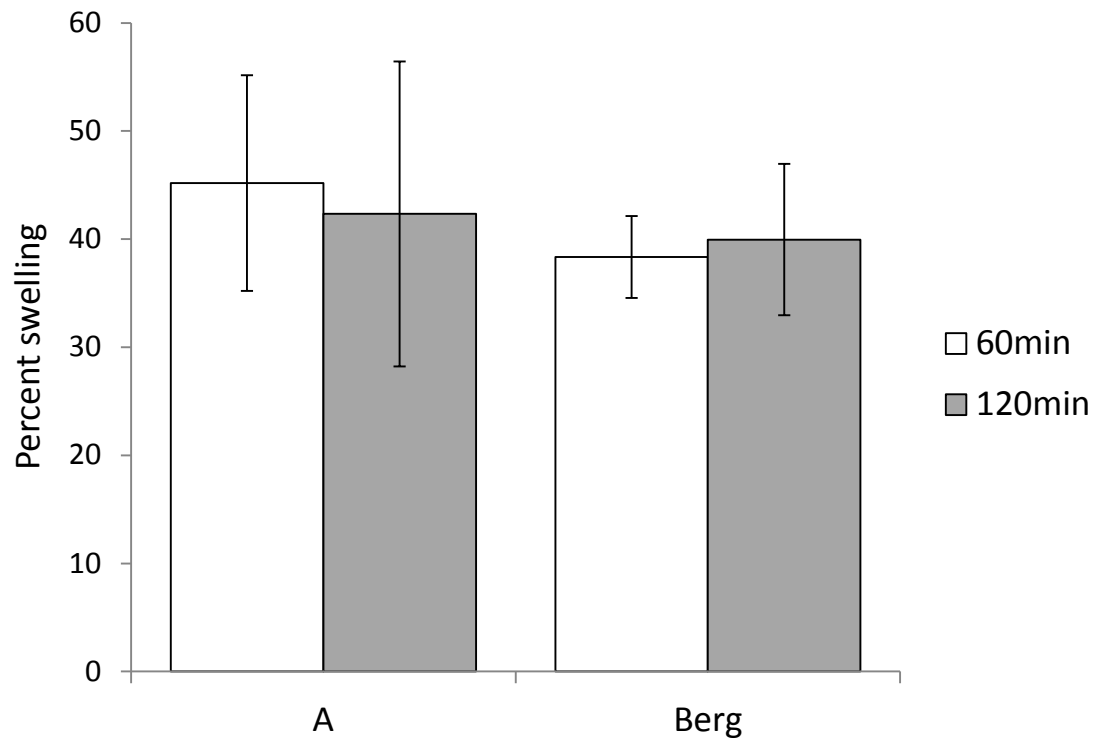
Figure 35 – Comparing fixative solution swelling

Fixative "A" contains a higher concentration of glutaraldehyde and higher osmolarity than fixative "Berg". There was no significant difference in the amount of swelling after 60 minutes or 120 minutes (n = 5).

Fixative A = 2.5% glutaraldehyde/0.1M NaCac (Osmolarity 450mOsm)

Fixative Berg = 2.0% glutaraldehyde/0.08 NaCac (Osmolarity 360mOsm)
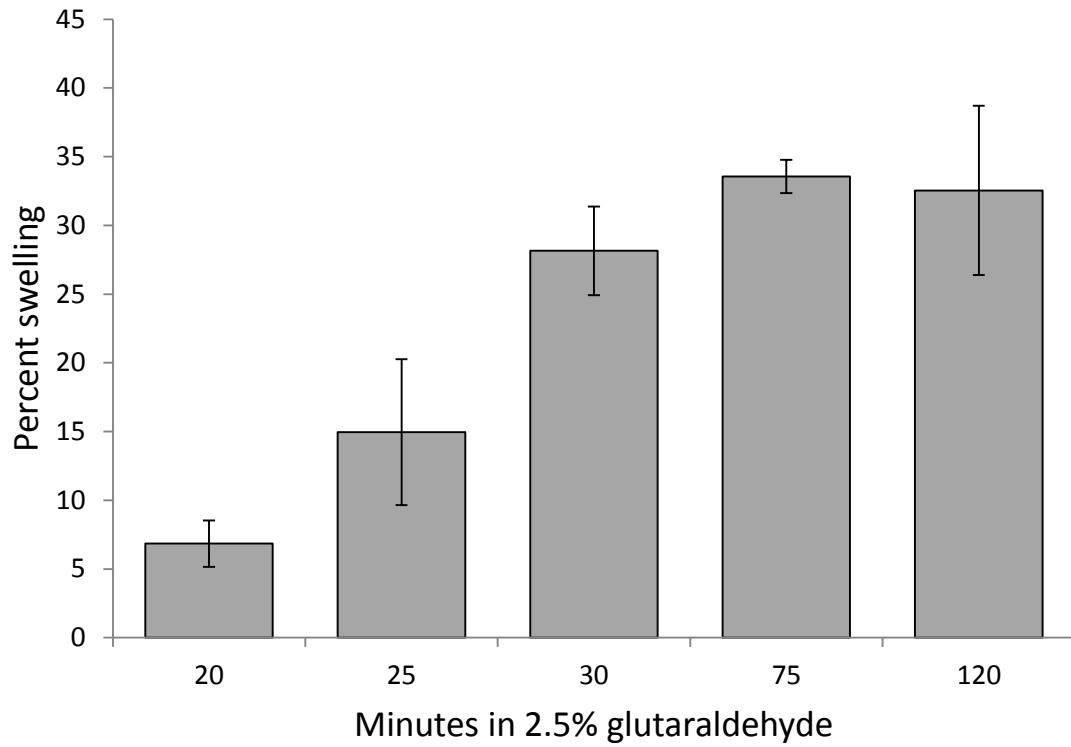
Figure 36 – Swelling as a result of time in fixative

Fixation with 2.5% glutaraldehyde is commonly used for tissue preservation with fixation

times typically 2 hours or more. Significant swelling occurs in less than 30 minutes

(n = 5). These values were slightly lower than thicknesses in Figure 35 from a different

set of mice.
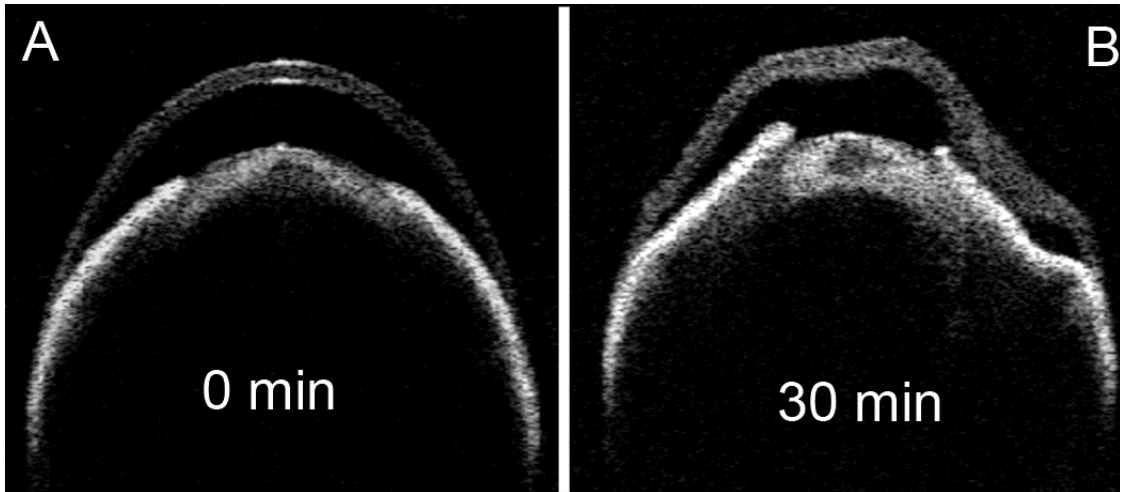
Figure 37 – Ex vivo images of fixation effects

Visante OCT image before (A) and 30 minutes after immersion in fixative "A" (B)

showing gross distortion of the eye. Spectralis OCT 3-D rendering (lower panel) shows

similar distortion with same time and fixative.

Microwave tissue preservation

To determine if histological artifacts could be reduced and thereby preserve the native

corneal thickness, corneas were prepared using an optimized microwave protocol.

Microwave fixed corneas had few or no lamellar separations (Figure 38, Panel B), when

compared to conventional fixation, (Figure 38, Panel A) were without gross corneal

distortion (Figure 38, Panel D), and appeared to be well fixed when examined by electron

microscopy. Figure 39 is a montage of images showing no lamellar separations across a

large portion of the cornea. At the ultrastructural level, the stroma of microwave

processed corneas was compact and did not exhibit interlamellar separations compared to

conventionally fixed corneas (Figure 40 Panels A and B) while the preservation of

keratocyte cytoplasmic structure was similar to that obtained with conventional fixation

(Figure 40 Panels C and D). The mean microwave processed CCT beyond 8 weeks was

99 ($\pm$2) μm and this value is in close agreement with *in vivo* CCT estimates made by SD-

OCT (Figure 41). In addition, the epithelial thickness determined from conventional

histology agreed with that obtained from measuring microwave-fixed sections,

suggesting that most of the artifactual increase in CCT following conventional processing

occurs within the stroma. Table 9 shows the values for collagen fibril diameter and Table

10 for the interfibrillar spacing in the anterior and posterior central cornea for specimens

prepared by conventional fixation versus microwave processed. No difference in fibril

diameter was observed between the two fixation processes. However, the interfibrillar

spacing was statistically different with approximately 20% less anteriorly, and 35% less

posteriorly in the microwave processed specimens compared to the conventional

processed corneas. Figure 42 shows representative sections of collagen fibrils used to

measure diameter and spacing. Collectively, our results support microwave-assisted histological processing as a method which produces CCT values not significantly different than SD-OCT values, while providing superior stromal ultrastructural preservation compared to conventional histological processing.
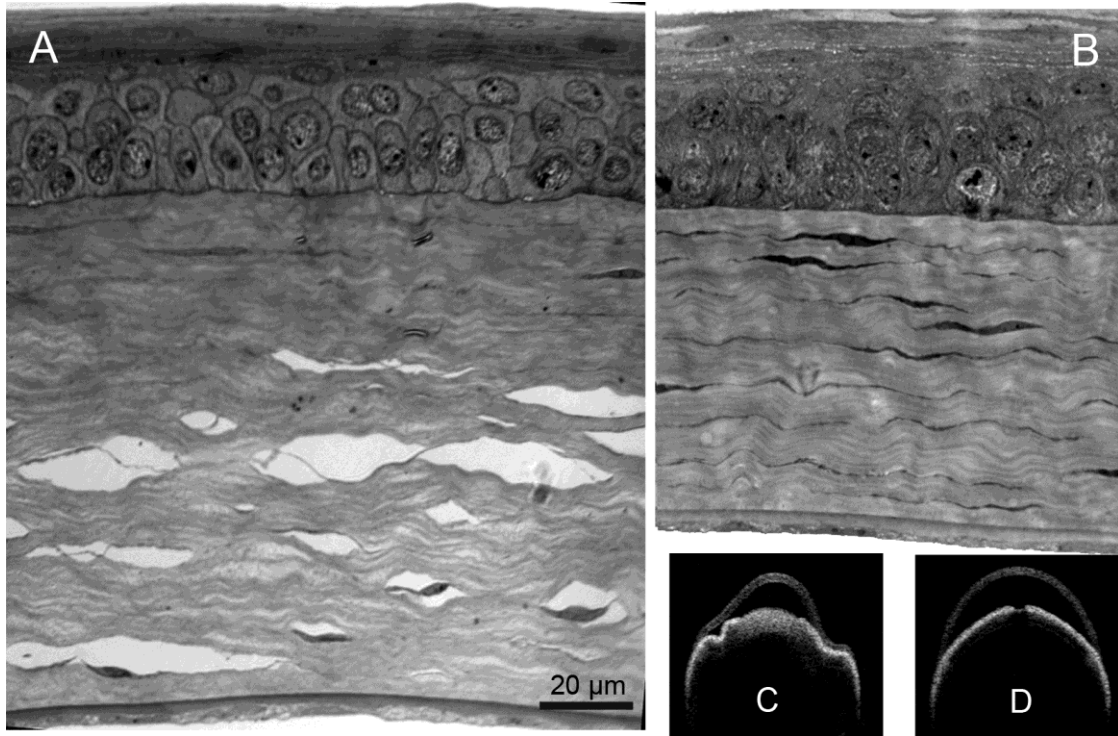
Figure 38 – LM conventional and MW images

A conventional histology specimen (A) with numerous large separations is compared to a microwave processed specimen (B) (same magnification for both). Panel (C) shows the OCT image of (A) and panel (D) shows OCT of (B).
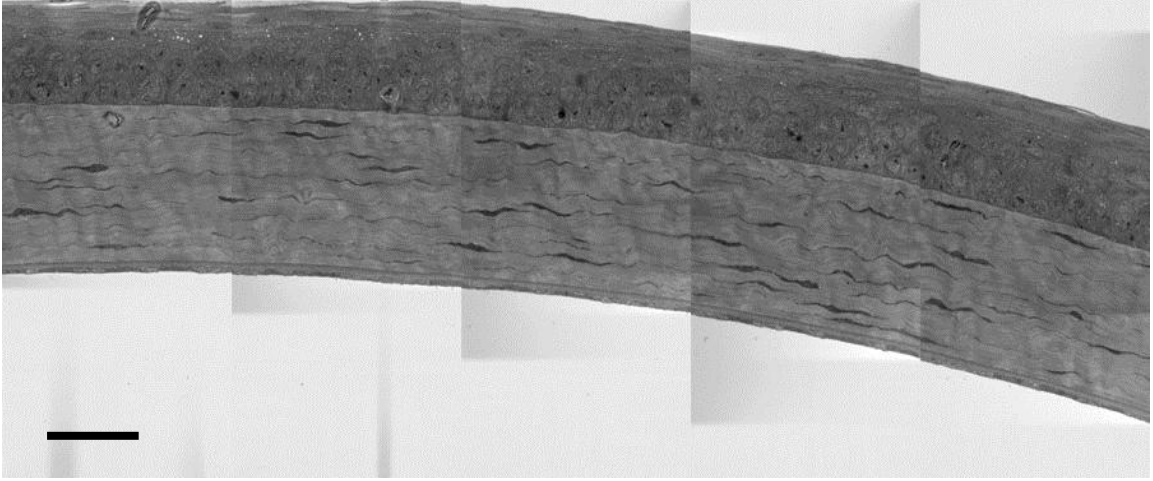
Figure 39 – Microwave processed montage

Microwave processed specimens were largely free of separations across the entire cornea.

Scale bar = 30 µm.
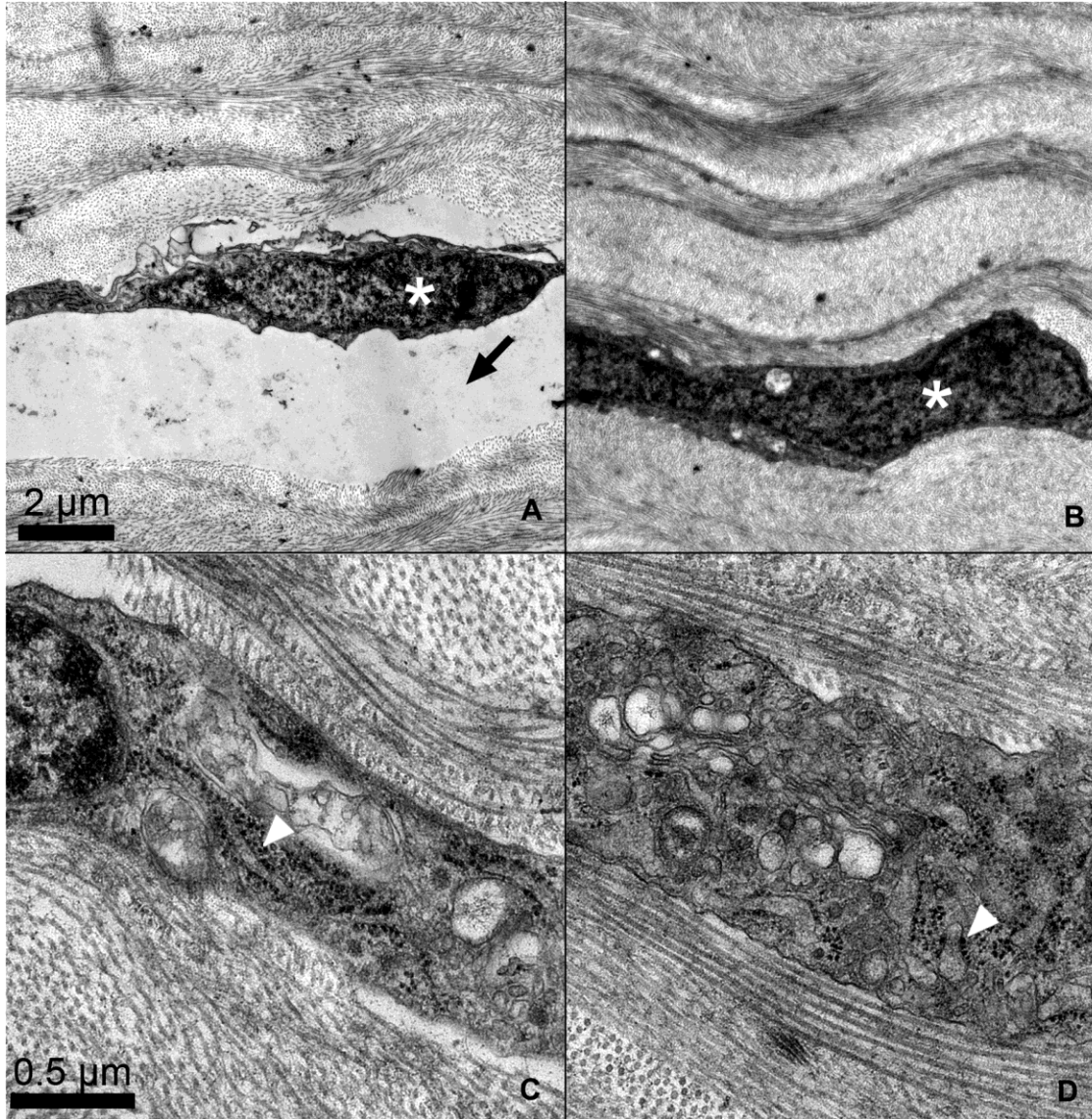
Figure 40 – EM conventional and MW images side-by-side

Left side panels (A and C) show conventional histology specimens and panels (B and D) were microwave processed. The white asterisks mark keratocytes and the arrow in (A) illustrates a separation between the keratocyte and the collagen. The white arrow heads in (C and D) point out the rough endoplasmic reticulum and show similar details.
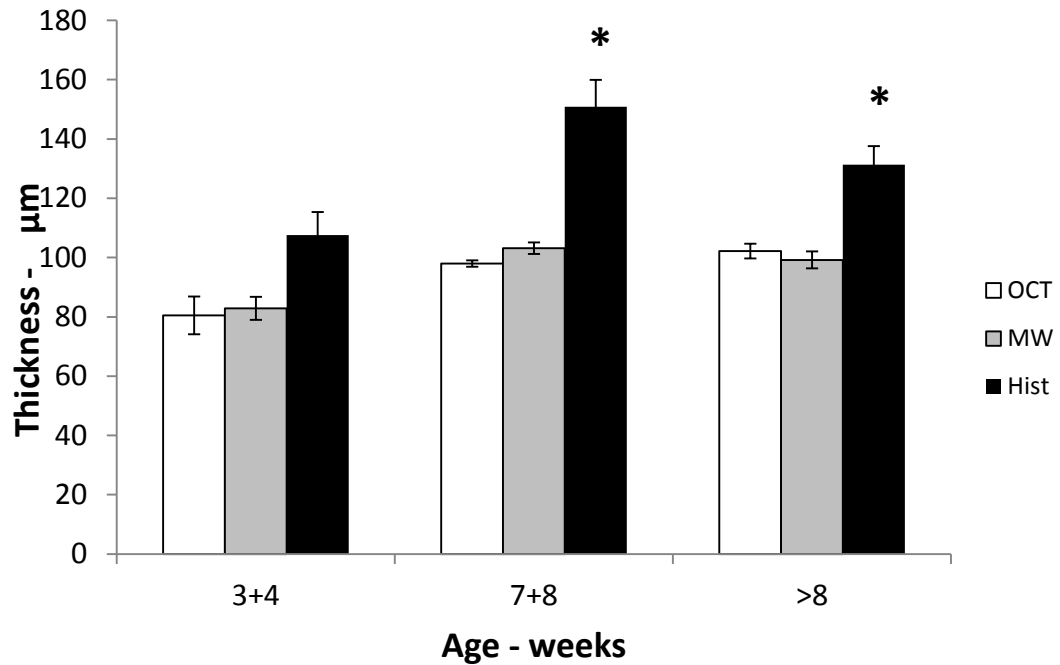
Figure 41 – Comparing 3 thickness measurement methods

The Spectralis OCT (OCT) and microwave prepared corneas (MW) were comparable at all ages, but conventional bench processed corneas (Hist) were significantly thicker at 7 weeks and beyond. Conventional bench processing included both 2.5% and 2.0% glutaraldehyde specimens as no difference in thickness was found between the two.

Table 9 – Collagen fibril diameter

Fibril Diameter (nm)		
	Conventional (n=3)	Microwave (n=4)
Anterior	24.3±0.5	25.8±0.6
Posterior	25.2±0.8	27.3±0.5

Table 10 – Spacing between collagen fibril centers

Interfibrillar Spacing (nm)		
	Conventional (n=3)	Microwave (n=4)
Anterior	67.8±2.8	53.6±1.1*
Posterior	75.8±1.1	55.9±2.3*

*$p < 0.05$ compared to conventional histology
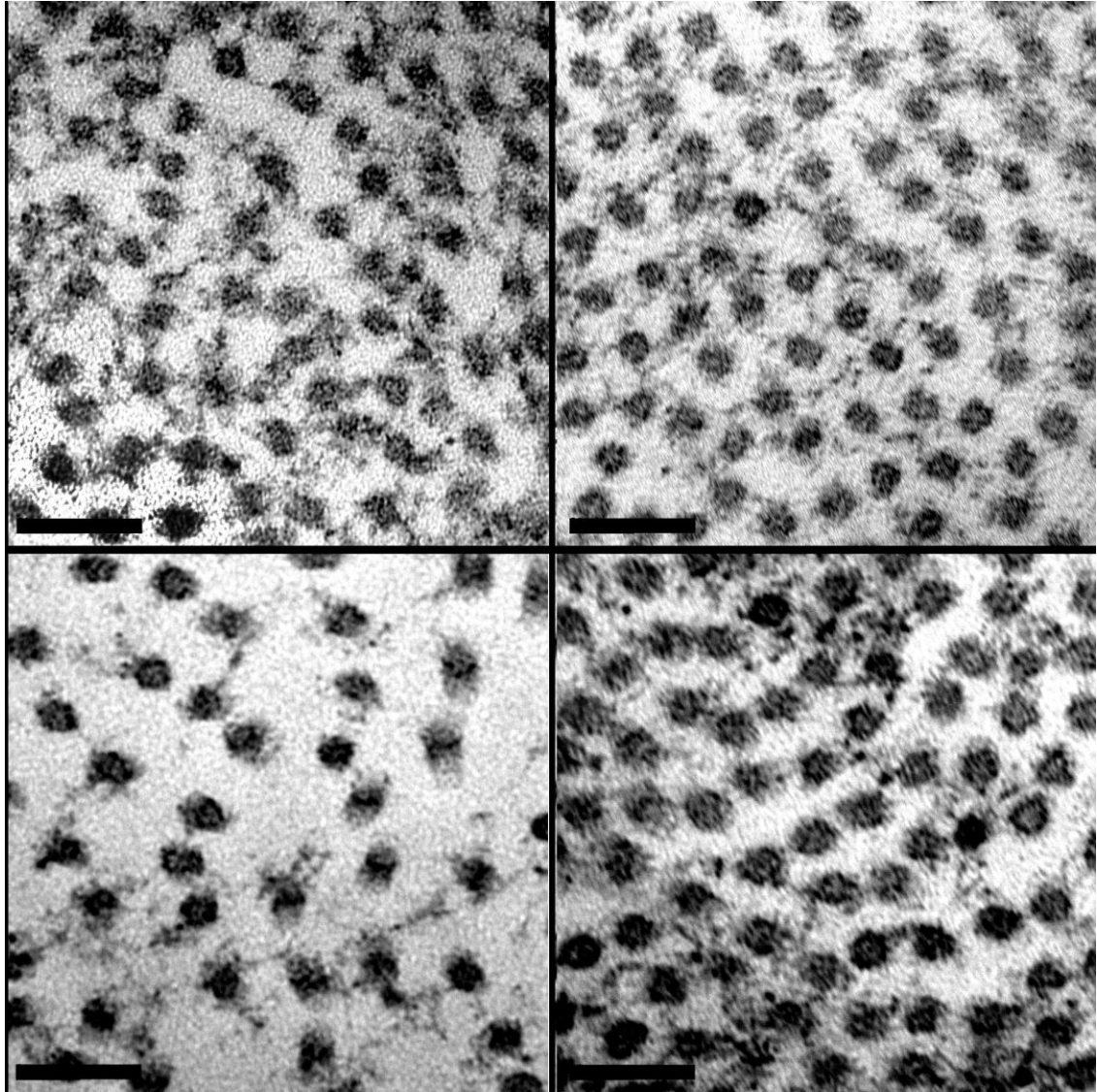
Figure 42 – EM conventional and MW collagen fibrils

In both the conventional (A) and microwave processed (B) corneas the anterior fibrils were slightly smaller than posterior (C and D). The spacing between fibrils was significantly greater in the posterior stoma with conventional histology (C). Scale bar = 100nm

3.1.3 Discussion

Consistent with the purpose of this study, postnatal corneal growth and development in C57BL/6 mice were elucidated by validating the SD-OCT as a method for obtaining accurate CCT values and measuring the CCT of mice from P0 to P250. These CCT data were used, not only to establish a minimum age for subsequent studies, but also as a benchmark for establishing an optimized histology protocol which minimized processing artifacts. In this way providing improved ability to observe structural changes beneath the wound areas that might alter migration speed and/or providing clues for structural changes induced by integrin-blocking antibodies.

A comprehensive normal growth curve was established for C57BL/6 mice and corroborated by measurements of microwave-fixed histological sections. Our results show that the C57BL/6 mouse is born with a CCT of approximately 50-60 μm. During the first 7-8 weeks it shows rapid thickening, more than doubling in thickness, after which it remains nearly constant at about 103 μm (SD-OCT, mean value >8 weeks) or 99 μm (microwave histology, mean value >8 weeks). The mouse is essentially born pre-mature with the eyelids not opening until approximately day 12-14, after which the cornea undergoes maturational changes for several weeks [1, 26, 27, 30-33]. Several parameters of eye growth and maturation either level off or slow to a minimal rate of change for the remainder of their adult life [27, 34]. The CCT developmental curve provides an important gauge for eye development in general, and suggests that animals younger than 7-8 weeks should not be considered adults for corneal research since they are still in a phase of rapid growth and development. However, in many murine corneal

studies, mice as young as 6 weeks of age are often used and assumed to represent the mature, fully developed cornea.

It has recently been reported that there is a range in mean CCT values in 17 different strains of adult mice ranging from approximately 90μm to 124 μm (similar measurements by cryosections and ultrasound pachymetry) [35]. Our study was confined to a colony of inbred C57BL/6 mice and it remains to be shown whether or not other strains of mice would exhibit an age-dependent growth curve temporally similar. When considering animal models for corneal research it is therefore important to consider the age of the mouse in the context of the specific strain.

Obtaining accurate CCT data is necessary, for example, for monitoring corneal development and for determining volumetric values to assess cell density and surface area ratios [9]. Frequently, the process of fixing corneal tissue results in separations between the stromal lamellae, and/or shrinkage or swelling of tissues, obviously adding error to thickness measurements. When measuring stromal or total corneal thickness, or calculating volume, these separations cannot be ignored. In addition, when investigators are looking at interactions between stromal cells and surrounding collagen, the separations may obscure the actual physical juxtapositions. Histology specimens are subjected to harsh fixative and preparatory procedures which have the potential to produce artifacts. Since there are many methods for fixing corneal tissue, they may all produce somewhat different results.

Corneal specimens prepared for light and electron microscopy are commonly preserved using glutaraldehyde as a primary fixative with fixation times varying from hours to a few days. For electron microscopy, osmium post-fixation is also typically

incorporated into the process, after which the tissue is dehydrated. In each step of the tissue preparation there is potential for artifactual alteration. During this process metabolic activity ceases, which results in cell permeability and ion concentration changes [29]. While the osmolarity of solutions used is a consideration for avoiding artifactual changes in tissue and cell volume, the specific ion concentration is even more important [20]. As observed in our *ex vivo* imaging, our standard fixative solution, with an osmolarity of approximately 450 mOsm caused considerable distortion (apparent overall shrinkage) of the intact eyeball and a paradoxical increase in corneal thickness (as much as 35%) beginning after about 15 minutes. *Ex vivo* scans with fixative solutions containing glutaraldehyde dramatically demonstrated significant distortion and swelling and separations between lamellae.

It has been shown that stromal lakes (inter/intralamellar spaces) are a typical consequence of stromal edema [36]. In our study, there was no reason to expect that the corneas would be edematous as the eyes were not inflamed and had been harvested from healthy mice and processed immediately after enucleation (the absence of edema was also confirmed with SD-OCT). An obvious conclusion was that the fixation process was inducing interlamellar separations (and distortions). This was confirmed with *ex vivo* imaging of the eyes during the process of fixation. It was also interesting to note that in nearly every case the separations occurred coincident with the location of keratocytes and were much more likely to occur in the posterior stroma, as opposed to the anterior. It was also noted that separations were minimal in mice prior to eyelid opening. These findings suggest keratocytes are the "weak link" in stromal tethering and prone to "letting go" during swelling. A possible explanation for the increased tendency of the posterior

stroma to exhibit interlamellar separations may lie in the organizational and compositional differences between anterior and posterior stroma. It has been well established that there is a higher keratocyte density, a lower keratan sulphate to chondroitin/dermatan sulphate ratio, and less prone to swelling in the anterior stroma [37]. Interestingly, very young corneas have more densely packed keratocytes and relatively low amounts of keratan sulphate [1], which may make them less susceptible to edema and interlamellar separation after fixation.

In the current study, CCT measurements obtained with SD-OCT avoided the potential for distortions and artifacts resulting from fixative effects and it was established as a valid and reliable method for CCT determination in the mouse. The SD-OCT, designed for scanning the retina, was easily modified with a 30D ophthalmic condensing lens attached to the front of the instrument. Measuring objects of known thickness established the validity of using the SD-OCT for thickness measurements. Results for CCT obtained by SD-OCT were much less variable and thinner on average than values obtained from conventional histology samples. This alone was evidence that CCT values obtained from conventional histology samples were influenced by artifacts occurring during fixation. This was corroborated by data obtained from microwave processed samples which showed minimal separations and CCT values within a few microns of the SD-OCT. SD-OCT yielded a CCT value that became the goal to maintain during tissue fixation. Microwave processing minimized the fixation time and eliminated the artifactual lamellar separations while maintaining the CCT values estimated from SD-OCT data and provided reliable morphometric data representative of the native, unfixed cornea. Collagen fibril diameter was essentially the same with microwave-processing as with

conventional histology processing and similar to values reported for x-ray diffraction analysis. However, collagen fibril packing was tighter in the microwave processed corneas (Table 10). This leads to the conclusion that, other than interlamellar separations, the thicker stroma seen in conventional histology sections is also due to an increase in interfibrillar spacing.

Microwave-assisted tissue fixation has been described in the literature since the early 1970's but is still not a commonly used method for either light or electron microscopy even though it accomplishes the entire fixation process in 1-2 hours with results as good, or better, than conventional fixation protocols requiring several days processing time [38-40] . The energy absorbed from microwave radiation produces heat and molecular motion. In the current study unwanted heating of specimens is averted by using a low wattage magnetron setting and incorporating a cold-spot water-filled heat sink [41]. The microwave-generated molecular motion combined with vacuum processing greatly enhances fixative penetration and reduces the distorting effects of fixative osmolarity [38].

Corneas prepared in the microwave were exposed to each of the chemicals for very brief times. For example the total time in glutaraldehyde-containing fixative was 10 minutes or less, which was less than the time in which distortion was seen to occur in the *ex vivo* experiments. The histological sections produced were, not only, generally free of lamellar separations, they showed evidence of satisfactory ultrastructural preservation. There was considerable discrepancy between the CCT of the conventionally-fixed corneas as compared to the microwave-fixed corneas. It is compelling to consider the microwaved corneas, without the separations, as representing the "truer" CCT. Using a

microwave-assisted histological protocol, it is possible to preserve the anatomical dimensions and ultrastructure of the mouse cornea and avoid the harsh deformational effects (shrinkage or swelling) that accompany routine histologic preparations. The microwave protocol, in conjunction with electron microscopy, further extends the morphologic detail provided by SD-OCT and light microscopy, and provides a superior method for obtaining high resolution corneal images free of fixation-induced distortional artifacts.

In summary, this study provides, for the first time, a comprehensive growth curve of CCT for C57BL/6 mice from birth through adulthood based on *in vivo/in situ* data obtained by SD-OCT and confirmed by histological sections prepared using microwave radiation. To our knowledge this is the first reported use of SD-OCT or microwave processed histological sections for murine CCT measurements. This study determined the age of stromal maturity which was used as minimum age for mice used in subsequent studies. This age, at which the stroma has stabilized, is important for *in vivo* motility characterization in order to minimize the potential for confounding factors when comparing various experimental manipulations. An optimized histology protocol which minimized processing artifacts was developed to improve our ability to observe structural changes beneath the wound areas that might alter migration speed and or providing clues for structural changes induced by integrin-blocking antibodies.

3.2 – Characterizing and Quantifying *in vivo* migration

3.2.1 Introduction

In a previous chapter some of the reasons that *in vivo* studies would be important especially for neutrophil migration were described. Because the cornea is transparent and requires the migrating neutrophils to traverse the avascular stroma for a considerable distance, it is particularly well suited for *in vivo* studies of interstitial migration of inflammatory cells *in situ* without tissue manipulation. The HRTIII-RCM provides a means to accomplish *in vivo* studies of interstitial migration in the cornea.

After transendothelial migration, the activated and transformed neutrophils must traverse avascular stromal tissue consisting of a dense matrix of near-orthogonally crossed layers of parallel collagen fibrils with interconnected keratocytes interspersed between these collagen lamellae. However keratocyte death directly beneath the wound begins shortly after an epithelial wound, even when the epithelial basement membrane remains intact [42, 43]. Infiltrating neutrophils then must migrate through regions with intact keratocytes as well as those with dead keratocytes; two distinctly different environments. *In vivo* time lapse HRT-RCM sequences provided the means, for the first time, to quantify speed and directionality of cellular movement while observing neutrophil interaction with stromal keratocytes in the living eye.

Following a central corneal epithelial abrasion, previous ultrastructural studies showed close contacts exist between neutrophils and keratocytes, suggesting the migrating neutrophils were using the keratocytes as a "cellular highway," a classic structure/function relationship [44]. Live imaging of neutrophils migrating along stromal keratocytes has never been documented. In vivo confocal microscopy is a novel tool for

examining the relative contribution of the keratocyte network to leukocyte migration within the corneal stroma.

Keratocytes die in the anterior stroma directly beneath the site of epithelial injury even though the basement membrane remains intact (Figure 43). Figure 44 compares a healthy keratocyte (A) beneath the uninjured epithelium as opposed to one that is beneath the wound and undergoing cell death (B) as noted by electron translucency of its vesiculated cytoplasm. Neutrophils that enter the region beneath the wound migrate without the presumed benefit of an intact keratocyte network. Observation and comparison of locomotion parameters in regions with and without viable keratocytes will provide additional data on how neutrophil locomotion is affected by the absence of a keratocyte network.

The purpose of this study was to use *in vivo* time lapse imaging to characterize and quantify neutrophil interstitial migration within regions where there were viable keratocytes and regions where keratocytes had died as a result of epithelial abrasion. Thus showing that neutrophils preferentially migrate along the keratocyte network and that migration is compromised in its absence.
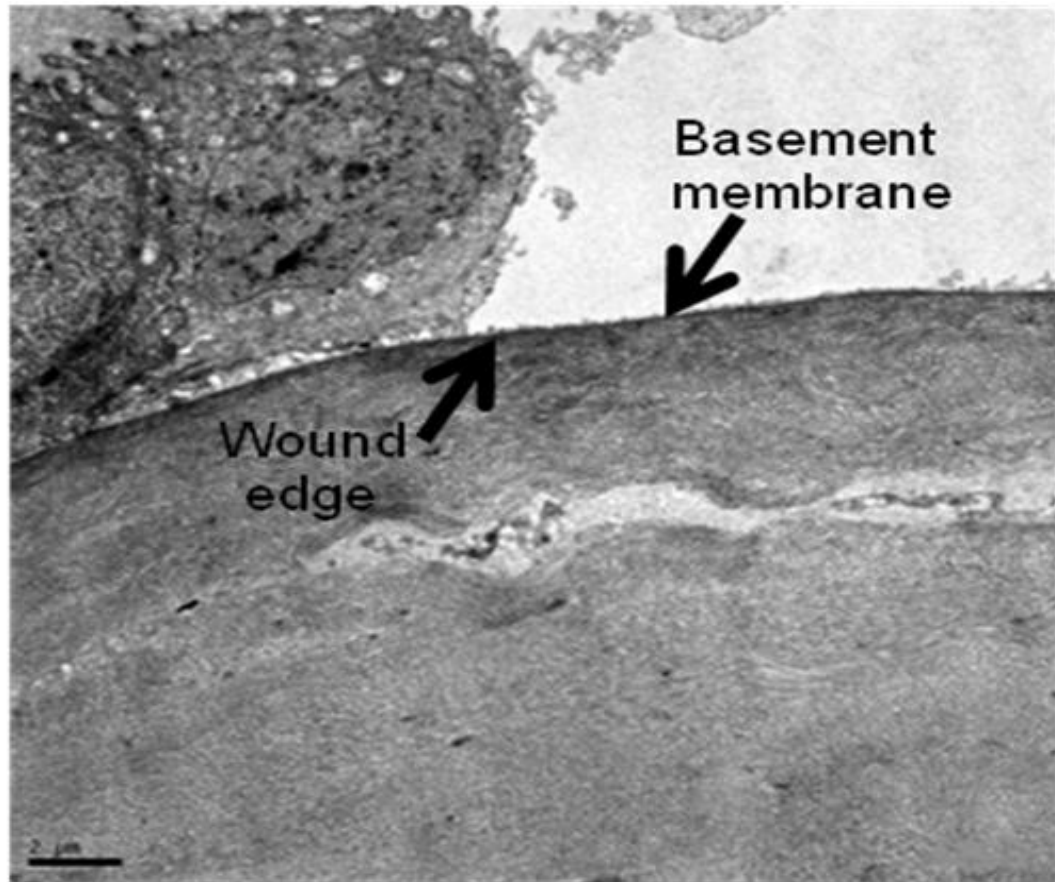
Figure 43 – Wound edge

As described earlier, the basement membrane remains intact after the epithelium has been

removed. This image shows a dead/dying keratocyte just beneath the basement

membrane. Keratocyte cell death was also evident with HRT-RCM images such as seen

in Figure 53. Scale bar = 2μm.
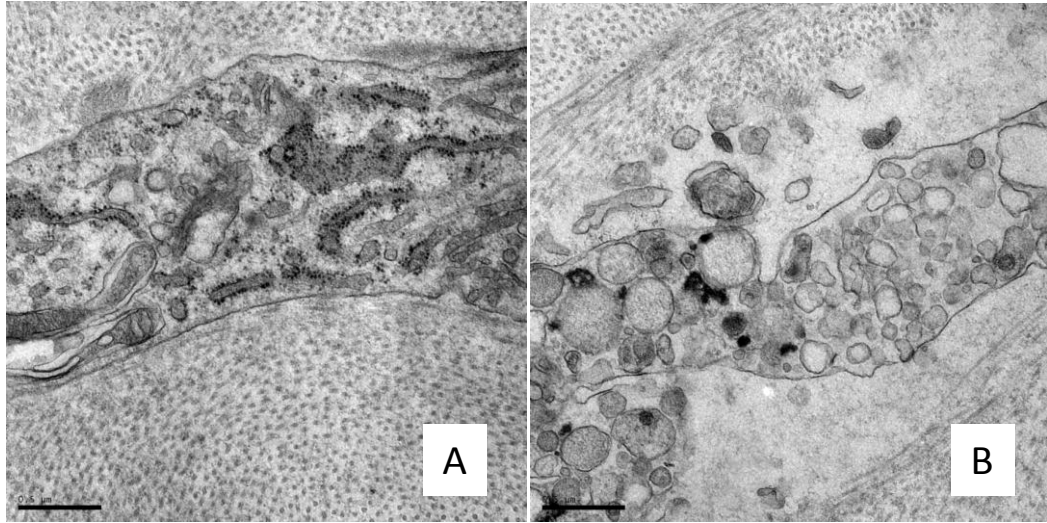
Figure 44 – Keratocyte apoptosis

Viable keratocyte beneath intact epithelium (A). Damaged (dying) keratocyte in anterior

stroma beneath epithelial abrasion (B).

 Scale bar 0.5 μm

Inflammtory cell imaging

Obtaining images of the mouse cornea with the HRT-RCM proved to be challenging at the onset but with repeated attempts and modifications in the procedure it proved to be relatively straight forward. Images of unwounded mice allowed visualization of the epithelium with distinct basal layer, somewhat indistinct stromal keratocytes which formed a continuous network, and a well defined endothelial layer. The sub-basal nerve plexus was easily visualized as were larger nerves within the stroma. Relatively large, irregular-shaped, highly reflective cells were frequently seen and presumed to be resident tissue macrophages (later confirmed) (Figure 47). Volume scanning with the HRT produced a z-stack of images captured every 2 microns and provided a good approximation of thickness values. Several time points (2 hours to 48 hours) after epithelial wounding were imaged. At times less than 8 hours very few inflammatory cells were noted, at 24 hours there were so many cells that it was hard to identify individual cells and by 48 hours there were none (Figure 45). Eight hours was chosen for the time after wounding for all subsequent experiments as it was a time before the peak influx and individual cells could be observed. At the 8 hour time point the cornea was edematous (45% swelling) according to the thickness obtained from volume scans (Figure 46, Table 11). It was also noted that the keratocytes were considerably more distinct and reflective as compared to the unwounded.
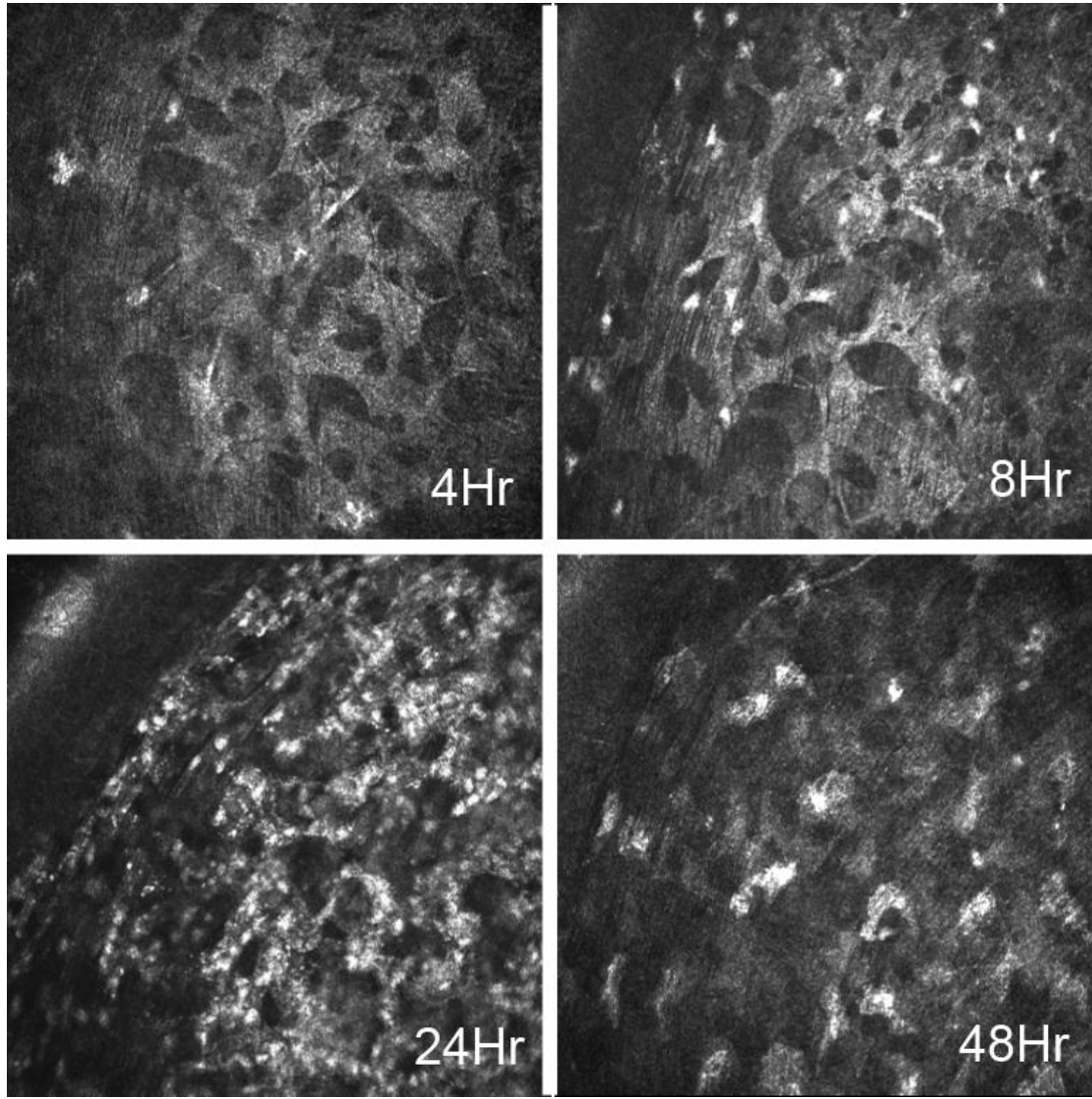
Figure 45 – Neutrophil peak influx

At 4 hours there were very few neutrophils (arrows) observed in the anterior stroma in the parawound area. At 8 hours there were enough to image 12 cells per frame and the cells were in the advancing phase of infiltration. At 24 hours masses of neutrophils were noted and at 48 hours few remained (large cells are macrophages).
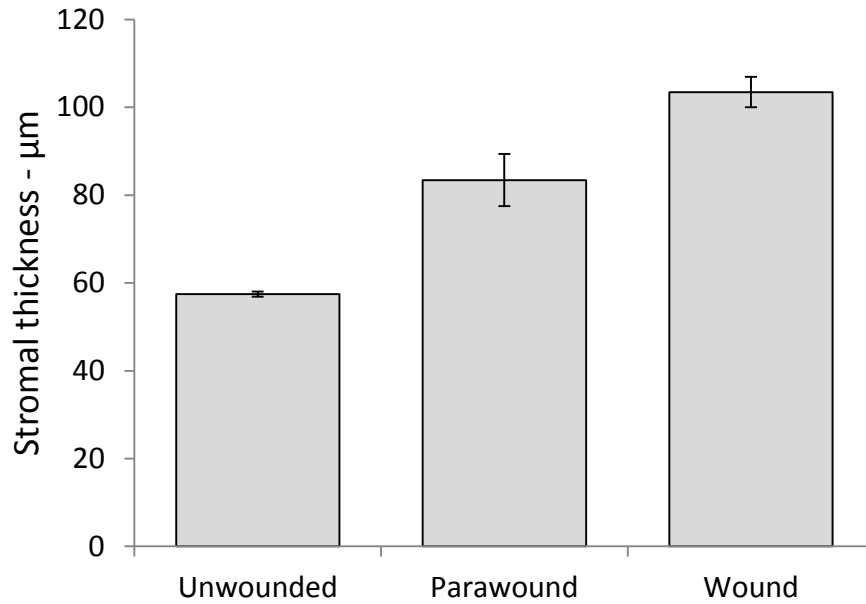
Figure 46 – Amount of swelling after wounding

Swelling begins shortly after an epithelial abrasion. At 8 hours after

wounding there was substantial overall swelling but significantly more

beneath the wound.

Table 11 – Swelling after wounding

	Thick	SEM	% increase
Unwounded	57.5 μm	±0.6	
Parawound	83.4 μm	±5.9	45.2 ±10.2
Wound	103.4 μm	±3.5	80.0 ±06.1
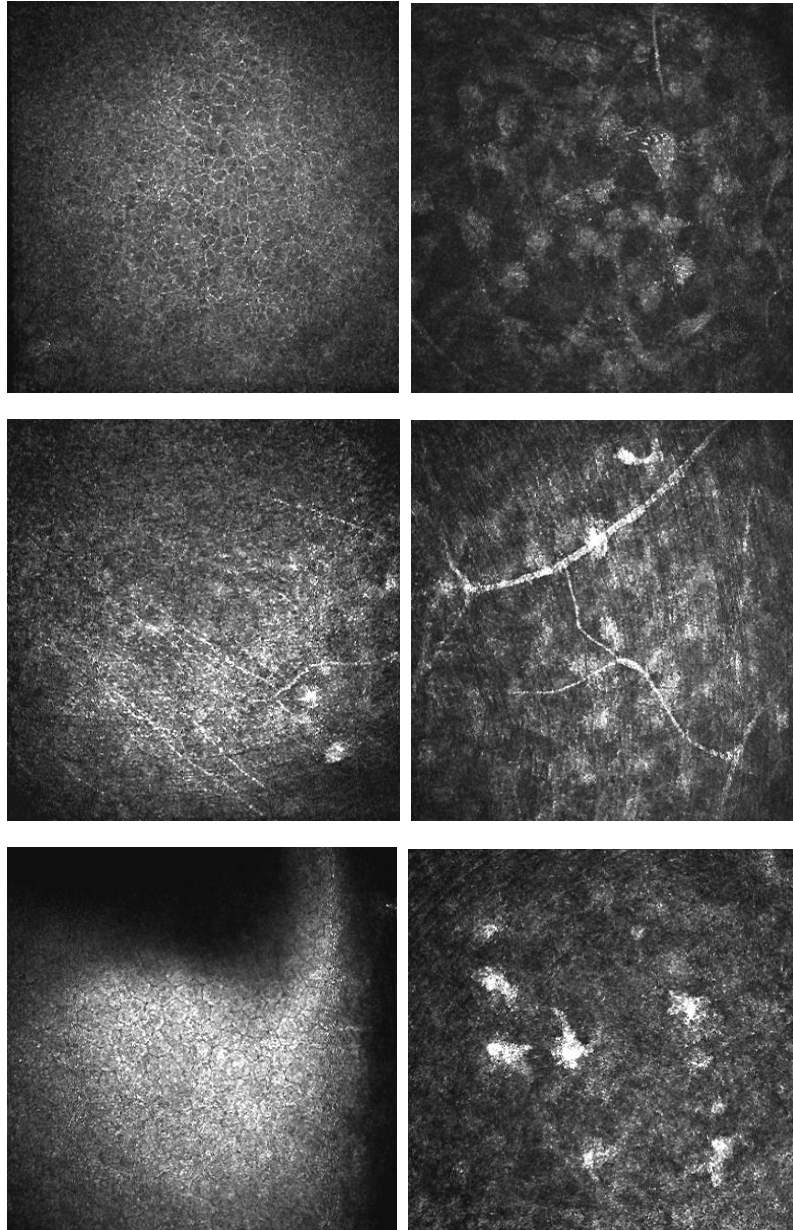
Figure 47 – Unwounded cornea HRT-RCM

In the unwounded cornea the basal epithelial layer (A) showed distinct cell borders, the keratocytes network was a little indistinct (B). Sub-basal nerves (C) and anterior stromal nerves (D) were easily visualized as was the endothelium (E). Resident macrophages (F) were a common finding. All images were in the paracentral region.

Time lapse motility characteristics

In order to determine the characteristics of inflammatory cell movement, for the first time within the living cornea, the HRT-RCM was used to capture a series of 100 second sequences in wounded corneas. Once a set of 100-second sequences was captured they were combined into a single movie file. The captured movie sequences required that they be stabilized due to respiratory and extraneous movements before cell motility could be analyzed. The longest sequence of images spanned a time of 45 minutes. Time was limited by the HRT instrument and/or the duration of anesthesia. In the mouse cornea the keratocyte network was readily visible in most instances along with the easily distinguishable, highly reflective infiltrating cells, within the 400x400μm area imaged.

The infiltrating cells, neutrophils as they are later confirmed to be, were observed to have a polarized morphology with a leading edge that probed the environment by briefly extending then retracting pseudopodia. Locomotion occurred as the extended pseudopodia gained a "foot hold" and the cell contracted to pull the trailing end of the cell forward (Figure 48). Typically the cells would follow a somewhat circuitous path but showed definite directional preference. However, in some instances the cell path would make a complete loop or re-trace portions of its path. Most cells showed persistence of motion though some occasionally paused momentarily. Although there was variability in how fast the cells were moving, there did not appear to be a sub-set of non-motile cells.
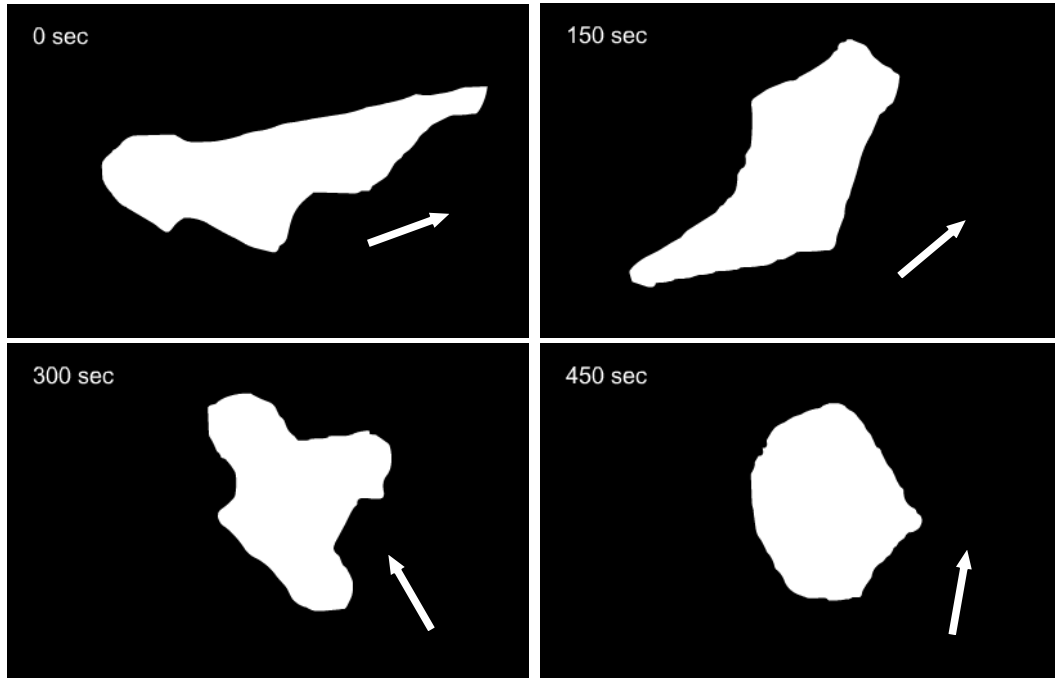
Figure 48 – Amoeboid shape changes

In the span of 7½ minutes the same cell has undergone significant shape changes as is typical of amoeboid cell locomotion. The white arrows indicate the direction of movement.

Neutrophil localization on keratocytes

Observation of cell movement showed a motility pattern that followed the keratocyte network. There were numerous instances where cells moved in single file across a narrow "bridge" between neighboring keratocytes (Figure 49). At times the migrating cells were seen stopping at a point where the network bifurcated and extending dual leading edges along the two competing paths until one leading edge collapsed and the cell was drawn along the "winning" path (Figure 50). It was quite rare ($< 1\%$ of the time) for a migrating cell not to be localized on the keratocyte network.

In order to quantify the preferential localization of the (neutrophils) on the keratocyte network, the percent of neutrophils localized on the keratocyte network was compared to randomly placed dots. After repeated counts, there was a significant difference ($p< 0.05$) in the number of neutrophils that coincided with the keratocyte network as compared to the random dots (99% vs. 75%). The keratocyte network covered about 75% of the image areas which corresponds with the random dot percentage of coincidence (Figure 51). Figure 52 cell tracking shows neutrophils following paths that coincide with the keratocyte network.
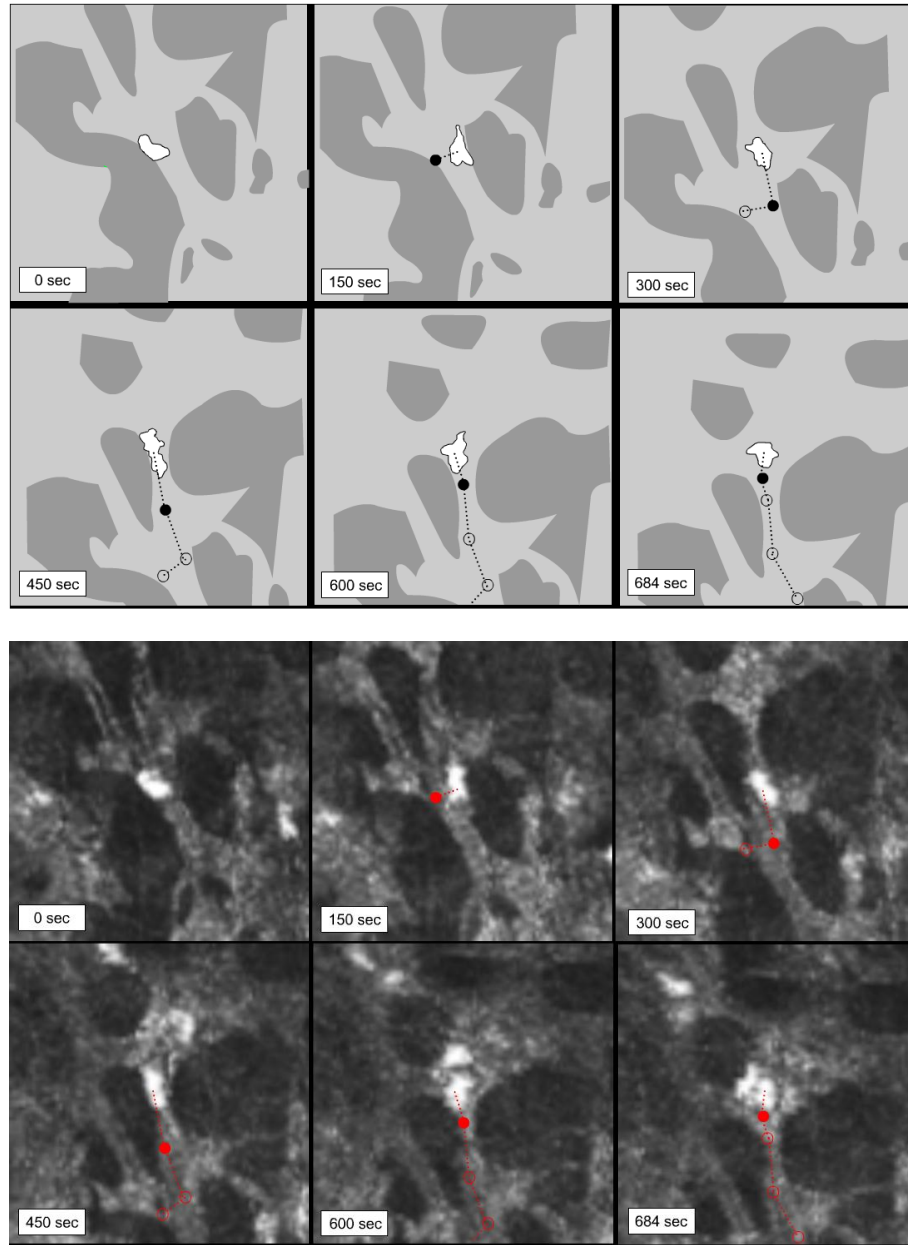
Figure 49 – Migration across keratocyte bridge

In (A) the light grey represents the keratocyte network and the darker grey the gaps in the network. This is a diagrammatic representation of the actual movie frames shown in the bottom panel (B). Frames are spaced 150 sec apart and clearly show the migrating cell following the keratocyte network in the parawound area.
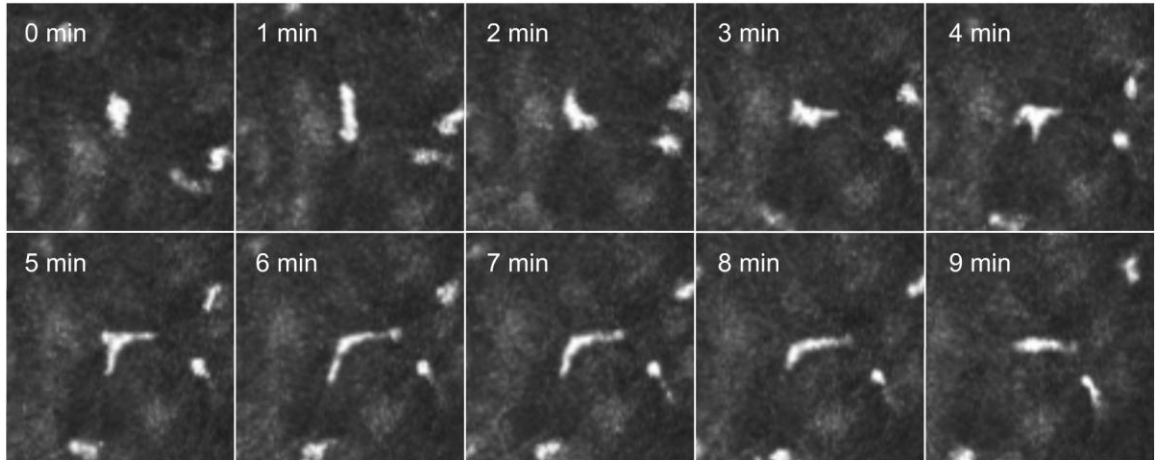
Figure 50 – Bi-directional decision

Cell in the center of the images goes from nearly round to a thin "V" shape (6 min) as it encounters a bifurcation in the network. If the neutrophil was not utilizing the network it would surely not have to make a "descision" and would simply continue moving randomly.
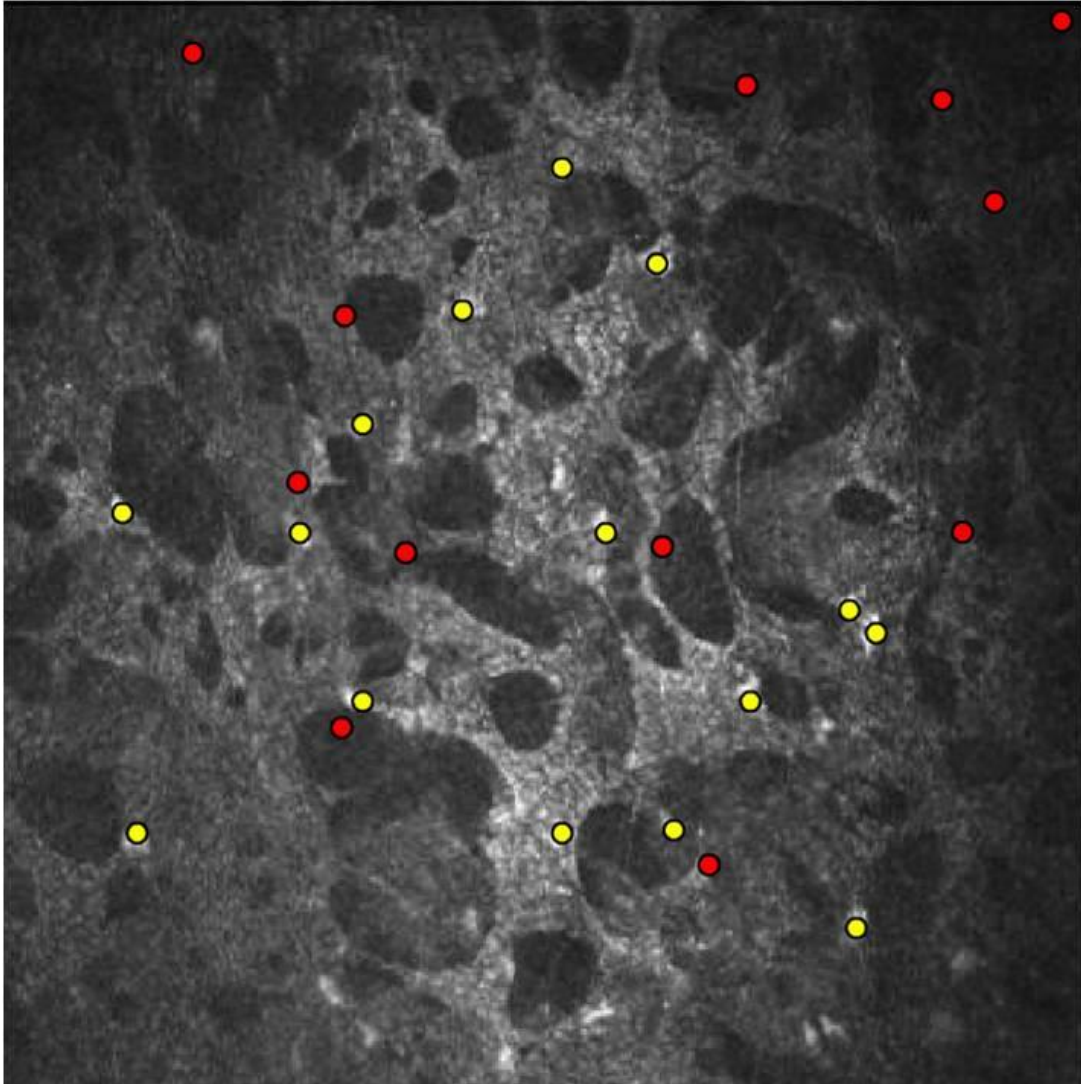
Figure 51 – Random dot placement

Neutrophils are marked with yellow dots. Red dots were randomly placed. More than

99% of the time yellow dots were determined to be on the keratocyte network, whereas

only 75% of the red dots. The keratocyte network covers about 75% of the image area.
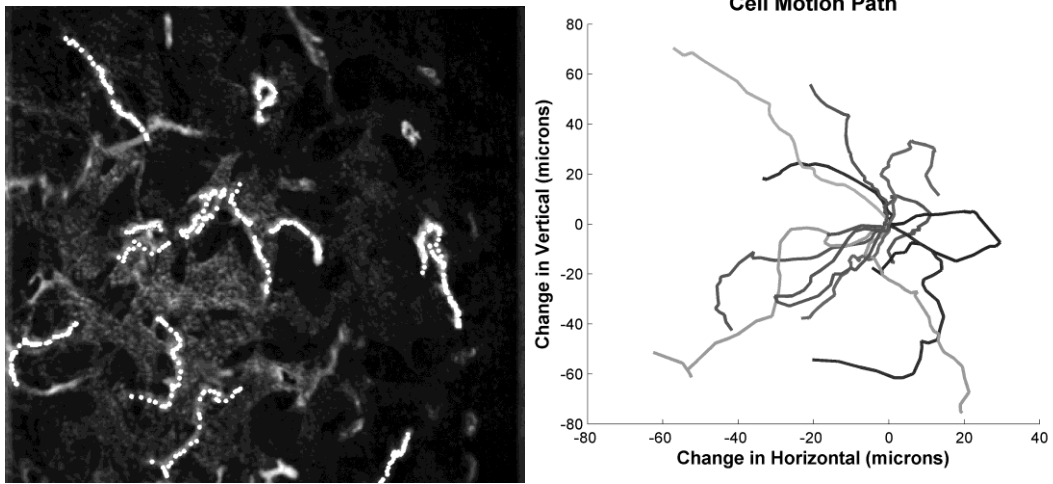
Figure 52 – Cell tracking

The left side image shows the actual cell tracks (white lines) over-laid on the HRT-RCM

image of the keratocyte network. On the right side is a polar plot of the cell paths placed

with a common point of origin.

Parawound vs. wound motility

At the 8 hour time after wounding used for all experiments, the epithelial wound was still incompletely healed with a gap of approximately 300 μm. Figure 53 shows a montage of images captured with the HRT-RCM where the wound is clearly visible after 8 hours and there is evidence of keratocyte death beneath the wound. Areas delineated with the yellow dotted lines represent the wound area and parawound area used for motility comparison. There was an obvious difference in cell motility with gross observation when comparing the areas beneath intact epithelium (parawound) to the area beneath the wound. Beneath the wound the neutrophils appeared to be restricted in their movement. Often they were seen to move back-and-forth along the same path and generally more random. Beneath the wound the keratocyte network was noticeably disrupted in the anterior half of the stroma, but normal in the posterior. Table 11 shows there was significantly more swelling within the wound as compared to the parawound area.

A semi-automated cell tracking MatLab program was developed to quantify individual cell motility using parameters described in the methods. The centroid of each of the randomly selected 12 cells was marked manually every 20th frame (1 frame per second) for the duration of the 10 minute sequences. Speed, velocity, and confinement ratio were compared between the parawound and wound areas and all three parameters were found to be significantly lower within the wound area (34.5%, 59.1%, and 41.7%, respectively) as shown in Figure 54 and Table 12.
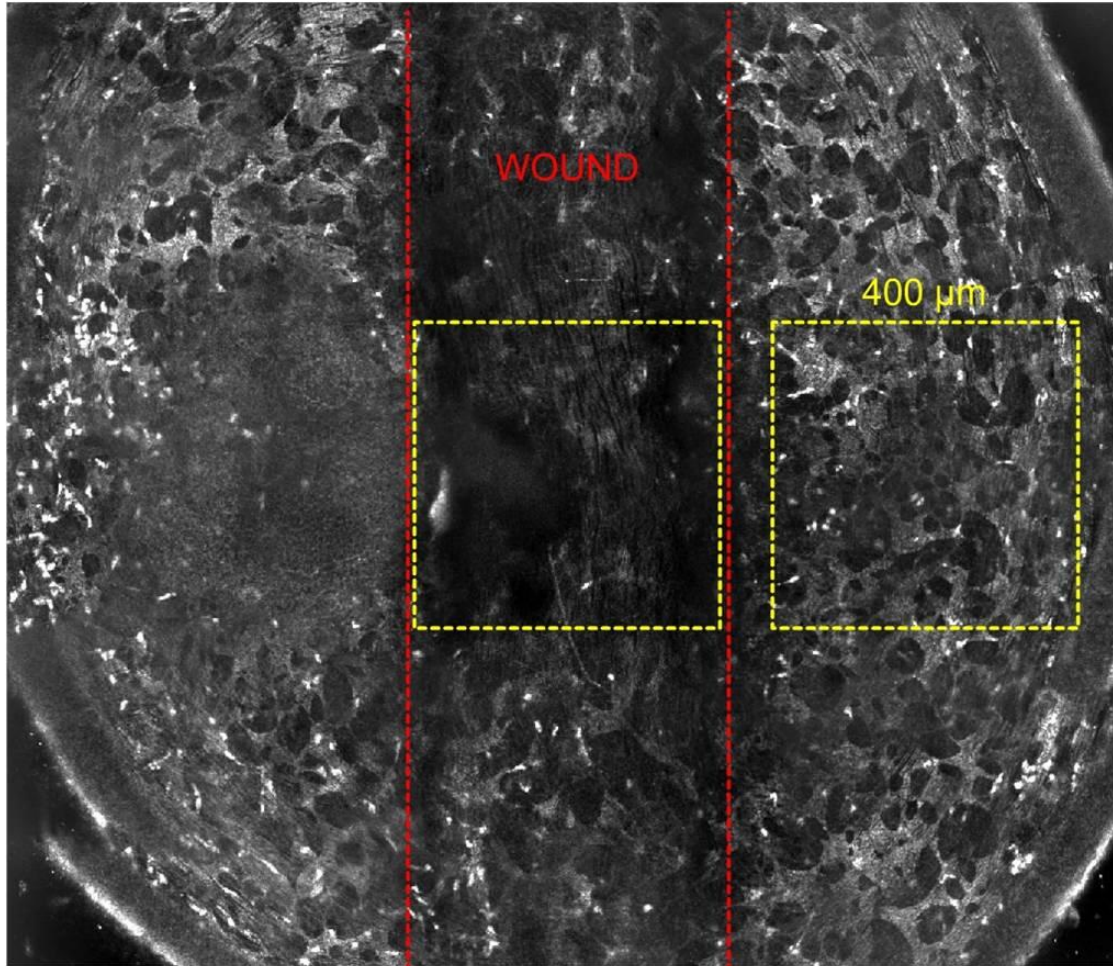
Figure 53 – HRT-RCM montage with wound

A montage created with images of the keratocyte network just beneath the epithelium (a

patch of epithelium is seen to the left of the wound). The yellow dotted-lines represent

the size of the area imaged with the HRT-RCM. The keratocyte network beneath the

wound (between red lines) is indistinct compared to the parawound area. This example is

displaced somewhat inferior to the cornea center and the bottom of the area between the

red dotted lines is outside the wound.
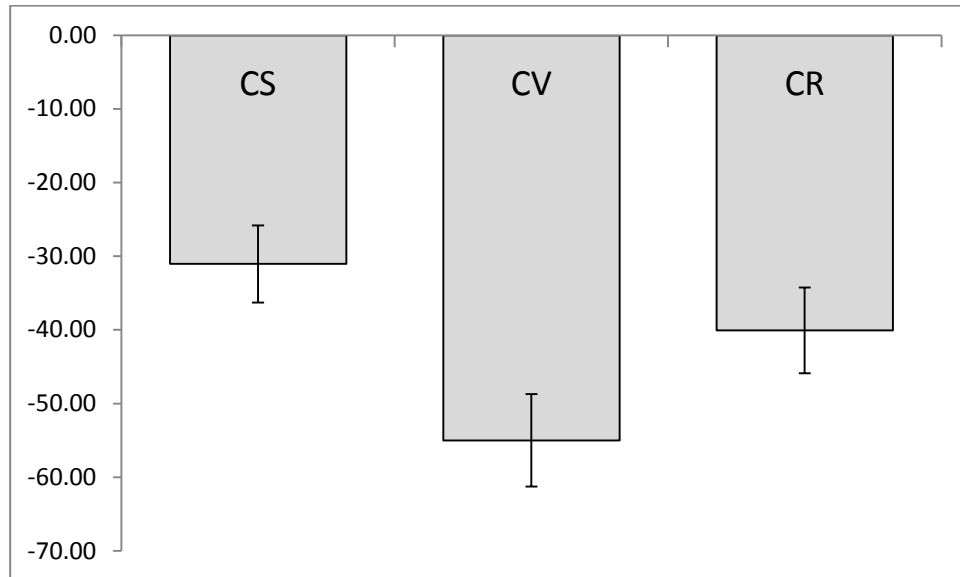
Figure 54 – Wound vs. parawound parameters

All three parameters were significantly reduced beneath the wound as compared to

the parawound area. Cell velocity was reduced even more than speed, resulting in

reduced confinement ratio and indicating cells were moving in a less straight path.

Table 12 – Wound vs. parawound parameters

Parameter	Parawound	Wound	% difference
Cell Speed	5.70±0.41 µm/min	3.73±0.25 *	-31.05±5.23
Cell Velocity	3.07±0.33 µm/min	1.26±0.33 *	-59.09±6.28
Confinement	0.51±0.03 µm/min	0.30±0.03 *	-40.08±5.82

(* = p<0.05)

3.2.3 Discussion

The HRT-RCM was developed as a clinical instrument, providing *in vivo* imaging of the

cornea, but over the past few years has been used for numerous animal and human

research studies. This instrument utilizes a 670nm scanning diode laser to obtain confocal

images with an acquisition time of 0.024 seconds and transversal optical resolution of

approximately 1µm/pixel (Heidelberg Engineering). The objective lens used in the

corneal module was the x60 immersion lens (0.90 N.A) which produced images 384 x

384 pixels covering an area of 400 x 400µm (Olympus, Hamburg, Germany). It has

previously been shown with the HRT-RCM rabbit and human keratocyte nuclei are easily

visualized whereas their cytoplasm is not [45, 46]. By contrast, in rats and mice, the

keratocytes are seen as hyperreflective stellate structures without visible nuclei [45]. It

has been shown that in chronic stromal edema (in humans) the keratocytes become

hyperreflective with well-defined cell bodies and processes but without visible nuclei

[47]. While some authors have described keratocytes with hyperreflective cell bodies as

"activated", there is no evidence showing phenotypic transformation and most likely the

hyperreflectivity is due to a difference in the ECM surrounding the keratocyte such as

occurs with edema. Consistent with these previous descriptions, our results allowed

visualization of the keratocyte cell bodies and their interconnecting processes however,

they were considerably more distinct and reflective 8 hours after wounding (with edema)

as compared to the unwounded corneas. Figure 55 illustrates the effect of applying a

hypotonic solution (nano-pure water) to the cornea and noting the change in appearance

of the keratocyte network.
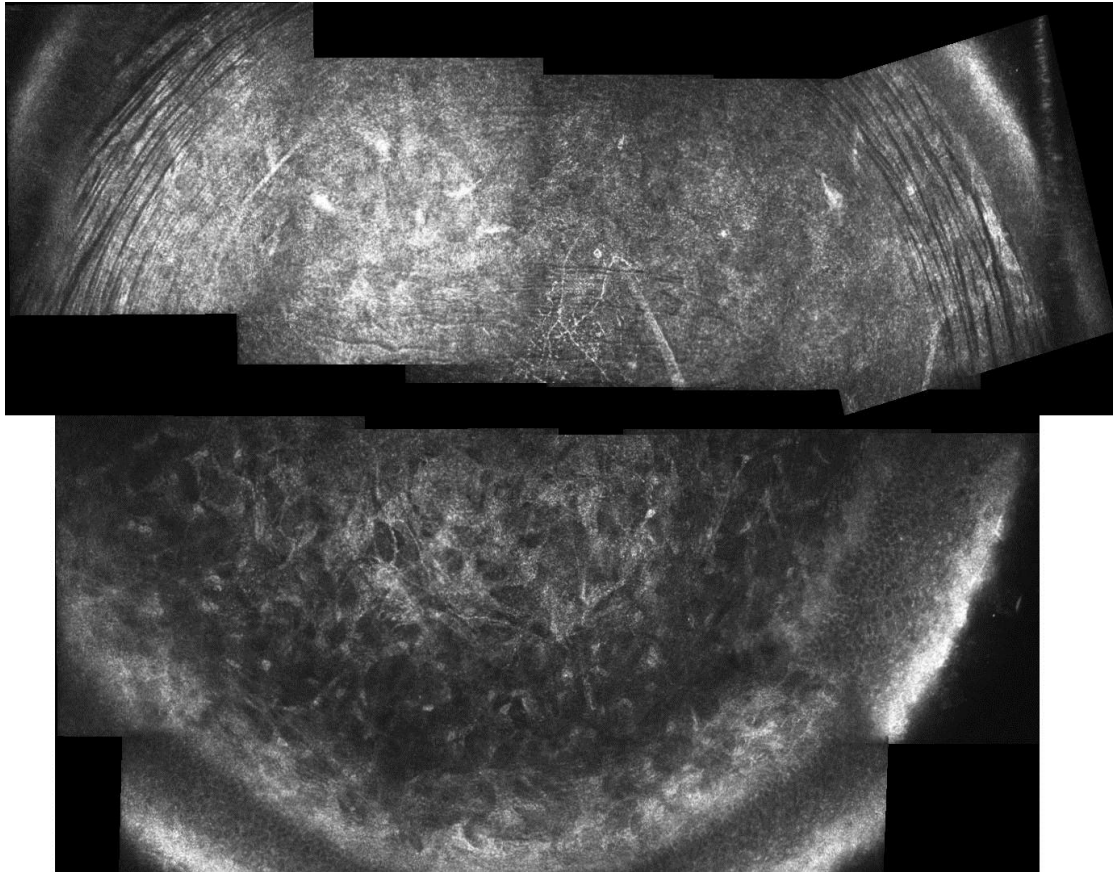
Figure 55 – Change in keratocyte network with water

Upper half of the image is an unwounded cornea in its normal state and lower half is the same cornea approximately 10 minutes after topical application of purified water. The keratocyte cell bodies are more easily visualized after the addition of water.

Neutrophil locomotion has been described as amoeboid where the leading edge extends one or more pseudopods while frictional forces or chemical adhesion holds the leading edge in place as the cell body contracts and pulls the rear of the cell forward [48, 49]. Neutrophil motility as noted with *in vivo* HRT-RCM time-lapse imaging was consistent with this type of locomotion.

Observations of neutrophil motility along with the quantification of neutrophil localization on the keratocyte network convincingly show that neutrophils preferentially migrate along the keratocyte network. Additionally, when neutrophils were tracked beneath the wound they showed reduced speed and less directed locomotion. These findings are consistent with previous studies showing CD18 and ICAM-1dependent surface contacts between neutrophils and keratocytes [9, 44]. However, there are other plausible explanations besides just loss of potential contact with keratocytes. As noted in Figure 46, there is significantly more edema beneath the wound compared to the parawound. Numerous authors have reported from *in vitro* 3-D migration experiments that the physical environment has a profound effect on neutrophil motility [50, 51]. It has been shown that there is an optimum spacing between matrix elements for efficient motility. Beyond that spacing distance, motility very likely switches from relying predominantly on physical/frictional forces to adhesion molecule binding [52, 53]. Therefore the amount of edema present in the wounded area may force the migrating cells to rely on other mechanisms of locomotion. An additional factor affecting neutrophil motility is the fact that keratocytes die beneath the wound and neutrophils are involved in clearing the area of debris. This may explain why they not only moved slower but also followed a less direct path. Chemokines that have likely diffused through the

stroma after injury would establish a gradient that guides neutrophils to the wound site. Once neutrophils have reached the source of chemokines (wound) there would be no more gradient to guide their migration.

Previous neutrophil motility studies have typically used *in vitro* methods or *in vivo* tissues other than the cornea with experimentally applied chemoattractants. Obviously there are many differences in the physical and molecular environment comparing these conditions to an *in vivo* model of inflammation induced by epithelial abrasion. However previously described motility parameters are useful for *in vivo* analysis in the cornea. Cell speed is the most commonly reported parameter. However, some studies fail to distinguish between speed and velocity. Speed is the total distance an object travels per interval of time, regardless of how many times it changes direction during the interval. Velocity, on the other hand, is the vector value representing the straight line displacement that occurred during the time interval. In this study cell speed (CS) was recorded as well as cell velocity (CV). Other studies have described the ratio of CS and CV using various names, such as chemotactic index, directionality, McCutcheon index, and confinement ratio (CR).

These parameters are reported as average values for individual cells. However, when looking at the migration characteristics of a population of cells, other parameters are more descriptive. One such parameter frequently reported is the mean squared displacement, or alternatively the mean displacement plot (MDP). These plots have been used to characterize cell motility, even implicating methods of locomotion such as random, guided, or confined movement.

3.3 – Role of integrins in neutrophil migration

3.3.1 Introduction

An epithelial abrasion compromises the anterior tight junctional barrier, releases

cytokines, and induces keratocyte death. It is important for the cornea to be repaired as

quickly as possible to maintain or restore sight and, as a result, insult to the cornea

invokes rapid and extensive inflammation with neutrophils providing the major cellular

response. Neutrophils are well known for their ability to destroy and remove invading

pathogens. However, it is well known that they also play an important role in wound

healing even in the absence of pathogens. As neutrophils are the major cellular element

of the inflammatory response, they have been the focus of considerable research relating

to corneal wound healing. While the sequence of rolling (selectin dependent), firm

adhesion to the vascular endothelium (integrin dependent), and diapedesis of neutrophils

(PECAM-1-dependent) has been extensively researched and described, relatively little is

known about extravascular interstitial migration through densely packed collagen within

the corneal stroma. Much of what we do know has come from *in vitro* 2-D or 3-D matrix

models which are limited by their ability to duplicate the nuances of the physiological or

physical native environment. Another consideration in *in vitro* studies that is often not

taken into consideration is the activation state of the neutrophils. Circulating neutrophils

and transmigrated neutrophils are significantly different in their expression of surface

molecules as well as other cellular processes [54].

Considered to be primarily adhesion molecules for cell-cell or cell-ECM binding,

integrins are also important for cellular functions such as cell migration and signaling

[55-58]. Neutrophil migration within the corneal stroma involves contact with extracellular matrix and resident stromal keratocytes, and cell surface integrin receptors have been implicated in these interactions [55]. It has recently been shown that neutrophils make close contact with keratocytes during the process of interstitial migration and these contacts are mediated by the leukocyte unique β2 (CD18) integrins (Figure 56) and ICAM-1, a β2 integrin ligand [9, 44].While members of β2 (CD18), and additionally, β1 (CD29) and β3 (CD61) integrin families are expressed on extravascular migrating neutrophils [55, 59, 60] it has been concluded from *in vitro* studies that locomotion of activated neutrophils is dependent on integrin binding on 2-D surfaces but is independent of integrin binding in 3-D matrixes [53, 57, 59, 61-64]. However, the role of integrin binding during *in vivo* corneal stroma migration has yet to be clearly defined.
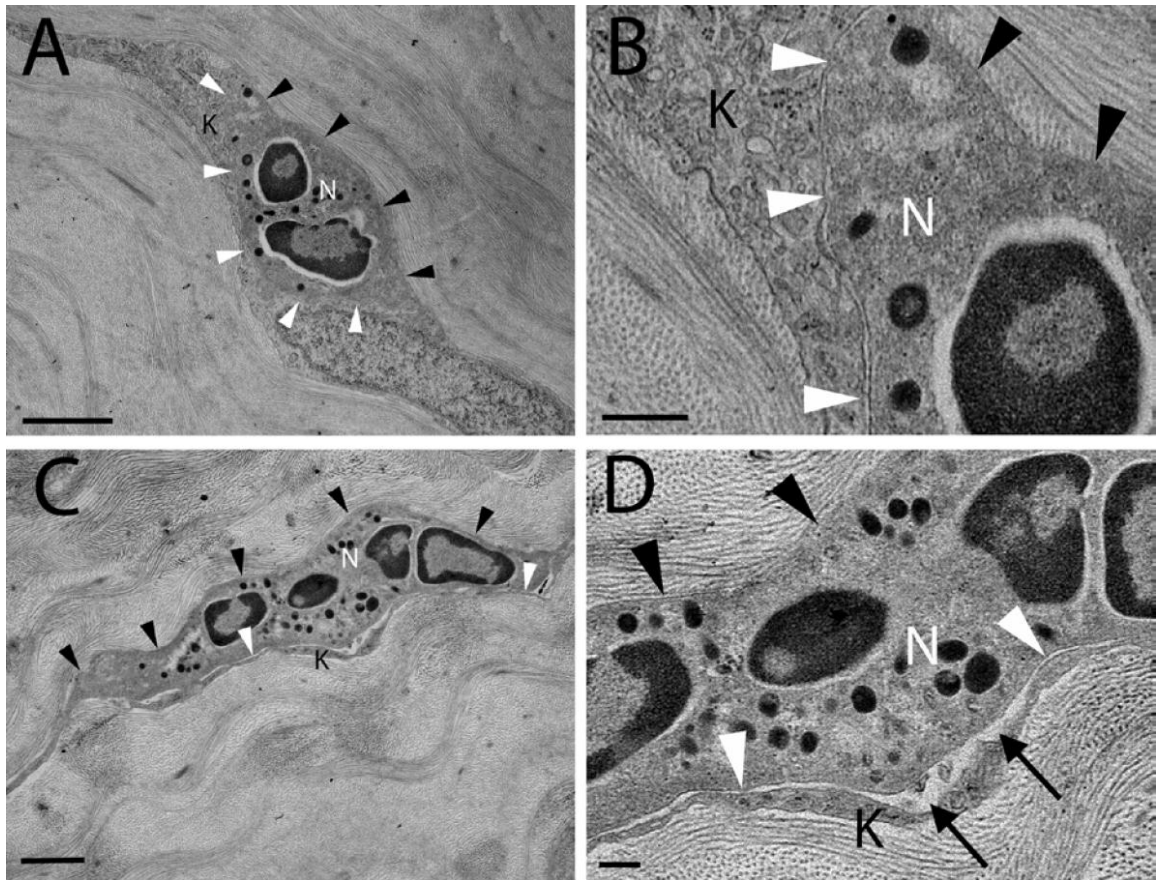
(images courtesy of D. Gagen)

Figure 56 – Loss of close contact

Electron micrographs (A, B) from wild type and (C, D) from CD18$^{-/-}$ mice. The 'N's"

identify neutrophils, the white arrow heads show interface between neutrophils and

keratocytes, black arrow heads the interface between neutrophils and collagen. The

enlarged view (D) of (C) shows gaps between the neutrophil and keratocyte. Scale bars

2μm (A),0.5 μm (B), 5 μm (C), 1 μm (D).

The purpose of this study was to determine the relative contribution of β1 (CD29), β2 (CD18) and β3 (CD61) integrins to neutrophil locomotion in the inflamed murine cornea by investigating *in vivo* effects of blocking antibodies against the indicated integrins. *In vivo* data obtained using Heidelberg Retinal Tomographer III with Rostock Corneal Module (HRT-RCM) time lapse sequences provided the means, for the first time, to quantify speed and directionality of cellular movement while observing neutrophil interaction with stromal keratocytes in the living eye.

3.3.2 Results

Identification of inflammatory cells

The Algerbrush provided an efficient means to remove the corneal epithelium in a vertical stripe that was approximately 0.5mm in width. Representative corneas previously examined by electron microscopy verified that the basement membrane remained intact (data not shown). At the time of imaging, eight hours after wounding, the wound remained open and the stromal thickness was increased compared to the unwounded as seen with the HRT through-focus. As others have reported, scanning with the HRT-RCM reveals a well defined keratocyte network in the mouse and rat cornea which was easily visualized in the regions of interest in our imaging [45]. Associated with this network, in the anterior stroma, we observed numerous, highly reflective bodies, ranging in shape from round to stretched-out oval with a typical size of approximately 3-4µm by 8-10µm. These bodies were not seen in uninjured corneas and were presumed to be infiltrating inflammatory cells.

In order to demonstrate the identity of these cells, harvested corneas were immuno-stained for Ly-6G, a specific neutrophil marker. A cornea whole-mount showing neutrophils labeled with Ly-6G is shown in Figure 57. At 8 hours after the epithelial injury there are still many neutrophils which have not reached the central wound area. The dotted rectangle in this figure is the area covered by the HRT-RCM montage in Figure 58. The distribution and density of cells appears comparable. In the close-up views in Figure 59 it is even more apparent that cell density was similar for the comparable areas imaged by HRT-RCM as compared to whole-mount Ly-6G labeled cells. This information, along with the size, speed of locomotion (as seen with time lapse imaging), and time of appearance in the stroma [65], positively identified the cells as neutrophils. The pattern of infiltrating neutrophils showed the greatest density in the paralimbus and gradually tapered off toward the center of the cornea. If the wound was slightly off center, there were considerably more neutrophils on the side with the least distance between the wound and the limbus, either nasal or temporal. Thus suggesting a stronger inflammatory stimulus is received at the limbus closest to the wound. Likewise, within the wound there were clusters of neutrophils at the top and bottom, which were obviously close to the limbus, but the rate of migration toward the center was apparently reduced, as seen by the distribution pattern (Figure 57). In a previous section it was shown with time-lapse imaging that the speed of neutrophil locomotion is reduced beneath the wound as compared to the parawound.
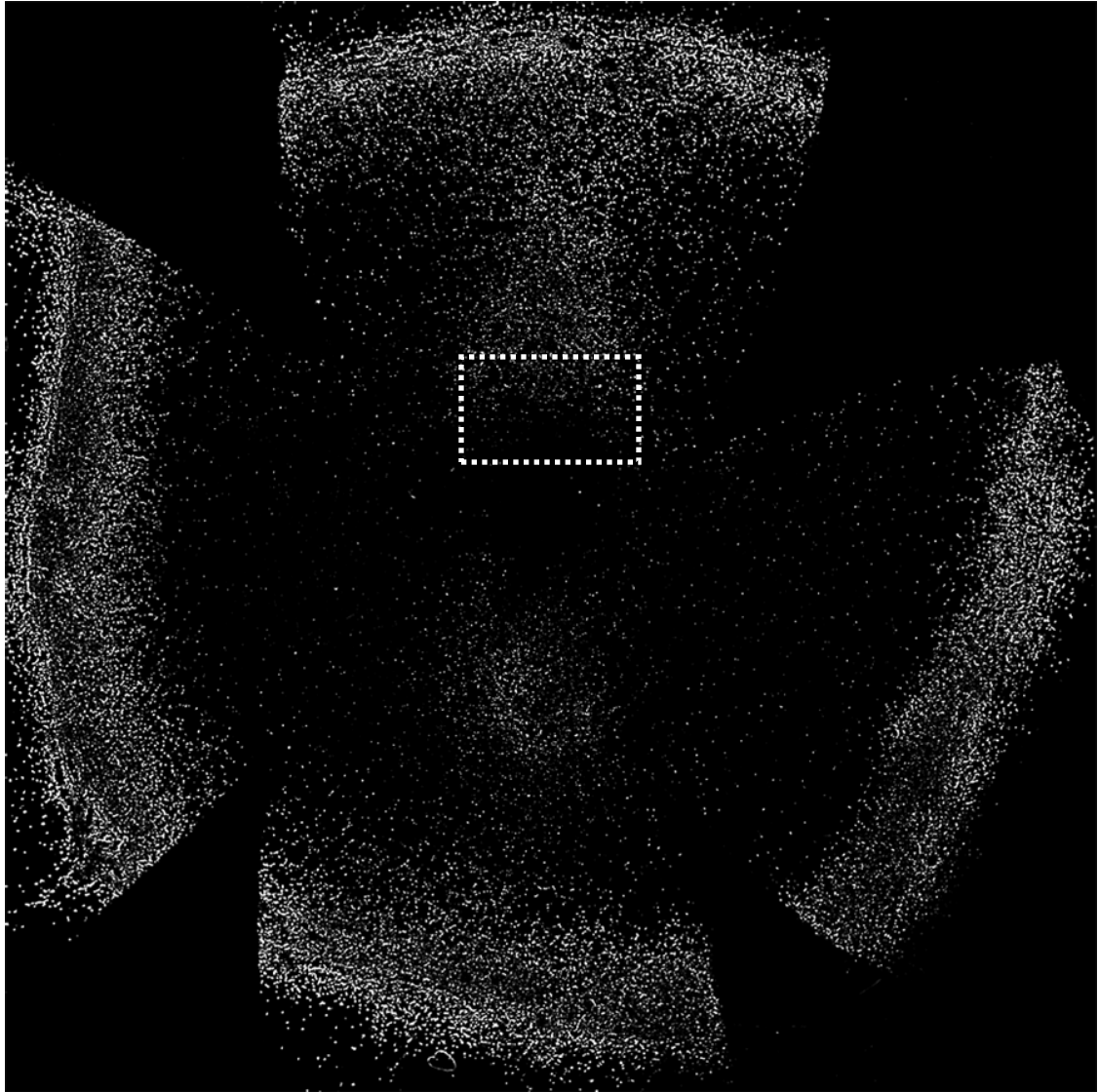
Figure 57 – Ly-6G immune montage

A montage of 10x images of the entire mouse cornea whole-mount showing the pattern of infiltrating neutrophils (light spots) 8 hours after epithelial injury. Neutrophils were labeled with a primary antibody against Ly-6G conjugated with FITC. The epithelial wound is oriented vertically in the center of the image with relatively higher density of neutrophils at both ends. The dotted rectangle (600 μm horizontally) represents the area shown in Figure 58.
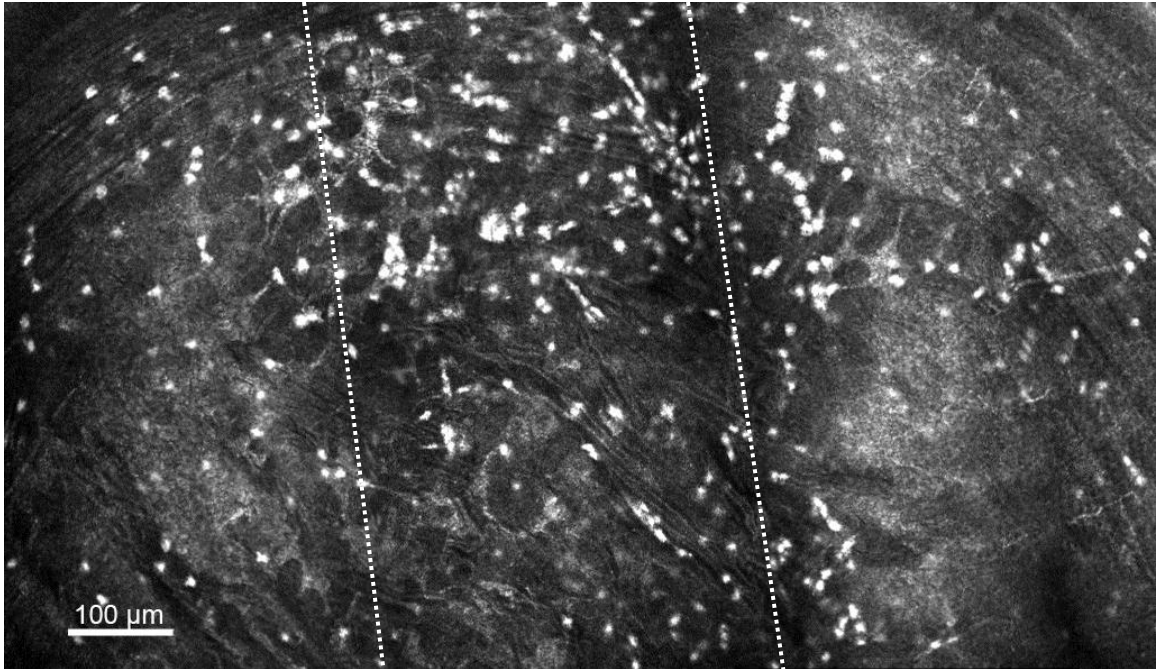
Figure 58 – HRT montage of same eye as Figure 57

This HRT-RCM montage covers approximately the same area marked on Figure 57 at the upper

end of the wound. In this image the dotted lines mark the edges of the wound at 8 hours after

injury. The density and distribution of highly reflective bodies corresponds with the labeled

neutrophils from Figure 57.
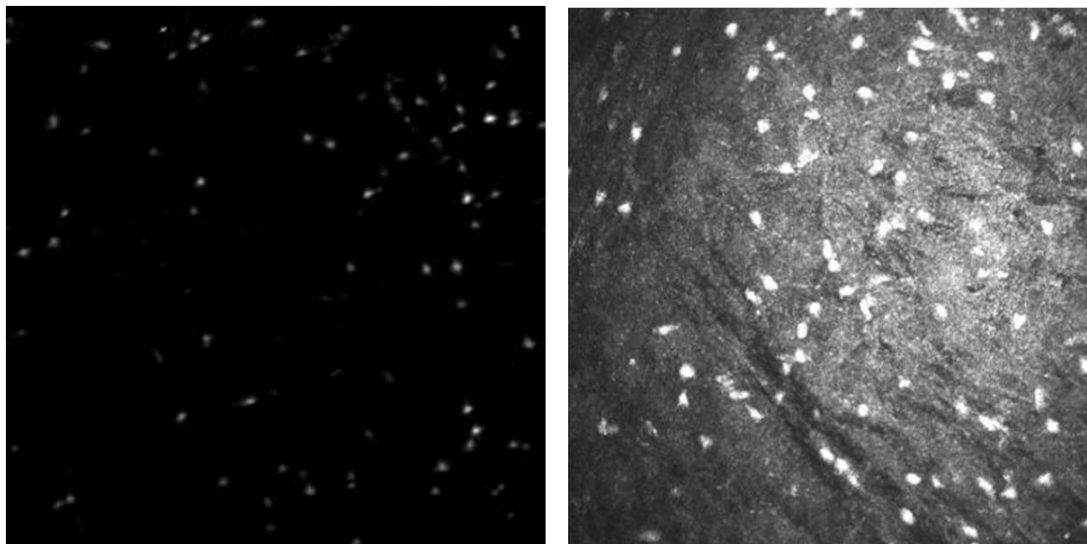
Figure 59 – Ly-6G compared to HRT

The image on the left is a close-up from Figure 57 (Ly-6G labeled) and the image on the

right a close-up from Figure 58 (HRT). Although not a perfect match the distribution of

cells is quite similar strongly suggesting they represent the same population.

Diffusion of blocking antibodies

Blocking antibodies against the β1 (CD29), β2 (CD18) and β3 (CD61) integrin families were topically applied at the time of wounding and imaged 8 hours later with HRT-RCM in order assess the relative contribution of each to neutrophil locomotion. Penetration and diffusion of the blocking antibody within the stroma was assessed by immunofluorescence microscopy after incubating the excised corneas in fluorophore-conjugated secondary antibodies. With the removal of the epithelial barrier in the wound and the small molecular size of the unconjugated blocking antibodies, diffusion of the antibody was evidenced by the labeling of neutrophils in all regions of the cornea (Figure 60).
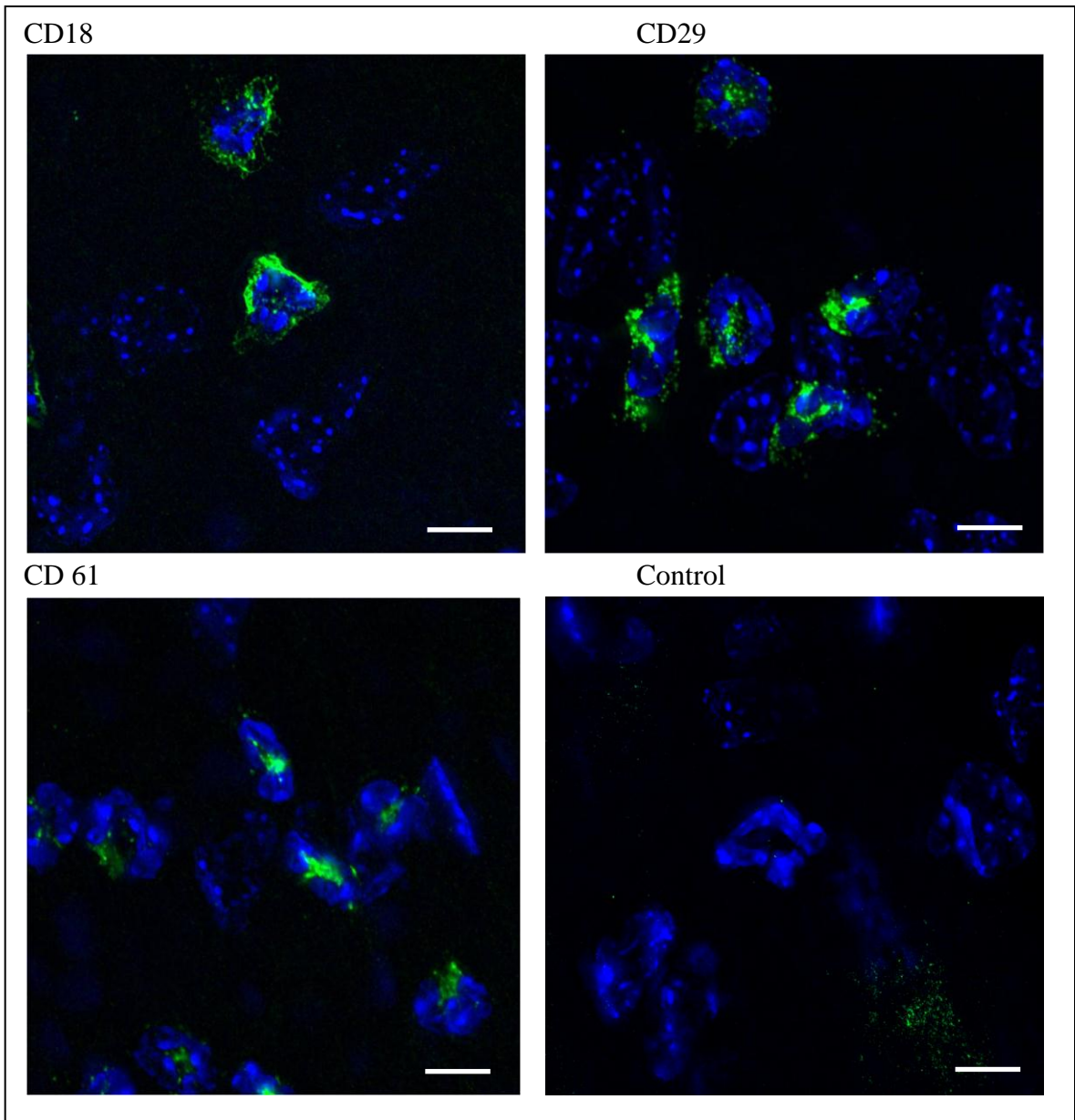
Figure 60 – Immuno-labeling to show antibody diffusion

In each case FITC (green) conjugated secondary antibodies labeled neutrophils throughout

the cornea showing that the primary blocking antibodies had diffused through the stroma

from the wound to the limbus. Each of the four images was obtained mid-way between the

wound and the limbus. Lower right corner of control image shows some green background

labeling. Scale bars = 10 μm.

Motility parameters

The effect of integrin blocking was assessed by the average cell speed (CS) and cell velocity (CV). The ratio of CV to CS confinement ratio (CR) served as an indicator of how closely a cell track followed a straight path. Table 13 shows the values for CS, CV and CR for each of the experimental conditions. There was no significant difference in CS (p=0.73) or CV (p=0.89) when the same observer analyzed the same corneas on two separate occasions.

The average CS in the IgG control eyes was 7.56±0.20 (SE) μm/minute with a CR of 0.58±0.02 (Figures 61 and 62). No significant difference in either parameter was found with blocking β2, or β3. However, β1 blockade produced significant reduction in CS and CR (31 %, 33% respectively). The reduction in speed indicates that β1 integrin binding facilitates neutrophil migration while the reduction in CR indicates the cells followed a less direct path and binding may help to steer the movement. In order to determine if blockade of one integrin was compensated by increased dependence on one of the others, the three blocking antibodies were combined into a single cocktail with results not different from β1 blockade alone (data not shown).

Figure 63 (A-D) shows representative mean displacement plots (MDP) for each of the experimental conditions. The mean displacement plot is a factor of velocity and the persistence of directional motion, or directedness. The slope for β1 blockade was significantly less than the control group which corresponds with the lower CV as well as the lower CR noted in Figure 62. The other experimental groups were not significantly different than the control group.
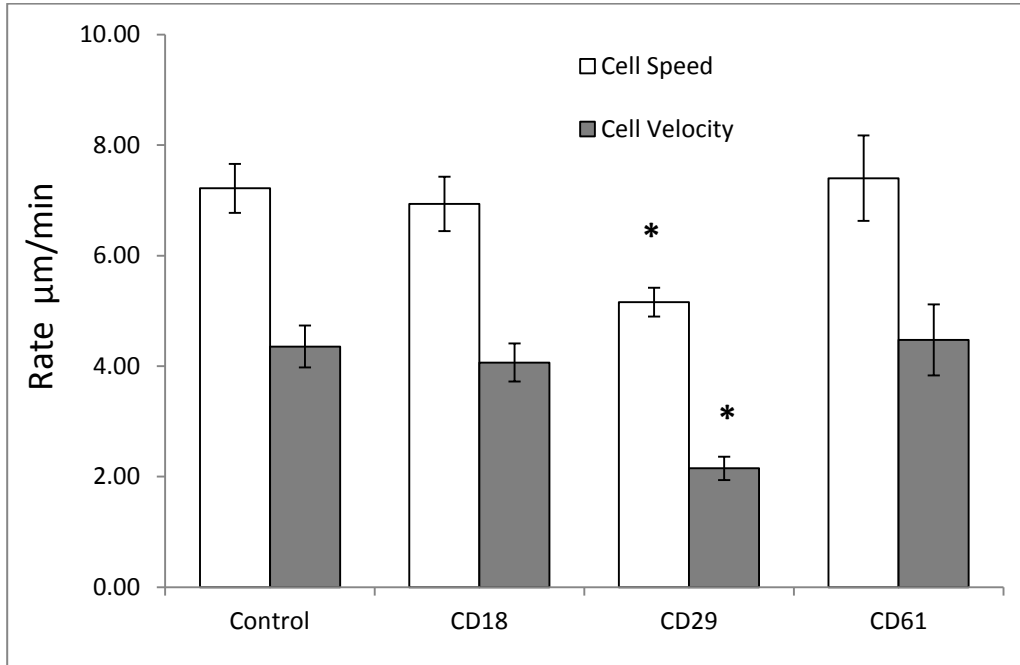
Figure 61 – Integrin blocking CS and CV

Both cell speed (CS) and cell velocity (CV) were significantly less with CD29 (β1) blockade.
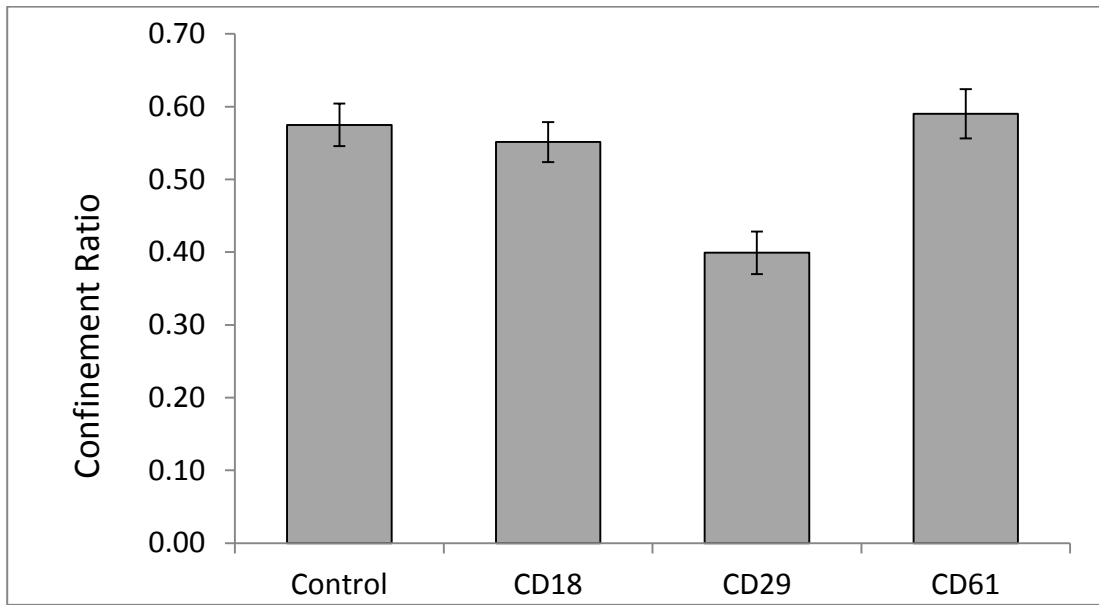
Figure 62 – Integrin blocking confinement ratio

The confinement ration (CR) was significantly less after blocking CD29, indicating the neutrophils were migrating in a less straight path.

Mean Displacement Plots (mean displacement in microns vs. sqrt of time)
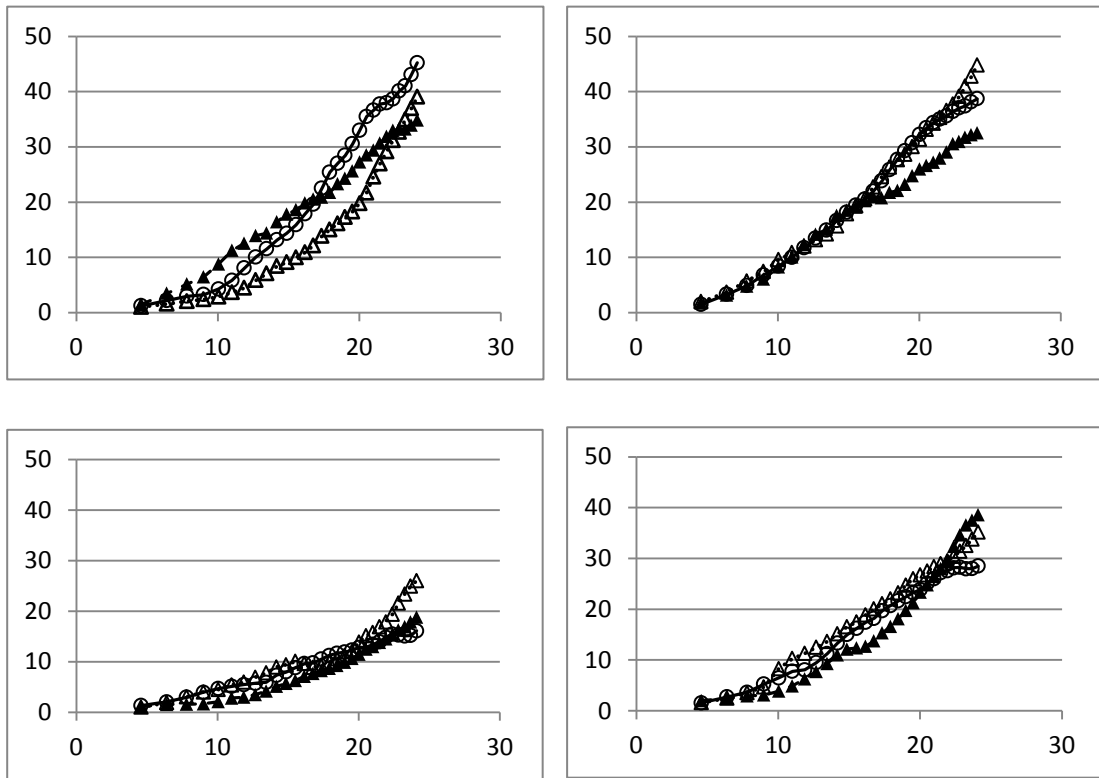
Figure 63 – Integrin blocking mean displacement plot

Mean displacement plots from 3 representative corneas in each experimental group show

a significantly flatter slope with the CD29 cells.
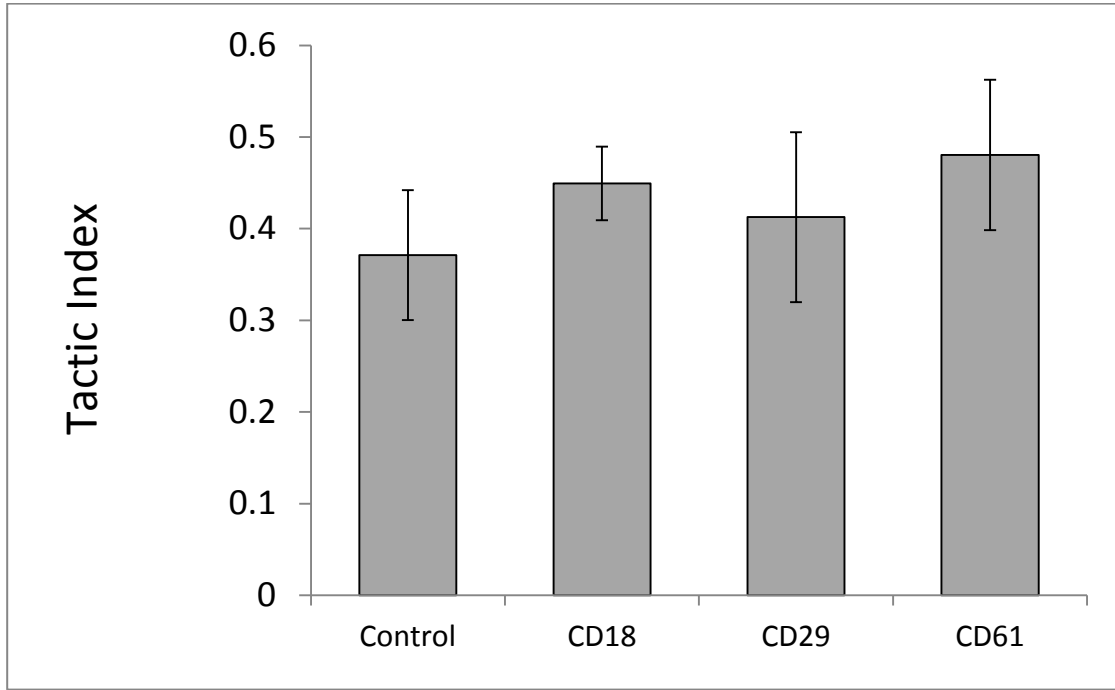
Figure 64 – Integrin blocking tactic index

The tactic index was not significantly different for any experimental group. Indicating

that integrin blocking had no effect on the group migration directionality.

Table 13 – Motility summary

	Control	CD18	CD29	CD61
CS	7.56±0.20	7.62±0.23	5.18±0.17*	7.41±0.23
CV	4.47±0.21	4.41±0.22	2.18±0.18*	4.43±0.25
CR	0.58±0.02	0.55±0.02	0.39±0.03*	0.58±0.02
TI	0.41±0.06	0.47±0.04	0.48±0.04	0.38±0.08
n	12x12	11x12	7x12	7x12

Speed and velocity μm/min ± standard error of the mean. The number of samples, n = number of corneas x number of cells per cornea (* = $p<0.05$)

The TI was not significantly different between the experimental groups (Figure 64), indicating that none of the blocking antibodies affected the guidance of the cell group. That is, migration of the population of cells in a specific direction was not affected, only the velocity. Out of 29 corneas imaged, 19 showed a population migration direction moving toward the wound, 7 were parallel, and 3 away from the wound. There was no trend for the different experimental conditions that would indicate an effect on direction of migration toward or away from the wound. The average TI for the groups was not significantly different and ranged from 0.37 ± 0.07 to 0.48 ± 0.08 which indicates that whatever guides cell migration is only about 40% effective in guiding the groups of cells in a particular direction, which in a few cases was away from the wound. The TI was not significantly different among the experimental groups, suggesting that none of the experimental conditions affected the group tendencies to move in a particular direction.

The migration angle which describes the average direction of displacement for a group of cells was determined to be positive (toward the wound) 59% of the time, neutral 26%, and negative 15% of the time (Figure 65).
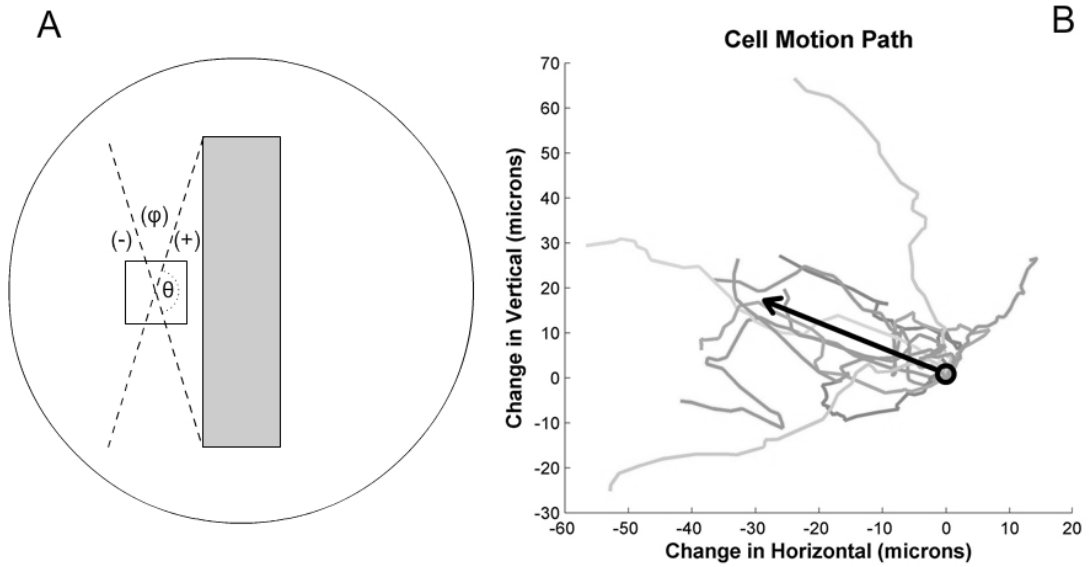
Figure 65 – Group migration angle

A group of cells was considered to be moving toward the wound (+) if the migration angle was within $\pm 75^{o}$ of perpendicular (angle θ) to the orientation of the wound, neutral movement if $\pm 15^{o}$ of parallel (angle φ), or (-) otherwise (A). The vector average for 12 tracked cells (B) defines the migration angle.

Stromal thickness and structure

In addition to recording image sequences with the HRT-RCM, volume scans were also obtained which provided a measure of stromal thickness. In comparing average thickness between the experimental groups, there was no significant difference. All of the experimental groups were significantly thicker (approximately 35%) than the uninjured average thickness (Figure 66).

Random corneas from each of the experimental groups were processed as histological sections using the biomicrowave and examined with the DeltaVision microscope. There were no observable differences among the corneas with particular attention given to the location and degree of interlamellar separations.

Our results then show that the blocking antibodies diffused throughout the stroma and β1 blockade alone reduced cell speed and velocity, and increased the deviation from a straight path without obvious physical differences in the stroma. However, none of the blocking antibodies prevented the migration of neutrophils or affected the group tactic response.
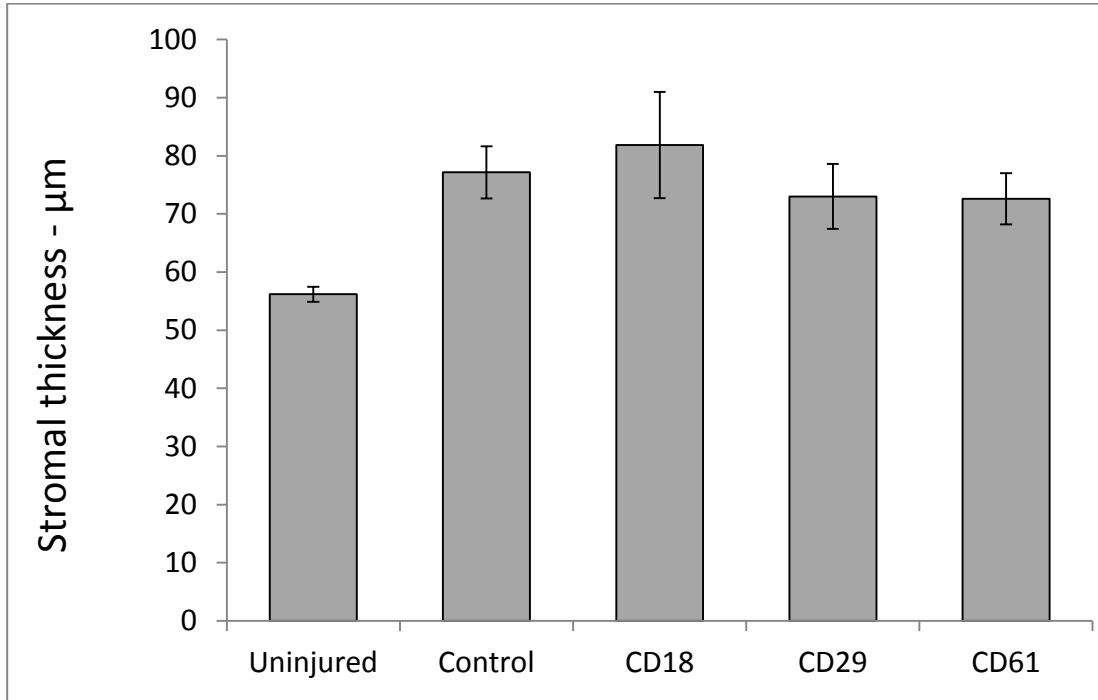
Figure 66 – Integrin blocking stromal swelling

Stromal thickness was determined by HRT-RCM through focus. Eight hours after

epithelial wounding there was approximately 35% swelling as compared to the

uninjured. The blocking antibodies had no significant effect on the amount of swelling

as compared to the IgG control.

3.3.3 Discussion

The purpose of the current study was to investigate the potential role of three integrin families in the interstitial migration of neutrophils in the inflamed murine cornea. I*n vivo* imaging with the HRT-RCM provided evidence that neutrophil locomotion within the inflamed corneal stroma is largely integrin-independent.

Histological sections can only provide information about a single instance in time and, as previously pointed out, they introduce the possibility of artifacts. In spite of these shortcomings, they have given us invaluable details about the physical environment, morphology of cells, and, with immunohistochemistry, they have shown expression and localization of molecules involved in cellular activities. Live cell *in vitro* studies have provided additional information about the dynamics of these cellular activities, but even the most robust 3-D matrixes fall short in terms of incorporating all the nuances of the *in vivo* environment. *In vivo* studies have been limited due to the lack of methods for observing cells in their unperturbed environment. Imaging technology is constantly advancing and developing tools for increasing our understanding of many of the cellular activities previously only speculated.

Although some aspects of motility research may require *in vitro* studies, where extraneous variables can be eliminated or accounted for, characterizing migration of neutrophils within the context of their native environment has to be considered in order to have a complete understanding of the mechanisms involved and the controlling factors. As described in chapter 1, the corneal stroma has a highly structured and compressed collagen fibril arrangement undergoing force applied by the intraocular pressure, as well

as osmotic forces. The physical structuring of the collagen fibrils into criss-crossed lamellae, in addition to the keratocyte network, interspersed between them, contribute to producing a unique physical environment and one that undoubtedly has significant impact on neutrophil migration through this area. Besides the physical challenges of migration in the stroma, there are interactions between neutrophils and their surrounding cells and ECM that potentially modulate neutrophil trafficking. There are numerous cytokines and chemokines present within the stroma that are temporally variable. The only way to observe neutrophils with all these variables in play is via *in vivo* microscopy.

The optical principal of a confocal microscope, simply stated, is a microscope that allows only in-focus light rays from a single focal plane to pass through the oculars or the image capturing device. The term confocal refers to the fact that the point in the image plane is coincident with or confocal with the point source [66]. The use of confocal microscopy for *in vivo* imaging has been particularly useful for the cornea. There have been several *in vivo* confocal microscopes developed for clinical use of the human cornea (see Patel, *et al.*, 2007 for a complete review) [67]. It is also becoming common for corneal research, as well [45]. The HRT, such as used for the experiments in this dissertation, has provided the opportunity to image dynamic processes such as leukocyte rolling along the vascular endothelium in response to inflammation [68].

The cornea, being an externally visible transparent structure that requires leukocytes to travel a considerable distance from the point of extravasation to the remote central cornea, lends itself to *in vivo* studies of leukocyte interstitial migration in the cornea. *In vivo* confocal microscopy using such instruments as the Heidelberg Retinal Tomographer (HRT) with the Rostock Corneal Module (RCM) provides such a means to record *in vivo*

188

imaging of inflammatory cells without surgical exposure of the tissue being examined. The HRT-RCM was designed for clinical use but requires no modification for imaging murine corneas and provides high resolution images [45, 46]. However, to the best of our knowledge, this is the first time it has been reported for time lapse migration studies of leukocytes in the murine cornea. The HRT-RCM provides a means for assessing *in vivo* dynamics that are not seen *in vitro* thus opening up the possibility of directly observing many tissue and cell processes.

Corneal insult results in pro-inflammatory signaling that engages the innate immune system and follows a well characterized cascade of events that initially involves extravasation of large numbers of leukocytes (primarily neutrophils) from systemic circulation within 1-2 hours. This process of neutrophil extravasation which has been thoroughly studied and well characterized, requires adhesion molecules. Selectins provide a means of slowing the passage of neutrophils, causing them to roll along the vascular endothelium and potentially become firmly adherent via integrins after which they transmigrate into the extravascular tissue, becoming activated in the process. The activated and transformed neutrophils must then provide intrinsic locomotion through avascular tissue consisting of a dense matrix of near-orthogonally crossed layers of parallel collagen fibrils with inter-connected keratocytes interspersed between these collagen lamellae. Keratocyte death directly beneath the wound begins shortly after an epithelial wound [42, 43, 69, 70] thus infiltrating neutrophils must migrate through regions with intact keratocytes as well as those with dead keratocytes; two distinctly different environments.

Neutrophils are among the fastest moving cells in mammals [62]. Studies have reported that neutrophils locomote in amoeboid fashion at average speeds of as low as 7um/min to possibly as high 30 µm /min [48, 51, 64, 71] Not surprisingly, our average cell speed in the parawound areas of control eyes (7.56±0.20 µm/minute) is somewhat slower than documented speeds for neutrophils in many other tissues (Table 14) likely due to the compact nature of the corneal stroma.

Table 14 - Neutrophil speed in other tissue

Tissue	Chemoattractant	Speed (um/min)
Cremaster	PAF	13.8±2.6
Cremaster	KC	10.9±1.8
Mesentery	PAF	14.7±1.4
Iris	Multiple endotoxin	7.6±4.7

(Planck, *et al*. 2008) [5]

Leukocyte motility has been previously studied primarily on two-dimensional surfaces and in three-dimensional culture media. The pattern of cell movement in 2D *in vitro* models has been described as random walk and is integrin dependent [48, 51, 64, 72] From 3-D *in vitro* experiments it has been reported that neutrophils may be integrin independent and operate by contact guidance, following paths of least resistance and using mechanical force to squeeze through the matrix [48, 53, 57, 59, 61]. These 2-D and 3-D experiments have provided much information however, neutrophils *in vivo* are in a complex, dynamic environment that can only partially be replicated *in vitro* and this environmental difference may have profound effects on how the migrating cells perform. For example, *in vivo* the stroma is composed of well organized compacted collagen

fibrils, which limits neutrophil migration to the potential spaces between lamellae. By contrast, 3-D collagen gel matrices are composed of randomly oriented collagen, which do not restrict migration to specific regions within the gel. Moreover, the phenotype of the extravasated neutrophil is known to be very different from that of the circulating neutrophil.

Since *in vitro* studies routinely use freshly isolated peripheral blood neutrophils, the behavior of these cells in 3-D matrices may differ markedly from that of neutrophils that have undergone diapedesis. In fact diapedesis likely prepares neutrophils for engagement with the ECM [54]. The corneal stroma has an organized architecture, contains cells and an assortment of proteoglycans, all of which may interact with migrating leukocytes. For example, Behzad *et al*. (1996) presented evidence that interstitial fibroblasts play a crucial role in providing directional information to migrating neutrophils [50]. Even though it has been shown that neutrophils migrate through 3-D matrices without integrin binding, the question of whether or not integrin binding affects neutrophil migration *in vivo* has not been definitively answered.

Integrins have been shown to be vital for cell migration in many situations however there are other locomotion mechanisms that may be employed. The role of integrins in neutrophil migration through the corneal stroma still remains unresolved. Results from our experiments indicate that neutrophil CS and CR were significantly decreased when blocking CD29 (β1) whereas, CD18 (β2) and CD61 (β3) integrin blockade had no effect. Suggesting at least a small role for CD29 (β1) integrins in neutrophil migration within the cornea interstitium.

β1 (CD29) integrin has been shown to be important in corneal development and in fact β1 (CD29) knockout mice die before birth [78]. However, conditional knockout of β1 (CD29) later in corneal maturation produced no structural differences compared to control corneas [79]. Dermal fibroblasts maintain the compactness of a collagen fiber network *in vitro* and control the tendency for the dermis to swell *in vivo* via CD29 (β1) mediated binding between fibroblasts and collagen [73]. Following this line of reasoning, it might have been expected that CD29 (β1) blocking would cause the keratocytes to release their binding to collagen fibrils resulting in increased swelling. If this were true, it might help to explain the decrease in motility parameters noted with CD29 (β1) blocking. However, our results showed this not to be the case as none of the blocking antibodies had a significant effect on the amount of stromal swelling after wounding.

β1 (CD29) integrins, also known as VLA (very late antigen) have several alpha units, are expressed in numerous cell types, and show high affinity interactions with proteins of the ECM [59]. Neutrophils have been shown to express α4β1, α5β1, α9β1 integrins which play a role in their adhesion and migration [55, 56, 74]. In addition, α2β1, α4β1, α5β1, α6β1 have been identified in stromal keratocytes. Their main ligands are laminin, fibronectin, and collagen [75, 76]. Our results showing that blocking β1 (CD29) reduced the speed of locomotion suggests that neutrophils use integrin(s) from this family to form "foot holds" (adhesive traction forces) that facilitate movement but the fact that speed was only reduced 28% shows that other mechanisms for movement co-exist. Werr, *et al*. [77] found more than 70% decrease in neutrophil speed in rat mesentery *in vivo* using β1 (CD29) blocking antibody while Friedl, *et al*. [63] reported that simultaneous blocking of β1 (CD29) , β2 (CD18) , β3 (CD61) , and αV integrins had no effect on T cell speed.

Our *in vivo* imaging showed neutrophils migrating preferentially along the keratocyte network in regions of the cornea where keratocytes were still intact. This is consistent with findings of Petrescu and colleagues who showed an extravascular role for neutrophil β2 (CD18) integrin in mediating close surface contacts with corneal keratocytes [44]. In addition Gagen, *et al*. showed that ICAM-1 (CD54), a ligand for β2 (CD18) integrin which is constitutively expressed on keratocytes and up-regulated during inflammation, is also required to maintain close contacts between neutrophils and keratocytes [9]. These findings raised the possibility of functional necessity of these adhesion molecules in the cornea. Burns and colleagues previously demonstrated a novel extravascular role for β2 (CD18) integrin in mediating PMN motility on cultured lung fibroblasts [80]. Indeed a recent study has shown that neutrophils and keratocytes make β2 (CD18) -dependent close contacts during corneal stroma migration and that the keratocytes act as a contact guidance mechanism, or "cellular highway" for neutrophil migration [44]. However our results support the notion that β2 (CD18) -dependent close contacts between neutrophils and keratocytes serves a purpose other than facilitating neutrophil migration. In agreement with our findings, previously it was shown that extravascular neutrophil accumulation at the limbus consisted of two waves, the first of which was β2 (CD18) dependent and the second was not. β2 (CD18) -/- integrin mice showed an absence of the first limbal wave, and were delayed at 24 hours in their accumulation at the limbus. After 24 hours they moved unhindered to the site of wound [65]. Thus showing that β2 (CD18) -independent mechanisms alone are adequate for neutrophil migration.

Even though several investigations have indicated a role for β2 (CD18) integrins in leukocyte chemotaxis, in our *in vivo* wound model, β2 (CD18) integrins did not appear to

have a significant role in extravascular neutrophil migration. The role of β2 (CD18) integrins is therefore likely to be through signaling, modulating activity of other integrins and/or cytoplasmic proteins rather than cell adhesion [59, 60, 81]. According to Saltzman, *et al*., 1999, neutrophil migration through collagen gels is CD18-dependent but only under conditions of high hydration, suggesting adhesion is only important when fiber density is relatively low [82]. As mentioned in chapter 1, the cornea stroma is maintained in a relatively deturgescent state and can undergo significant swelling if homeostasis is disrupted such as after an epithelial injury. Thus suggesting that stromal edema may have a bearing on the mechanism of neutrophil locomotion. Neutrophils, however, migrate between collagen lamellae rather than between individual collagen fibrils so *in vivo* studies are needed to confirm this possibility.

The third family of integrins investigated in this study, β3 (CD61) is essentially represented by only one member, αVβ3 found on both neutrophils and stromal keratocytes [75, 83]. Its ligands include fibronectin, vitronectin, fibrinogen, and tenascin-C which have been found to be present in inflamed corneal stroma [60]. Our results indicate that β3 (CD61) serves a purpose other than facilitating neutrophil migration.

The lack of effect when blocking β2 (CD29) or β3 (CD61) could have been due to a compensatory shift to dependence on one of the other integrins. However, when the three integrin blocking antibodies were combined the results were not different from what was seen with β1 (CD29) alone.

What are most informative for migration of a group of cells into the cornea are parameters which describe the group movement. In this study the vector average was used to represent the movement of a group of cells. This vector average gives a velocity

(migration velocity, MV) and a direction (migration angle, MA). The vector average takes into consideration the direction of displacement: to the right and up are positive, and to the left and down are negative. The MV and MA quantify the group movement as a single cell representing the group. A parameter not previously used but included in our analysis is the ratio of the average CV to the resultant MV. We chose to call this parameter the "tactic index" (TI). It indicates how closely the cells within the group follow a single direction of displacement. In our experiment the MA was compared to the location of the wound as a means to illustrate whether the infiltrating cells were being accurately guided to the site of inflammation.

The average TI (Tactic Index) for the groups was not significantly different from one another and ranged from 0.37±0.07 to 0.48±0.08, indicating that migration guidance is only about 40% effective in guiding the groups of cells in a particular direction. This would suggest a certain amount of randomness as well as lack of a strong or non-ambiguous directional guidance stimulus. Our *in vivo* model finds the neutrophils in a very complex environment with varying physical constraints as well as multiple competing local transient chemoattractant gradients. In a few cases the MA (Migration Angle) was away from the wound. Heit, *et al*. observed a similar behavior when they reported that a small percentage moved against gradient, even with fMLP stimulation [84].

In summary, the HRT-RCM provided the means to observe and quantify neutrophil migration *in vivo* and assess the effect of blocking each of three integrin families, β1 (CD29), β2 (CD18) and β3 (CD61), known to be expressed on extravascular neutrophils. Our results show that β2 (CD18) and β3 (CD61) blockade had no significant effect on

migration while β1 (CD29) blockade produced a significant, but not total, reduction in CS (Cell Speed), CV (Cell Velocity), and CR (Confinement Ratio), thus indicating that neutrophil locomotion within the corneal stroma does not require integrin binding, though β1 (CD29) binding facilitates the process, the details of which remain to be determined. Our experimental results are from an epithelial wound model in the murine cornea and it may be quite likely, as others have reported, that dependence on integrin binding for migration is specific to the site and stimulus of inflammation and may change over time as the inflammatory response evolves [51, 53, 56, 61, 63, 65, 84].

Chapter 3 References

1. Song, J., Lee, Y.G., Houston, J., Petroll, W.M., Chakravarti, S., Cavanagh, H.D., Jester, J.V. (2003) Neonatal corneal stromal development in the normal and lumican-deficient mouse. *Invest Ophthalmol Vis Sci* **44**, 548-57.

2. Chakravarti, S., Magnuson, T., Lass, J.H., Jepsen, K.J., LaMantia, C., Carroll, H. (1998) Lumican regulates collagen fibril assembly: skin fragility and corneal opacity in the absence of lumican. *J Cell Biol* **141**, 1277-86.

3. Cornuet, P.K., Blochberger, T.C., Hassell, J.R. (1994) Molecular polymorphism of lumican during corneal development. *Invest Ophthalmol Vis Sci* **35**, 870-7.

4. Akhtar, S., Kerr, B.C., Hayes, A.J., Hughes, C.E., Meek, K.M., Caterson, B. (2008) Immunochemical localization of keratan sulfate proteoglycans in cornea, sclera, and limbus using a keratanase-generated neoepitope monoclonal antibody. *Invest Ophthalmol Vis Sci* **49**, 2424-31.

5. Miyagawa, A., Kobayashi, M., Fujita, Y., Hamdy, O., Hirano, K., Nakamura, M., Miyake, Y. (2001) Surface ultrastructure of collagen fibrils and their association with proteoglycans in human cornea and sclera by atomic force microscopy and energy-filtering transmission electron microscopy. *Cornea* **20**, 651-6.

6. Rada, J.A., Cornuet, P.K., Hassell, J.R. (1993) Regulation of corneal collagen fibrillogenesis in vitro by corneal proteoglycan (lumican and decorin) core proteins. *Exp Eye Res* **56**, 635-48.

7. Chakravarti, S., Petroll, W.M., Hassell, J.R., Jester, J.V., Lass, J.H., Paul, J., Birk, D.E. (2000) Corneal opacity in lumican-null mice: defects in collagen fibril

structure and packing in the posterior stroma. *Invest Ophthalmol Vis Sci* **41**, 3365-73.

8. Ecoiffier, T., Yuen, D., Chen, L. (2009) Differential distribution of blood and lymphatic vessels in the murine cornea. *Invest Ophthalmol Vis Sci* **51**, 2436-40.

9. Gagen, D., Laubinger, S., Li, Z., Petrescu, M.S., Brown, E.S., Smith, C.W., Burns, A.R. (2010) ICAM-1 mediates surface contact between neutrophils and keratocytes following corneal epithelial abrasion in the mouse. *Exp Eye Res*.

10. Chintakuntlawar, A.V., Chodosh, J. (2009) Chemokine CXCL1/KC and its receptor CXCR2 are responsible for neutrophil chemotaxis in adenoviral keratitis. *J Interferon Cytokine Res* **29**, 657-66.

11. Carlson, E.C., Sun, Y., Auletta, J., Kao, W.W., Liu, C.Y., Perez, V.L., Pearlman, E. (2010) Regulation of corneal inflammation by neutrophil-dependent cleavage of keratan sulfate proteoglycans as a model for breakdown of the chemokine gradient. *J Leukoc Biol* **88**, 517-22.

12. Carlson, E.C., Liu, C.Y., Chikama, T., Hayashi, Y., Kao, C.W., Birk, D.E., Funderburgh, J.L., Jester, J.V., Kao, W.W. (2005) Keratocan, a cornea-specific keratan sulfate proteoglycan, is regulated by lumican. *J Biol Chem* **280**, 25541-7.

13. Lee, S., Bowrin, K., Hamad, A.R., Chakravarti, S. (2009) Extracellular matrix lumican deposited on the surface of neutrophils promotes migration by binding to beta2 integrin. *J Biol Chem* **284**, 23662-9.

14. Hayashi, Y., Call, M.K., Chikama, T., Liu, H., Carlson, E.C., Sun, Y., Pearlman, E., Funderburgh, J.L., Babcock, G., Liu, C.Y., Ohashi, Y., Kao, W.W. (2010)

Lumican is required for neutrophil extravasation following corneal injury and wound healing. *J Cell Sci* **123**, 2987-95.

15.   Ashwin, P.T., Shah, S., Pushpoth, S., Wehbeh, L., Ilango, B. (2009) The relationship of Central Corneal Thickness (CCT) to Thinnest Central Cornea (TCC) in healthy adults. *Cont Lens Anterior Eye* **32**, 64-7.

16.   Montiani-Ferreira, F., Petersen-Jones, S., Cassotis, N., Ramsey, D.T., Gearhart, P., Cardoso, F. (2003) Early postnatal development of central corneal thickness in dogs. *Vet Ophthalmol* **6**, 19-22.

17.   Hager, A., Wegscheider, K., Wiegand, W. (2009) Changes of extracellular matrix of the cornea in diabetes mellitus. *Graefes Arch Clin Exp Ophthalmol* **247**, 1369-74.

18.   Insull, E., Nicholas, S., Ang, G.S., Poostchi, A., Chan, K., Wells, A. (2010) Optic disc area and correlation with central corneal thickness, corneal hysteresis and ocular pulse amplitude in glaucoma patients and controls. *Clin Experiment Ophthalmol*.

19.   Fontes, B.M., Ambrosio, R., Jr., Jardim, D., Velarde, G.C., Nose, W. (2010) Corneal biomechanical metrics and anterior segment parameters in mild keratoconus. *Ophthalmology* **117**, 673-9.

20.   Doughty, M.J. (2000) Swelling of the collagen-keratocyte matrix of the bovine corneal stroma ex vivo in various solutions and its relationship to tissue thickness. *Tissue Cell* **32**, 478-93.

21.   Maldonado, M.J., Lopez-Miguel, A., Nieto, J.C., Cano-Parra, J., Calvo, B., Alio, J.L. (2009) Reliability of noncontact pachymetry after laser in situ keratomileusis. *Invest Ophthalmol Vis Sci* **50**, 4135-41.

22.   Martin, R., de Juan, V., Rodriguez, G., Cuadrado, R., Fernandez, I. (2007) Measurement of corneal swelling variations without removal of the contact lens during extended wear. *Invest Ophthalmol Vis Sci* **48**, 3043-50.

23.   Oh, J.H., Yoo, C., Kim, Y.Y., Kim, H.M., Song, J.S. (2009) The effect of contact lens-induced corneal edema on Goldmann applanation tonometry and dynamic contour tonometry. *Graefes Arch Clin Exp Ophthalmol* **247**, 371-5.

24.   Haddadin, R.I., Oh, D.J., Kang, M.H., Filippopoulos, T., Gupta, M., Hart, L., Sage, E.H., Rhee, D.J. (2009) SPARC-null mice exhibit lower intraocular pressures. *Invest Ophthalmol Vis Sci* **50**, 3771-7.

25.   Henriksson, J.T., McDermott, A.M., Bergmanson, J.P. (2009) Dimensions and morphology of the cornea in three strains of mice. *Invest Ophthalmol Vis Sci* **50**, 3648-54.

26.   Schmucker, C., Schaeffel, F. (2004) A paraxial schematic eye model for the growing C57BL/6 mouse. *Vision Res* **44**, 1857-67.

27.   Zhou, X., Shen, M., Xie, J., Wang, J., Jiang, L., Pan, M., Qu, J., Lu, F. (2008) The development of the refractive status and ocular growth in C57BL/6 mice. *Invest Ophthalmol Vis Sci* **49**, 5208-14.

28.   Doughty, M.J., Bergmanson, J.P., Blocker, Y. (1997) Shrinkage and distortion of the rabbit corneal endothelial cell mosaic caused by a high osmolality

glutaraldehyde-formaldehyde fixative compared to glutaraldehyde. *Tissue Cell* **29**, 533-47.

29. Hayat, M.A. (1981) *Fixation for electron microscopy*. Academic Press, New York.

30. Chakravarti, S., Zhang, G., Chervoneva, I., Roberts, L., Birk, D.E. (2006) Collagen fibril assembly during postnatal development and dysfunctional regulation in the lumican-deficient murine cornea. *Dev Dyn* **235**, 2493-506.

31. Zieske, J.D. (2004) Corneal development associated with eyelid opening. *Int J Dev Biol* **48**, 903-11.

32. Jester, J.V., Lee, Y.G., Huang, J., Houston, J., Adams, B., Cavanagh, H.D., Petroll, W.M. (2007) Postnatal corneal transparency, keratocyte cell cycle exit and expression of ALDH1A1. *Invest Ophthalmol Vis Sci* **48**, 4061-9.

33. Nagasaki, T., Zhao, J. (2003) Centripetal movement of corneal epithelial cells in the normal adult mouse. *Invest Ophthalmol Vis Sci* **44**, 558-66.

34. Jun, A.S., Chakravarti, S., Edelhauser, H.F., Kimos, M. (2006) Aging changes of mouse corneal endothelium and Descemet's membrane. *Exp Eye Res* **83**, 890-6.

35. Lively, G.D., Jiang, B., Hedberg-Buenz, A., Chang, B., Petersen, G.E., Wang, K., Kuehn, M.H., Anderson, M.G. (2009) Genetic dependence of central corneal thickness among inbred strains of mice. *Invest Ophthalmol Vis Sci* **51**, 160-71.

36. Quantock, A.J., Meek, K.M., Brittain, P., Ridgway, A.E., Thonar, E.J. (1991) Alteration of the stromal architecture and depletion of keratan sulphate proteoglycans in oedematous human corneas: histological, immunochemical and X-ray diffraction evidence. *Tissue Cell* **23**, 593-606.

37. Meek, K.M., Leonard, D.W., Connon, C.J., Dennis, S., Khan, S. (2003) Transparency, swelling and scarring in the corneal stroma. *Eye (Lond)* **17**, 927-36.

38. Wendt, K.D., Jensen, C.A., Tindall, R., Katz, M.L. (2004) Comparison of conventional and microwave-assisted processing of mouse retinas for transmission electron microscopy. *J Microsc* **214**, 80-8.

39. Ferris, A.M., Giberson, R.T., Sanders, M.A., Day, J.R. (2009) Advanced laboratory techniques for sample processing and immunolabeling using microwave radiation. *J Neurosci Methods* **182**, 157-64.

40. Giberson, R.T., Demaree, R.S., Jr., Nordhausen, R.W. (1997) Four-hour processing of clinical/diagnostic specimens for electron microscopy using microwave technique. *J Vet Diagn Invest* **9**, 61-7.

41. Josephsen, G.D., Josephsen, K.A., Beilman, G.J., Taylor, J.H., Muiler, K.E. (2005) Microwave processing for sample preparation to evaluate mitochondrial ultrastructural damage in hemorrhagic shock. *Microsc Microanal* **11**, 500-5.

42. Wilson, S.E., Kim, W.J. (1998) Keratocyte apoptosis: implications on corneal wound healing, tissue organization, and disease. *Invest Ophthalmol Vis Sci* **39**, 220-6.

43. Zhao, J., Nagasaki, T. (2004) Mechanical damage to corneal stromal cells by epithelial scraping. *Cornea* **23**, 497-502.

44. Petrescu, M.S., Larry, C.L., Bowden, R.A., Williams, G.W., Gagen, D., Li, Z., Smith, C.W., Burns, A.R. (2007) Neutrophil interactions with keratocytes during corneal epithelial wound healing: a role for CD18 integrins. *Invest Ophthalmol Vis Sci* **48**, 5023-9.

45. Labbe, A., Liang, H., Martin, C., Brignole-Baudouin, F., Warnet, J.M., Baudouin, C. (2006) Comparative anatomy of laboratory animal corneas with a new-generation high-resolution in vivo confocal microscope. *Curr Eye Res* **31**, 501-9.

46. Rieth, S., Engel, F., Buhner, E., Uhlmann, S., Wiedemann, P., Foja, C. (2010) Comparison of data from the rostock cornea module of the heidelberg retina tomograph, the oculus pentacam, and the endothelial cell microscope. *Cornea* **29**, 314-20.

47. Alomar, T.S., Al-Aqaba, M., Gray, T., Lowe, J., Dua, H.S. (2011) Histological and confocal microscopy changes in chronic corneal edema: implications for endothelial transplantation. *Invest Ophthalmol Vis Sci* **52**, 8193-207.

48. Friedl, P., Weigelin, B. (2008) Interstitial leukocyte migration and immune function. *Nat Immunol* **9**, 960-9.

49. Downey, G.P. (1994) Mechanisms of leukocyte motility and chemotaxis. *Curr Opin Immunol* **6**, 113-24.

50. Behzad, A.R., Chu, F., Walker, D.C. (1996) Fibroblasts are in a position to provide directional information to migrating neutrophils during pneumonia in rabbit lungs. *Microvasc Res* **51**, 303-16.

51. Planck, S.R., Becker, M.D., Crespo, S., Choi, D., Galster, K., Garman, K.L., Nobiling, R., Rosenbaum, J.T. (2008) Characterizing extravascular neutrophil migration in vivo in the iris. *Inflammation* **31**, 105-11.

52. Tan, J., Shen, H., Saltzman, W.M. (2001) Micron-scale positioning of features influences the rate of polymorphonuclear leukocyte migration. *Biophys J* **81**, 2569-79.

53. Mandeville, J.T., Lawson, M.A., Maxfield, F.R. (1997) Dynamic imaging of neutrophil migration in three dimensions: mechanical interactions between cells and matrix. *J Leukoc Biol* **61**, 188-200.

54. Christenson, K., Bjorkman, L., Karlsson, J., Sundqvist, M., Movitz, C., Speert, D.P., Dahlgren, C., Bylund, J. (2011) In vivo-transmigrated human neutrophils are resistant to antiapoptotic stimulation. *J Leukoc Biol* **90**, 1055-63.

55. Gonzalez, A.L., El-Bjeirami, W., West, J.L., McIntire, L.V., Smith, C.W. (2007) Transendothelial migration enhances integrin-dependent human neutrophil chemokinesis. *J Leukoc Biol* **81**, 686-95.

56. Ridger, V.C., Wagner, B.E., Wallace, W.A., Hellewell, P.G. (2001) Differential effects of CD18, CD29, and CD49 integrin subunit inhibition on neutrophil migration in pulmonary inflammation. *J Immunol* **166**, 3484-90.

57. Lammermann, T., Bader, B.L., Monkley, S.J., Worbs, T., Wedlich-Soldner, R., Hirsch, K., Keller, M., Forster, R., Critchley, D.R., Fassler, R., Sixt, M. (2008) Rapid leukocyte migration by integrin-independent flowing and squeezing. *Nature* **453**, 51-5.

58. Muether, P.S., Dell, S., Kociok, N., Zahn, G., Stragies, R., Vossmeyer, D., Joussen, A.M. (2007) The role of integrin alpha5beta1 in the regulation of corneal neovascularization. *Exp Eye Res* **85**, 356-65.

59. Lindbom, L., Werr, J. (2002) Integrin-dependent neutrophil migration in extravascular tissue. *Semin Immunol* **14**, 115-21.

60. Carter, R.T. (2009) The role of integrins in corneal wound healing. *Vet Ophthalmol* **12 Suppl 1**, 2-9.

61.   Koenderman, L., van der Linden, J.A., Honing, H., Ulfman, L.H. (2010) Integrins on neutrophils are dispensable for migration into three-dimensional fibrin gels. *Thromb Haemost* **104**, 599-608.

62.   Friedl, P., Brocker, E.B. (2000) The biology of cell locomotion within three-dimensional extracellular matrix. *Cell Mol Life Sci* **57**, 41-64.

63.   Friedl, P., Zanker, K.S., Brocker, E.B. (1998) Cell migration strategies in 3-D extracellular matrix: differences in morphology, cell matrix interactions, and integrin function. *Microsc Res Tech* **43**, 369-78.

64.   Khandoga, A.G., Khandoga, A., Reichel, C.A., Bihari, P., Rehberg, M., Krombach, F. (2009) In vivo imaging and quantitative analysis of leukocyte directional migration and polarization in inflamed tissue. *PLoS One* **4**, e4693.

65.   Li, Z., Burns, A.R., Smith, C.W. (2006) Two waves of neutrophil emigration in response to corneal epithelial abrasion: distinct adhesion molecule requirements. *Invest Ophthalmol Vis Sci* **47**, 1947-55.

66.   Bohnke, M., Masters, B.R. (1999) Confocal microscopy of the cornea. *Prog Retin Eye Res* **18**, 553-628.

67.   Patel, D.V., McGhee, C.N. (2007) Contemporary in vivo confocal microscopy of the living human cornea using white light and laser scanning techniques: a major review. *Clin Experiment Ophthalmol* **35**, 71-88.

68.   Lim, L.L., Hoang, L., Wong, T., Planck, S.R., Ronick, M.B., Gould, R.R., Mathers, W.D., Rosenbaum, J.T. (2006) Intravital microscopy of leukocyte-endothelial dynamics using the Heidelberg confocal laser microscope in scleritis and allergic conjunctivitis. *Mol Vis* **12**, 1302-5.

69. Pal-Ghosh, S., Pajoohesh-Ganji, A., Tadvalkar, G., Stepp, M.A. (2011) Removal of the basement membrane enhances corneal wound healing. *Exp Eye Res* **93**, 927-36.

70. Wilson, S.E., Chaurasia, S.S., Medeiros, F.W. (2007) Apoptosis in the initiation, modulation and termination of the corneal wound healing response. *Exp Eye Res* **85**, 305-11.

71. Li, L., Norrelykke, S.F., Cox, E.C. (2008) Persistent cell motion in the absence of external signals: a search strategy for eukaryotic cells. *PLoS One* **3**, e2093.

72. Ambravaneswaran, V., Wong, I.Y., Aranyosi, A.J., Toner, M., Irimia, D. (2010) Directional decisions during neutrophil chemotaxis inside bifurcating channels. *Integr Biol (Camb)* **2**, 639-47.

73. Rodt, S.A., Reed, R.K., Ljungstrom, M., Gustafsson, T.O., Rubin, K. (1994) The anti-inflammatory agent alpha-trinositol exerts its edema-preventing effects through modulation of beta 1 integrin function. *Circ Res* **75**, 942-8.

74. van den Berg, T.K., Puklavec, M.J., Barclay, A.N., Dijkstra, C.D. (2001) Monoclonal antibodies against rat leukocyte surface antigens. *Immunol Rev* **184**, 109-16.

75. Stepp, M.A. (2006) Corneal integrins and their functions. *Exp Eye Res* **83**, 3-15.

76. Andresen, J.L., Ledet, T., Hager, H., Josephsen, K., Ehlers, N. (2000) The influence of corneal stromal matrix proteins on the migration of human corneal fibroblasts. *Exp Eye Res* **71**, 33-43.

77.   Werr, J., Johansson, J., Eriksson, E.E., Hedqvist, P., Ruoslahti, E., Lindbom, L. (2000) Integrin alpha(2)beta(1) (VLA-2) is a principal receptor used by neutrophils for locomotion in extravascular tissue. *Blood* **95**, 1804-9.

78.   Pajoohesh-Ganji, A., Ghosh, S.P., Stepp, M.A. (2004) Regional distribution of alpha9beta1 integrin within the limbus of the mouse ocular surface. *Dev Dyn* **230**, 518-28.

79.   Parapuram, S.K., Huh, K., Liu, S., Leask, A. (2011) Integrin beta1 is necessary for the maintenance of corneal structural integrity. *Invest Ophthalmol Vis Sci* **52**, 7799-806.

80.   Burns, A.R., Simon, S.I., Kukielka, G.L., Rowen, J.L., Lu, H., Mendoza, L.H., Brown, E.S., Entman, M.L., Smith, C.W. (1996) Chemotactic factors stimulate CD18-dependent canine neutrophil adherence and motility on lung fibroblasts. *J Immunol* **156**, 3389-401.

81.   Mayadas, T.N., Cullere, X. (2005) Neutrophil beta2 integrins: moderators of life or death decisions. *Trends Immunol* **26**, 388-95.

82.   Saltzman, W.M., Livingston, T.L., Parkhurst, M.R. (1999) Antibodies to CD18 influence neutrophil migration through extracellular matrix. *J Leukoc Biol* **65**, 356-63.

83.   Rainger, G.E., Buckley, C.D., Simmons, D.L., Nash, G.B. (1999) Neutrophils sense flow-generated stress and direct their migration through alphaVbeta3-integrin. *Am J Physiol* **276**, H858-64.

84.   Heit, B., Colarusso, P., Kubes, P. (2005) Fundamentally different roles for LFA-1, Mac-1 and alpha4-integrin in neutrophil chemotaxis. *J Cell Sci* **118**, 5205-20.

CHAPTER 4 - DISCUSSION

4.1 - General summary

In general terms, inflammation is an organism's response to injury which defends against invading pathogens that may accompany the injury, as well as being an initial step in the healing process. Thus inflammation is critical to survival. Neutrophils are key constituents of inflammation and their migration to the site of injury is necessary for them to participate.

The purpose of this dissertation was to provide insights into the mechanisms of neutrophil migration through the corneal stroma, specifically addressing the influence of the keratocyte network on migrating neutrophils and the relative contribution of β1 (CD29), β2 (CD18) and β3 (CD61) integrins to neutrophil locomotion in the inflamed murine cornea. Even though the emphasis was on migration and the role of integrins in the process, it must be kept in mind that integrins do more than simply provide a physical adhesion point, and that migration involves more than simple locomotion. While neutrophils are moving through the interstitium they are interacting with the extracellular matrix and the cells which it contains. These interactions likely trigger important events in the inflammatory cascade. Thus, interstitial migration is a critical step but only a single step in the complex process of inflammation.

The significance of this dissertation is highlighted by the fact that experiments were performed *in vivo*. Migrating cells were therefore interacting with their "normal" corneal environment, which cannot be duplicated *in vitro* nor with tissues other than the cornea. The benefits of *in vivo* studies are only present when the animal being studied is maintained at a stable, homeostatic state. Therefore every effort was made to keep the

animal physiologically normal during the imaging process to be sure that all the subtleties of the interstitium were in-play.

In order for *in vivo* experiments to be representative, the animals used must be at an age of maturity that provides a relatively stable environment. As described in chapter 1, in the early postnatal period the mouse cornea undergoes major structural and physiological changes that would undoubtedly have an effect on neutrophil migration. In order to avoid confounding variables that could have a significant impact on *in vivo* neutrophil migration, it was necessary to determine the age at which the corneal stroma reaches maturity. This was the rationale for expending considerable time and effort in establishing a minimum age for the animals used in these experiments as part of Aim 1. Additionally from Aim 1, accurate histological representation was necessary to be able to compare the stroma beneath the wound to the parawound, and potentially reveal evidence of gross structural changes that may have occurred with the addition of blocking antibodies.

Chapter 1 described the complex nature of the corneal stroma. The cornea has been a scientific curiosity for centuries due to its unique qualities. In spite of enormous research efforts over the years, there is still more to be learned. Electron microscopy, X-ray diffraction, and other methods have given us a concept of its structure, while other methodologies have given us information about its biomechanical properties. However, the question of how neutrophils (leukocytes) are able to migrate through the stroma is still somewhat of an enigma. The stroma is tightly compacted with keratocytes squeezed in between the lamellae. Many forces combine to hold the stroma together. Yet, somehow, neutrophils are able to rapidly migrate through the stroma without apparent

alterations in their wake. Aim 2 showed that neutrophils preferentially (exclusively?) migrate along the network of keratocytes, between lamellae. The question then arose whether neutrophils use integrin-dependent binding to move along the keratocytes or whether the keratocyte network is a "path of least resistance". This question was addressed in aim 3.

Aim 3 investigated the role of integrins in neutrophil migration by blocking three separate integrin families known to be expressed by activated neutrophils and/or keratocytes. *In vivo* studies such as this are particularly important for determining the role of integrins during neutrophil migration since there is still debate whether they are required or not, based on 3-D *in vitro* studies. If integrin binding were responsible for the preferential migration of neutrophils along the keratocyte network, it would have been expected that motility decrease with blockade of β2 (CD18) integrins (on neutrophils) since keratocytes upregulate surface expression of ICAM-1, a ligand for β2 (CD18) integrins. However, this was not the case. β1 (CD29) integrins, which are found on keratocytes and neutrophils, bind with elements of the ECM but one study showed them to make homophilic cell-cell binding [1]. Although, this is not a widely reported finding, it does raise the possibility that β1 (CD29) integrin homophilic binding could potentially be involved in neutrophil-keratocyte adhesion. Indeed, when β1 (CD29) integrins were functionally blocked, the neutrophils migrated significantly slower and followed a more random path. However, their preferential migration along the keratocyte network was not affected. αVβ3 integrin is also present on both neutrophils and keratocytes but it has not been shown to have homophilic interactions and showed no effect on neutrophil motility when it was blocked. It was therefore shown that, of the three integrin families tested,

only β1 is involved in facilitating neutrophil locomotion in the corneal stroma, but even if it is blocked migration continues at a somewhat slower rate. The conclusion is that neutrophil migration through the murine cornea stroma following a non-infective epithelial abrasion is partially dependent on β1 binding. Whether this effect is due to loss of homophilic interaction between neutrophils and keratocytes, loss of heterophilic interaction between neutrophils and components of the ECM, or alterations in the extracellular environment remains to be determined.

Significance of research

Acute inflammation is an initial phase of the innate immune response and is of critical importance for an individual's survival. Not only is it a defense against invading microbes but is also an integral component of wound healing. Neutrophils are key players in acute inflammation and have multiple roles including pro-inflammatory signaling, killing pathogens, aiding in the resolution of inflammation, and releasing cytokines and growth factors to promote healing. It is important for neutrophils to reach the site of injury as quickly as possible to prevent the spread of invading microbes introduced through the wound. Anything that slows the process puts the tissue at risk for infection. The whole cascade of events is complex and our understanding of it is only partial. Every event is interrelated with others and therefore research aimed at one event may have implications for others as well. While understanding the mechanism of neutrophil locomotion is important for a number of reasons, the process of migration is more than locomotion. The migrating cells interact with other cells and their extracellular

environment, initiating signal transduction which in turn initiates or modulates other events. Therefore research designed to elucidate migration mechanisms, the molecules or events that are involved or not involved, provides details to aid in the overall understanding of inflammation.

Normally inflammation is a necessary and well controlled process. However, for many reasons, the inflammatory response may be exaggerated or depressed and may not resolve properly leading to chronicity. Modulation of inflammation, when appropriate, without interrupting or interfering with the overall process is the desired outcome. By and large treatment for inflammation has been aimed at suppressing pro-inflammatory factors. However, these same treatments ironically also suppress some of the naturally occurring anti-inflammatory agents. They also make one more susceptible to infection and slower to heal. Perhaps medical treatment needs to be more concentrated on promoting the anti-inflammatory processes to encourage the individual's own defenses to resolve inflammation. The goal should be "bringing closure" rather than interrupting the process. Having a thorough understanding of the intricate cascade of events is prerequisite to successful management of inflammation.

Neutrophils were shown to preferentially migrate along the keratocyte network and predominantly in the anterior stroma. We have no solid evidence for why they prefer the anterior stroma but it is likely that it may be due to structural differences between anterior and posterior stroma. Refractive corneal procedures target the anterior stroma and it therefore seems plausible that this type of stromal alteration may have an effect on the ability of neutrophils to migrate. Collagen cross-linking has been used for treatment of keratoconus. Whether keratoconic corneas are treated with collagen cross-linking or not,

in either case their stromal architecture is abnormal and undoubtedly has ramifications for neutrophil migration. Even though cross-linking may have benefits for preventing the progression of corneal ectasia, it could possibly have a deleterious effect on neutrophil migration. There are many situations where the stromal architecture and/or keratocyte network are altered. Perhaps in these situations neutrophils must switch their means of locomotion from mechanical squeezing ("chimneying") to integrin-dependent binding to components of the ECM.

It is clearly evident that much additional research is needed in order to fully understand the intricate processes involved in neutrophil interstitial migration and through this understanding will emerge improved treatment and management of corneal wounding.

Limitations of this research:

1. These studies only looked at a single time point in the inflammatory process. It is possible that blocking antibodies would have other effects not seen at 8 hours which is early in the infiltration wave.

2. The mouse cornea is different in many ways. It is possible that integrins play more or less of a role in human corneal neutrophil migration.

3. A single strain of mouse was used and they were all female. The experiments could be repeated with and males and females compared, as well as comparison with other strains.

4. These studies used a non-infectious wound model. In the presence of other molecules produced by infectious agents there is likely to be a stronger chemoattractant which may alter the mechanism of neutrophil motility.

5. Cells were tracked for 10 minutes. Longer tracking times may provide additional clues to changes in motility resulting from integrin blocking.

6. These studies were in the cornea only. Neutrophil migration in other tissues is very likely different. The surrounding extracellular matrix undoubtedly has a significant effect and the cornea structure is unique in many ways.

7. There are possibly other adhesion molecules involved. Other potential adhesion molecules present could be identified with Western blotting and each blocked with the appropriate antibody.

4.2 - Future Directions

Using the HRT-RCM for *in vivo* time-lapse imaging of neutrophils many other research questions can be investigated in mice, as well as in other animals, including humans. There are numerous corneal diseases, surgical and medical treatments that may alter the normal stromal environment and subsequently have an impact on the inflammatory process. A common example would be the effects noted with contact lens wear. Minimizing the pro-inflammatory effects from contact lenses and their associated solutions is of significant concern to product developers. In many instances the HRT-RCM may provide valuable *in vivo* insights for product development and for management of product-related complications.

Before considering altered corneas, more investigation of the normal corneal response to inflammation is needed. In this dissertation the role integrins play in neutrophil migration was addressed. It was shown that neutrophils are capable of migrating through the stroma without the aid of β1 (CD29), β2 (CD18), or β3 (CD61) integrin binding. The presumed alternative mechanism of migration would be mechanical squeezing through the confined space between collagen lamellae. This remains to be shown, but *in vivo* imaging can help in this regard. It might be that if the space between lamellae were expanded beyond a certain point, the neutrophils would be unable to use frictional forces for squeezing and would then revert to integrin binding. In order to test this hypothesis, corneas could be made hyper-edematous and neutrophil migration parameters compared to baseline. With the wounding that is applied to the corneas, there is some amount of edema. However this may not be enough to produce the change in migration method.

Additional edema can be induced by applying hypotonic solutions to the anterior surface and blocking the action of the endothelial cell pump.

Another question remains to be addressed. What is the relationship between neutrophil migration and keratocytes? The present study indicates that integrin binding between neutrophils and keratocytes is not necessary for the neutrophils to follow the keratocyte network. If keratocytes were induced to undergo apoptosis and then wounded, would neutrophils be able to migrate through an area void of keratocytes? This may also be like a secondary wound where more neutrophils are recruited before keratocyte numbers are back to baseline. In chapter 3 it was shown that neutrophils moved significantly slower beneath the wound where keratocytes were lost. As mentioned, there are several reasons why this may occur. If the experiments were repeated and a potent neutrophil chemoattractant applied to one side of the cornea it might be shown that the neutrophils deviated from the keratocyte network as a result.

There have been several suggestions for the attractants which guide infiltrating neutrophils toward the wound site. Chemokines released from the damaged epitheium or those from the tears that found their way into the stroma once the epithelial barrier was breeched have been implicated. Another possibility that has not been explored in the cornea is the contribution of necrotaxis. It has been shown that dead cells release formyl-Methionyl-Leucyl-Phenylalanine (fMLP) and neutrophils have fMLP receptors [2]. Neutrophil fMLP signaling could be blocked with fMLP receptor antagonists in order to determine the relative contribution of this potential attractant to neutrophil migration in the corneal stroma.

Macrophages are also reported to be intimately involved with neutrophil migration, but *in vivo* dynamics of their involvement have yet to be shown. Macrophages are readily visualized with the HRT-RCM and their densities determined and followed over the wound healing period in the same mouse. It might be possible to determine whether macrophages proliferate in the cornea or are recruited from the limbus [3]. The timing of the neutrophil peak and clearance as compared to macrophage peak and return to baseline may provide insight into their interaction dynamics. When they do return to baseline what happens to the lost macrophages? There is some evidence they may transform into other cell types [4, 5] .

Along the same lines, it has been reported by numerous researchers that neutrophils die once they reach the site of inflammation and are then cleared by macrophages. *In vivo* imaging may provide evidence supporting this or may show that some neutrophils go beyond the site and possibly return to the limbus, and possibly intravasate as recently described to occur in zebra fish [6].

Once some of the normal dynamics are explored, the same dynamics can be explored in abnormal corneas. An area of interest is the effects of obesity induced insulin resistance and diabetes on the cornea and in particular how the inflammatory dynamics are altered. It has been shown that the corneal stroma is altered in diabetes, thus potentially affecting the ability of neutrophils to migrate efficiently. Obesity induced insulin resistance, a precursor to diabetes, has been shown to cause a shift in macrophage polarity from the non-inflammatory to the pro-inflammatory phenotype [7]. Thus these individuals are in a sense in a state of chronic inflammation.

The global prevalence of diabetes in the year 2000 was estimated to be 2.8% (171 million) and is projected to be 4.4% (366 million) by 2030. Among those who are diabetic many have corneal complications ranging from mild dry eye symptoms to vascularization, severe stromal scarring and ulceration. Diabetic keratopathy is under-diagnosed largely because there has not been a practical means for diagnosing early/mild forms of the disease. Even with minor or no obvious keratopathy, diabetics have abnormal corneal wound repair. Histologically they have thickened epithelial basement membrane, hemidesmosomes with poor penetration of anchoring fibrils into the stroma, collagen irregularities, and degeneration of keratocytes and endothelial cells. A greater understanding of the effects of diabetes on leukocyte motility may provide clues to why wound healing is abnormal in these individuals.

Visualizing the dynamics of neutrophil migration in the living eye using instruments such as the HRT-RCM has countless possibilities for experimental application. Undoubtedly the area of intravital microscopy/imaging will continue to evolve and, as it does, elucidate many details surrounding neutrophil migration.

Chapter 4 References

1.	Sriramarao, P., Steffner, P., Gehlsen, K.R. (1993) Biochemical evidence for a homophilic interaction of the alpha 3 beta 1 integrin. *J Biol Chem* **268**, 22036-41.

2.	McDonald, B., Pittman,K., Menezes, G. B., Hirota, S. A., Slaba, I., Waterhouse, C. C., Beck, P. L., Muruve, D. A., Kubes, P. (2011) Intravascular danger signals guide neutrophils to sites of sterile inflammation. *Science* **330**(6002), 362-366.

3.	Mahdavian Delavary, B., van der Veer, W.M., van Egmond, M., Niessen, F.B., Beelen, R.H. Macrophages in skin injury and repair. *Immunobiology* **216**, 753-62.

4.	Lin, M.L., Li, Y.P., Li, Z.R., Lin, J.X., Zhou, X.L., Liang, D. Macrophages acquire fibroblast characteristics in a rat model of proliferative vitreoretinopathy. *Ophthalmic Res* **45**, 180-90.

5.	Takayama, T., Kondo, T., Kobayashi, M., Ohta, K., Ishibashi, Y., Kanemaru, T., Shimazu, H., Ishikawa, F., Nakamura, T., Kinoshita, S., Nakamura, K. (2009) Characteristic morphology and distribution of bone marrow derived cells in the cornea. *Anat Rec (Hoboken)* **292**, 756-63.

6.	Yoo, S.K., Huttenlocher, A. (2011) Spatiotemporal photolabeling of neutrophil trafficking during inflammation in live zebrafish. *J Leukoc Biol* **89**, 661-7.

7.	Mosser, D.M., Edwards, J.P. (2008) Exploring the full spectrum of macrophage activation. *Nat Rev Immunol* **8**, 958-69.